SEA SURFACE COMPUTATIONS FROM LOCAL SATELLITE TRACKING AND SATELLITE ALTIMETRY

DEMITRIS DELIKARAOGLOU

October 1980

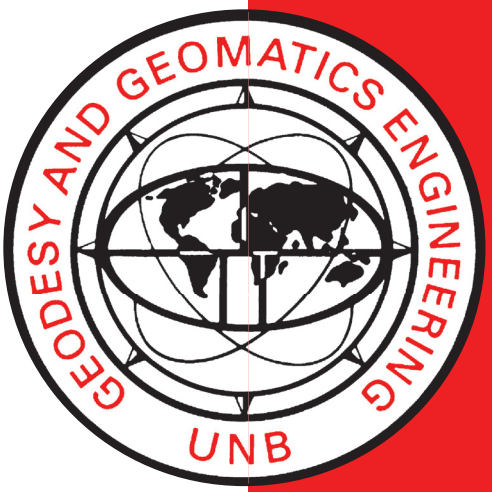

TECHNICAL REPORT
NO. 74

PREFACE

In order to make our extensive series of technical reports more readily available, we have scanned the old master copies and produced electronic versions in Portable Document Format. The quality of the images varies depending on the quality of the originals. The images have not been converted to searchable text.

AN INVESTIGATION ON THE SHORT WAVELENGTH ORBIT IMPROVEMENT AND SEA SURFACE COMPUTATIONS FROM LOCAL SATELLITE TRACKING AND SATELLITE ALTIMETRY

by

Demitris Delikaraoglou

B.Sc. National Technical University, Athens, 1974

M.Sc. University of Oxford, 1976

A thesis submitted in partial fulfilment of the

requirements for the degree of

Doctor of Philosophy in Engineering

in the Department

of

Surveying Engineering

THE UNIVERSITY OF NEW BRUNSWICK

June, 1980

Reprinted April 1986

ABSTRACT

The use of satellite radar altimetry in acquiring geodetic data over oceanic areas is investigated using precise ephemeris information for satellite coordinates and GEOS-3 altimetry data collected within the context of a Canadian GEOS-3 altimetry experiment conducted in the Hudson Bay area. GEOS-3 Doppler tracking data from four stations in the vicinity of Hudson Bay are analyzed for the purpose of establishing the extent of local improvement of the orbits required to reduce the altimetry data.

The a priori decisions involved in the computation of mean sea surface were to use precise ephemeris information; to use the available Doppler tracking data to reduce the ephemeris errors by means of the semi short-arc technique in the translocation mode; to use these Doppler fitted orbits to reduce and adjust the altimetry data; and to compare the results to various versions of the geoid to establish the degree of usefulness of the satellite altimetry technique for the determination of the sea surface topography.

The estimation of sea surface from satellite altimetry data is discussed. The problem areas and the various sources of errors inherent in the satellite altimetry observables used to define the sea surface are identified and their respective modelling within the context of this study is examined in detail.

The basic principles of the semi short-arc method, conventionally used in Canada for geodetic positioning, are related here to the intended local improvement of the orbits required to utilize the altimetry data.

From numerical results based on the combination of the available GEOS-3 Doppler data with reference orbits described in this case by a set of DMA precise ephemerides, precise ephemeris errors exceeding occasionally 10 m in the radial direction were found.

The formulation of the least squares model of intersecting altimetry arcs used here to remove long wavelength errors primarily due to unmodelled gravity field effects in the orbit determination is examined in detail. Residual orbit biases are found to be well represented by an absolute bias and a tilt parameter for each arc. From the study of a regional network of GEOS-3 orbital arcs in Hudson Bay the internal consistency of the estimated sea surface is found to be less than one metre, whereas the rms difference of the sea surface heights at the intersection points is found to be 1.1 m.

Comparisons of the altimetry-derived sea surface with a GEOS-3 sea surface independently determined by DMA indicated a relative consistency of 0.98 m (rms), attributed primarily to the presence of unmodelled time varying effects in the sea surface and anticipated differences induced by the different reduction procedures used to obtain the adjusted altimetry data. Comparisons with two combined geoids indicated an agreement of the order of 1.2 m (rms), attributed mainly to errors in the computed geoids and some level of spurius structure possibly introduced into the sea surface because of the Doppler orbit adjustment.

Based on the analysis and the results of this study, several contributions relevant to the problem of acquiring geodetic data in oceanic areas from satellite altimetry have resulted from this research. Of these, the following are considered, in the author's opinion to be the most significant:

1. The practical demonstration of the feasibility of improvement of the orbits required to utilize the altimetry data from local satellite tracking; the implications from the present results are that if local Doppler tracking can improve orbital information as good as the precise ephemeris, it should be even more important in the case of worse available reference orbits.

2. A complete discussion into the diverse kinds of information which needs to be considered in any attempt of utilizing satellite altimetry data. While the results presented herein are based on assumptions and decisions pertaining to the intended application of the Hudson Bay experiment, the information contained in this thesis should serve to highlight the strengths and weaknesses of the estimation process used in this study and hence usefully direct further investigations towards future applications.

3. The development of a complete computer package of programs (available at the Department of Surveying Engineering at UNB) designed to combine information similar to the one used in this study.

TABLE OF CONTENTS

PAGE

LIST OF TABLES

LIST OF FIGURES

FIGURE PAGE

LIST OF SYMBOLS

A	Satellite radar altimetry range
a	Semi-major axis of ellipsoid, orbital ellipse
b_A	Altimetry bias
D	Doppler cound
d	Sea depth
E	Eccentric anomaly
e	Satellite eccentricity
f	Frequency
f	Satellite true anomaly
f	Flattening of ellipsoid
f_k	Phase of tidal constituent k
G	Mean value of gravity
g	Gravity acceleration
H_k	Amplitude of tidal constituent k
h	Height above geocentric ellipsoid
N	Geoid undulation
n	Satellite mean motion
P	Atmospheric pressure
R	Mean radius of the earth
r	Satellite radius
S	Wind pile-up effect
U	Wind velocity
t	Time
x,y	Local cartesian coordinates
X,Y,Z	3-D geocentric cartesian coordinates
z	Sea surface height above geocentric ellipsoid

z_s	Sea surface topography
z_m	Time invariant part of sea surface height
z_t	Time varying part of sea surface height
β_k	Phase of tidal constituent k
Δg	Gravity anomaly
δa	Across-track orbit error component
δE	Along-track orbit error component
$\delta \eta$	Out-of-plane orbit error component
ε	Observational error
θ	Greenwich Sidereal Time
$\imath$	Satellite inclination
λ	Longitude
σ	Standard deviation
τ	UTC time epoch
ϕ	Geocentric latitude
Ω	Right ascension of the ascending node
Ω_k	Frequency of tidal constituent k
ω	Argument of the perigee

ACKNOWLEDGEMENTS

This work was funded by the Bedford Institute of Oceanography under research contract DSS Ref. 6AD FP806-9-G042. Dr. Dave E. Wells, who served as project coordinator, provided valuable support both in supplying the altimetry data and through valuable discussions that helped me to understand many of the more interesting aspects of satellite altimetry.

Thanks are extended to Shell Canada Limited and the Institute für Angewandte Geodäsie, Frankfurt, for their valuable assistance in the collection of GEOS-3 Doppler used in Section 3.

I am sincerely thankful to my thesis advisor and research supervisor Dr. Petr Vanicek for his valuable guidance, constant support and encouragement he has given me throughout this study. I have profited greatly from many discussions with him, as well as his detailed critisism of the manuscript.

Dr. Gerard Lachapelle of the Geodetic Survey of Canada showed a keen interest in this study. His help in providing the geoid and gravity data used in this study and allowing the use of computer time in the computer facilities of the Geodetic Survey is gratefully acknowledged.

The reduction of the GEOS-3 Doppler data would have not been possible without the extensive computing support given by Mr. J. Kouba of the Earth Physics Branch, who most willingly spared the time to give the benefit of his experience and help in utilizing the available data.

The valuable assistance given in this respect by Mr. David J. Doal of the Geodetic Survey is much appreciated. Thanks are also extended to Ms. Laura Mills and Mr. Saburi John and Mr. William Mersereau of the Computing Centre of the University of New Brunswick where nearly all of the computer programming and processing of the altimetry data was carried out.

The faultless typing job is due to Ms. Susan Perrott, whose patience and help in preparing the manuscript is much appreciated.

Last but not least, I would like to extend my appreciation to my colleagues of the Geodesy Group in the Department of Surveying Engineering where there was always an atmosphere of enthusiastic learning and true friendship. Those to whom I owe special thanks are Messrs. Brad Nickerson, who is no longer at UNB, and Robin Steeves. Discussing this work with them has been extremely helpful in many instances.

SECTION 1

INTRODUCTION

1.1 General Background and Outline of the Present Study

Between 1973-1975, Canada's participation in the GEOS-3 satellite programme (*NASA, 1972a*) was planned with two closely related satellite altimetry experiments which were to be conducted in the Hudson Bay area and the Northwestern Atlantic region. These experiments were initiated in view of the upcoming launch of the GEOS-3 satellite which was to carry a radar altimeter designed to measure the vertical distance to the ocean surface with geodetic accuracy. The primary objective was to develop experience in the analysis of radar altimetry data and to evaluate the data's utility to contribute to the physical study of the surrounding and interior oceanic areas of Canada for possible future altimeter bearing satellites (*Hodgson, 1973*). For the Hudson Bay Experiment in particular, embedded to this primary objective two more detailed objectives were (*Wells, 1976*):

a. to investigate alternative approaches which would eliminate dependence on precise orbits required in satellite altimetry reductions; and

b. to compute from altimetry data the sea level in Northern Canada and compare it with gravimetric geoids for the purpose of determining the extent to which satellite altimetry would contribute to the knowledge of the geoid in that area.

A premise widely held at the outset of the GEOS-3 programme was that in order to exploit fully the designed resolution ($\pm$ 1 m or better) of the GEOS-3 radar altimeter for geoid improvement, it was necessary that the radial component of the satellite orbit be known to at least this accuracy. Ordinarily, conventional approaches to the reduction of altimetry data were to utilize orbits from long arc solutions which require extensive worldwide tracking coverage to maintain such accurate reference orbits. A major problem that makes such a requirement very difficult is that errors in the long arc orbits resulting from unmodelled effects on the adopted geopotential model used in the orbit integration, unmodelled perturbations caused by air drag and solar radiation pressure, as well as unresolved biases in the tracking data would induce systematic errors in the orbits which in turn could be transferred to the local geoid.

For the intended application to the Canadian Hudson Bay Experiment the awareness of these difficulties led to the investigation of the feasibility of an approach which would utilize the long experience in Doppler satellite control that Canada had developed during previous satellite projects with the NNSS (TRANSIT) satellites (*Wells, 1974; Kouba and Wells, 1976*). Such an approach was envisioned to refine locally the GEOS-3 orbits by using simultaneous supplementary

Doppler tracking from several stations in the area of interest (Wells, 1976).

An effort in this direction is a major task set forth in this study. Accordingly the goals of the work reported here are twofold, namely to consider the application of satellite radar altimetry to the determination of the sea surface (and hence the geoid) in general; and secondly, within this context to utilize the radar altimetry data collected by the GEOS-3 satellite in the region of Hudson Bay together with Canadian Doppler for the same satellite to model and map the Hudson Bay sea surface.

In the subsequent sections the procedures for processing, combining and evaluating the data will be described. Section 2 discusses the application of satellite altimetry measurements to the estimation of the sea surface and geoid improvement. The various sources of errors affecting satellite altimetry are identified and their modelling within the context of the present study is examined. Section 3 deals with the treatment of the GEOS-3 Doppler data with regard to the intended local improvement of the orbits required to utilize the altimetry data. Section 4 deals with the formulation of the basic adjustment model of intersecting arcs. The estimation of orbital errors for each arc is examined and a computationally convenient solution of the normal equations using a partitioned regression technique is given. Results of the analysis of the GEOS-3 altimetry in Hudson Bay are given in section 5 together with results of the comparison of the features of the estimated sea surface with known geoidal features. An assessment of the results obtained is discussed in section 6. The

decisions upon which the results of section 5 depend are discussed, conclusions are drawn and recommendations are made.

1.2 The GEOS-3 Data Bank for the Hudson Bay

A GEOS-3 data bank maintained at UNB contains four basic data sets and a number of regional subsets used in this investigation to study the problem of orbital errors and the estimation of the ses surface in the Hudson Bay. These data sets and their sources are briefly described below, with more detailed descriptions given in the sequel as required.

(1) GEOS-3 radar altimetry for the Hudson Bay was received from NASA through the Bedford Institute of Oceanography (BIO). The originally received data sets consist of 238 GEOS-3 altimetry passes over the Hudson Bay and the Northwestern Atlantic which were acquired by a portable telemetry station at Caribou, Maine during the period from September to December, 1976. The data used in this study is in a BIO subset form of the original NASA standard format described by *Leitao et al (1975)*. The main omission of originally supplied NASA data, not in the BIO subsets, was the header timing records (*ibid, p. 57*) and the altimeter data related to the second main application of the altimeter, i.e. the determination of significant waveheight from the shape of the return pulse. Included in the BIO subsets (see appendix B for a complete list) were all altimeter related measurements (radar altimeter average return samples including waveform samples, return pulse parameters, timing information relating the UTC/GEOS-3 telemetry relationships, etc.), calculated parameters (satellite coordinates (ϕ,λ,h) interpolated from satellite ephemerides computed by the agencies listed in table 1.1, corresponding geoid heights based on a global gravimetric geoid by *Vincent and Marsh (1973)*, atmospheric corrections, etc.), as well as various indicators (operational status

parameters, tracker regime identification parameters, etc.).

It is pertinent to note here that the original data contain information (also retained in the BIO subsets) which represents averages of measurements in a certain time interval. Depending on the mode of transmission (low data rate or high data rate) these averages represent a "frame" value of 10 points/sec or 100 points/sec grouped into variable 2.048 sec or 3.477 sec "major frames". It is these frame averages which we shall make use of in section 5 to extract the required sea surface information.

(2) The orbits initially provided within the above altimetry records were accorded an accuracy code A in the classification by the Wallops Flight Center (WFC) - see table 1.1. It is worth noting here that for the altimetry data provided to us, the WFC orbits were derived from precise ephemerides, which was not generally the case with the data supplied by NASA to various investigators. At a later stage, a set of GEOS-3 precise ephemerides was received from the Defence Mapping Agency Aerospace Center (DMAAC) through the Earth Physics Branch, Energy, Mines and Resources Canada. This data was in the standard precise ephemeris format in the form of state vectors referenced to the NWL 9D coordinate system (*White et al, 1975*) and was of the standard precise ephemeris accuracy (1 m).

Table 1.1

Wallops Flight Center Accuracy Classification of GEOS-3 Orbits

Code	Source	Quality (rms)	Orbit Type
A	WFC	10 metres	1 Day Arc
D	WFC	3 - 10 metres	1 - 8 Rev Arc
G	NSWC	5 metres	3 Day Arc
J	NSWC	3 metres	3 Rev Arc
N	GSFC	1 - 2 metres	5 Day Arc

WFC = Wallops Flight Center
NSWC = Naval Surface Weapons Center
GSFC = Goddard Space Flight Center

(3) During the primary altimetry data acquisition period NASA tracking was supplemented by GEOS-3 Doppler tracking from 5 satellite tracking stations in Calgary, Churchill, Great Whale River, Ottawa and Fredericton. Using preprocessed GEOS-3 Doppler tracking data made available to us by BIO, along with the DMA precise ephemeris of the GEOS-3 orbits it was felt that a significant orbit improvement was to be expected from this data. For details of this investigation see Section 3.

(4) Finally, two geoids against which the results of the GEOS-3 altimetry in the Hudson Bay were to be assessed include a 20' x 20' detailed geoid computed at UNB from the GEM-10 gravity field model (*Lerch et al, 1977*) and terrestrial gravity data, and a 0°.5 x 1° geoid undulation set computed in the Geodetic Survey of Canada (GSC) from the GEM-10B gravity field model (*Lerch et al, 1978*) and terrestrial gravity. A data set of GEOS-3 derived sea surface in the Hudson Bay computed independently by DMA was also provided by GSC and used for an additional intercomparison with our altimetry results.

SECTION 2

ESTIMATION OF THE SEA SURFACE FROM SATELLITE ALTIMETRY

2.1 General Considerations

In any attempt to use a radar altimeter in acquiring geodetic data over the oceans there are various aspects which need to be considered. The altimeter measures the distance between the satellite and the instantaneous sea surface over a footprint as shown in figure 2.1. Evidently, the altimetry measurement is affected from both orbital errors and altimeter instrument biases, as well as sea variations such as tides, storm surges, wind pile ups, etc. The situation can be explained with the aid of figure 2.2a which illustrates the geometry of an individual altimetry observation. At the epoch of such an observation for which corrections to the altimetry measurement for atmospheric influences is assumed to be completed the relationship between the satellite height and the sea surface height is

$$h_s = z + A = N + z_s + A \qquad (2.1)$$

where

h_s is the satellite height above the reference ellipsoid (as derived from the satellite ephemeris);

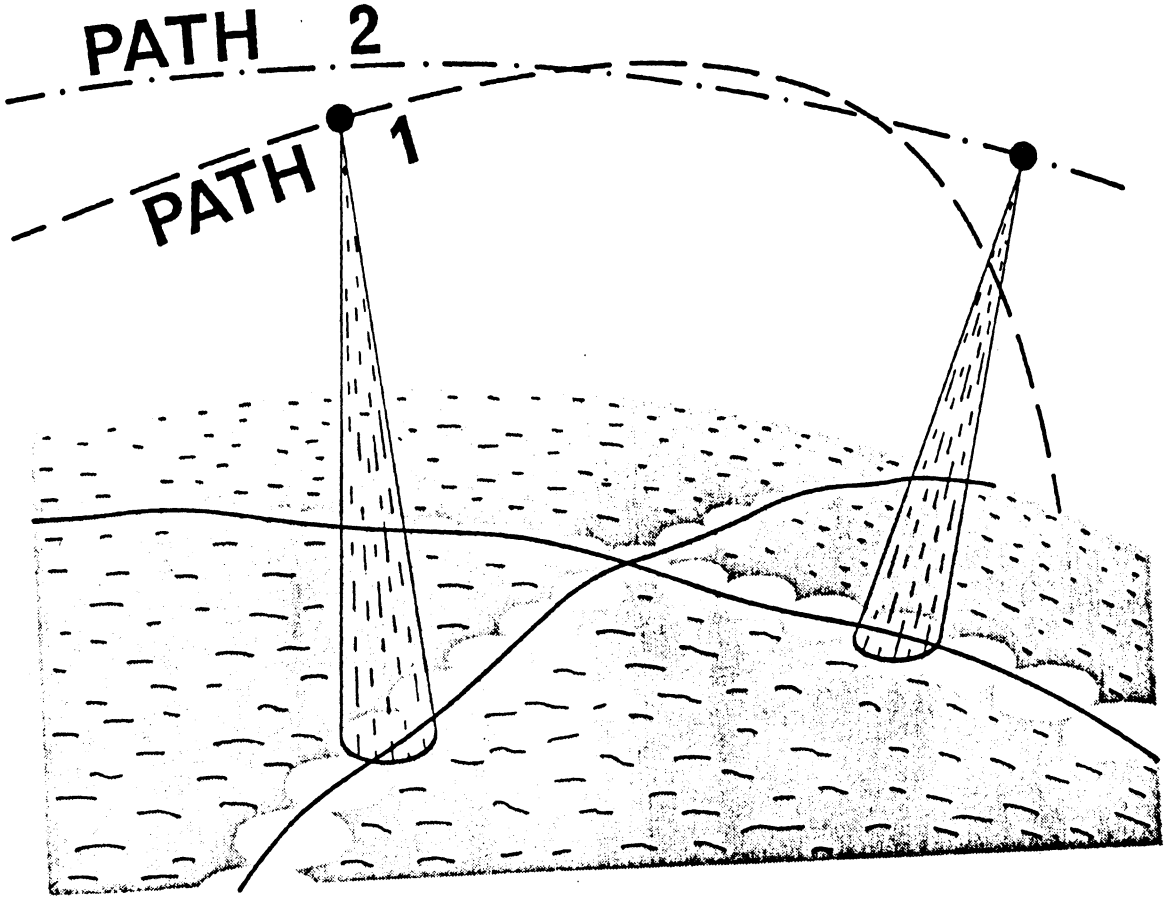

Figure 2.1 Basic Concept of Satellite Altimetry

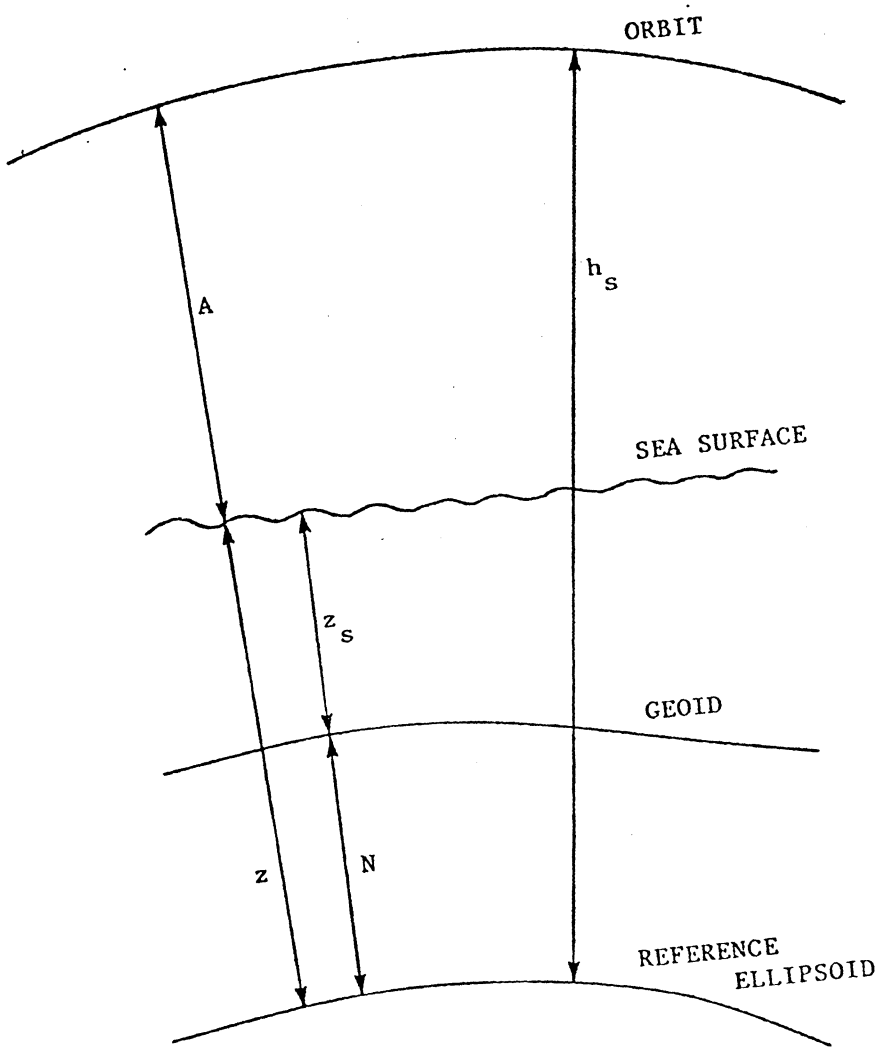

Figure 2.2a

Simplified Geometry of an Altimetry Observation

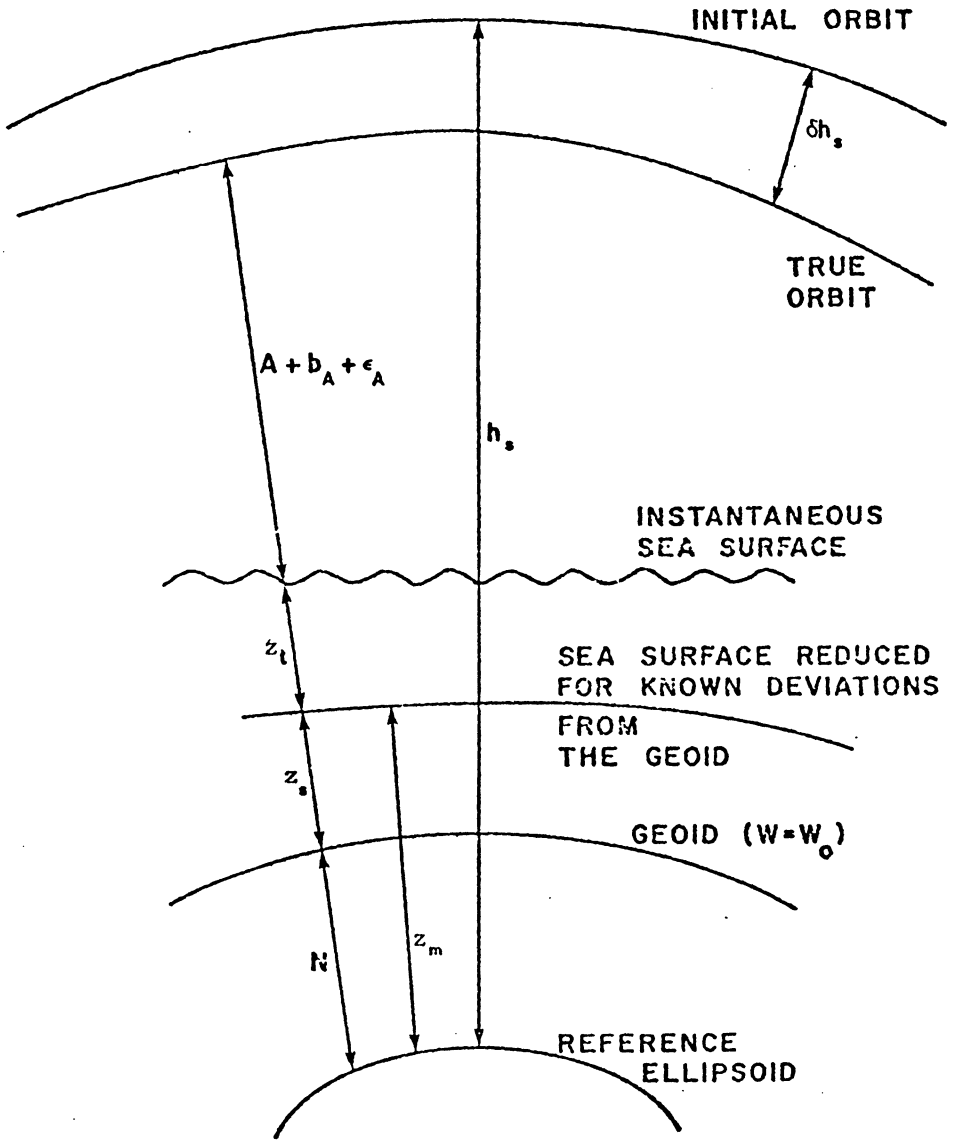

Figure 2.2b

Geometry of an Altimetry Observation

A is the altimetry measurement corrected for atmospheric influences;

z is the sea surface height (ssh) above the reference ellipsoid;

z_s is the sea surface topography, and

N is the geoid undulation.

Taking orbit error and time varying effects on the sea surface into account equation (2.1) becomes

$$(h_s - \delta h_s) = z_m + z_t + (A + \varepsilon_A + b_A) \qquad (2.2)$$

where

z_m is the time invariant part of the ssh

z_t is the time varying part of the ssh

δh_s is the orbit error

ε_A is the altimetry measurement error, and

b_A is the altimeter bias (if any).

In the context of the intended application of geoid improvement from satellite altimetry, the only quantity in (2.2) likely to be capable of modelling is the time varying term z_t. This term contains both the sea tide effect, which can be corrected for if a suitable tidal model is available, and other non-tidal time varying effects which can be accounted for by modelling, provided that relevant data (e.g. synoptic weather data) permitting such modelling is available.

The bias term b_A and δh_s may be thought of as representing the parameters of an error model s of the form

$$s = AX \qquad (2.3)$$

where A is the design matrix transforming the bias parameters into the

observation space. It is readily seen that a major task confronting any altimetry reductions is to devise a suitable parameter model for s in such a way that the sea surface height can be obtained from an adjustment whereby the obvious goal is the removal of the biases X without any loss of information about the geometry of the sea surface. In the following subsections the modelling of z_t and the development of a model for s within the context of the present study are discussed.

2.2 Modelling of the Sea-Tide Effect

Over the past two decades considerable progress has been made in the quantitative mapping of the global ocean tides. Several researchers have addressed the problem of tidal prediction by using empirical methods, that is, by means of vast numbers of tidal recordings taken at continental, island and deep-sea gauges (*Munk and Cartwright, 1976; Munk et al, 1970; Zettler et al, 1975*). Others have made use of theoretical methods based on a wealth of novel mathematical tools designed to address the problems of integration of appropriate hydrodynamic equations with theoretical and/or empirical boundary conditions (*Hendershott, 1972, 1975; Estes, 1977; Schwiderski, 1978*).

For the present study , although in each frame of the original NASA altimetry records a tidal correction coming from the *Henderschott (1972)* global tide model is supplied , it was felt that this model was inadequate for such a confined water body as the Hudson Bay. It was therefore decided to develop and use an analytical tidal model representative of the tidal regime of the Hudson Bay. Considering different possible approaches we chose to base our modelling on the work of *Freeman and Murty (1976)*. Their tidal model in its original

form is rather complex; it uses basically a linearized system of Laplace tidal equations with specific boundary conditions. For our specific purposes, the necessity to evaluate the desired tidal effect for different time instances suggested an approach similar to the one described in *Vanicek and Krakiwsky (in prep)*.

For each considered tidal frequency ω_k, corresponding to different tidal constituents M_2, S_2, N_2, etc. the tide h at an instant t can be written as

$$H(t) = \sum_k f_k H_k \cos(\omega_k t + \beta_k) \qquad (2.4)$$

where the amplitude H_k and phase β_k are obtained from cotidal charts as functions of positions alone and the node factors f_k can be obtained e.g. from *Schureman (1971)*.

To further by-pass the need of storing H_k, β_k for each point one can approximate the spatial distribution of these effects by a linear form *(Okenwa, 1978)*

$$\tilde{H}_k(x_i, y_i) = \sum_{j=0}^{J} C_j^H \psi_j(x_i, y_i) \qquad (2.5a)$$

$$\tilde{\beta}_k(x_i, y_i) = \sum_{j=0}^{J} C_j^\beta \psi_j(x_i, y_i) \qquad (2.5b)$$

with chosen base functions

$$\psi \equiv \{\psi_j = x^\ell y^m\} \quad \ell, m = 0, 1, 2, \ldots n, \quad j = 0, 1, \ldots, J$$

where J is the number of base functions, n is the degree of approximating polynomial and x_i, y_i are local orthogonal coordinates defined as

$$x_i = R_o (\phi_i - \phi_o)$$

$$y_i = R_o (\lambda_i - \lambda_o) \cos \phi_o$$

where ϕ_o, λ_o, R_o are the latitude, longitude and mean earth radius of curvature at an arbitrarily chosen local origin.

The vectors of coefficients C_j^H, C_j^β, which differ for each considered frequency, can be determined using ordinary least squares methodology (*Vanicek and Wells, 1972*) and in turn be stored in the computer for subsequent computations.

For the present study, cotidal charts for four major tidal constituents, M_2, S_2, N_2 and K_1 constructed from the Freeman-Murty model were digitized and used as input to a specially developed program to compute the coefficients vectors C_j^H, C_j^β for the four constituent frequencies. In the course of these computations it became apparent that a separate modelling of the M_2, S_2 and N_2 tide was necessary for the areas east and west of longitude 85° W. This is because, as it can be seen from figure 2.3 which illustrates the M_2 tide, the latter rotates about two major amphidromic points located in the central and east central Hudson Bay (similar behaviour is true for the S_2 and N_2 tide).

To check the efficiency of the derived coefficients amplitudes and phases were predicted along the 85° W longitude boundary, as well as on a 1° x 1° grid points. Generally agreement of the predicted values with their respective input values was within 10° in phase and 15 cm in amplitude; however, more extreme discrepancies occurred near the major amphodromic points, where, of course, any phase error

Figure 2.3

M_2 Tide in Hudson Bay

(After Freeman and Murty, 1976)

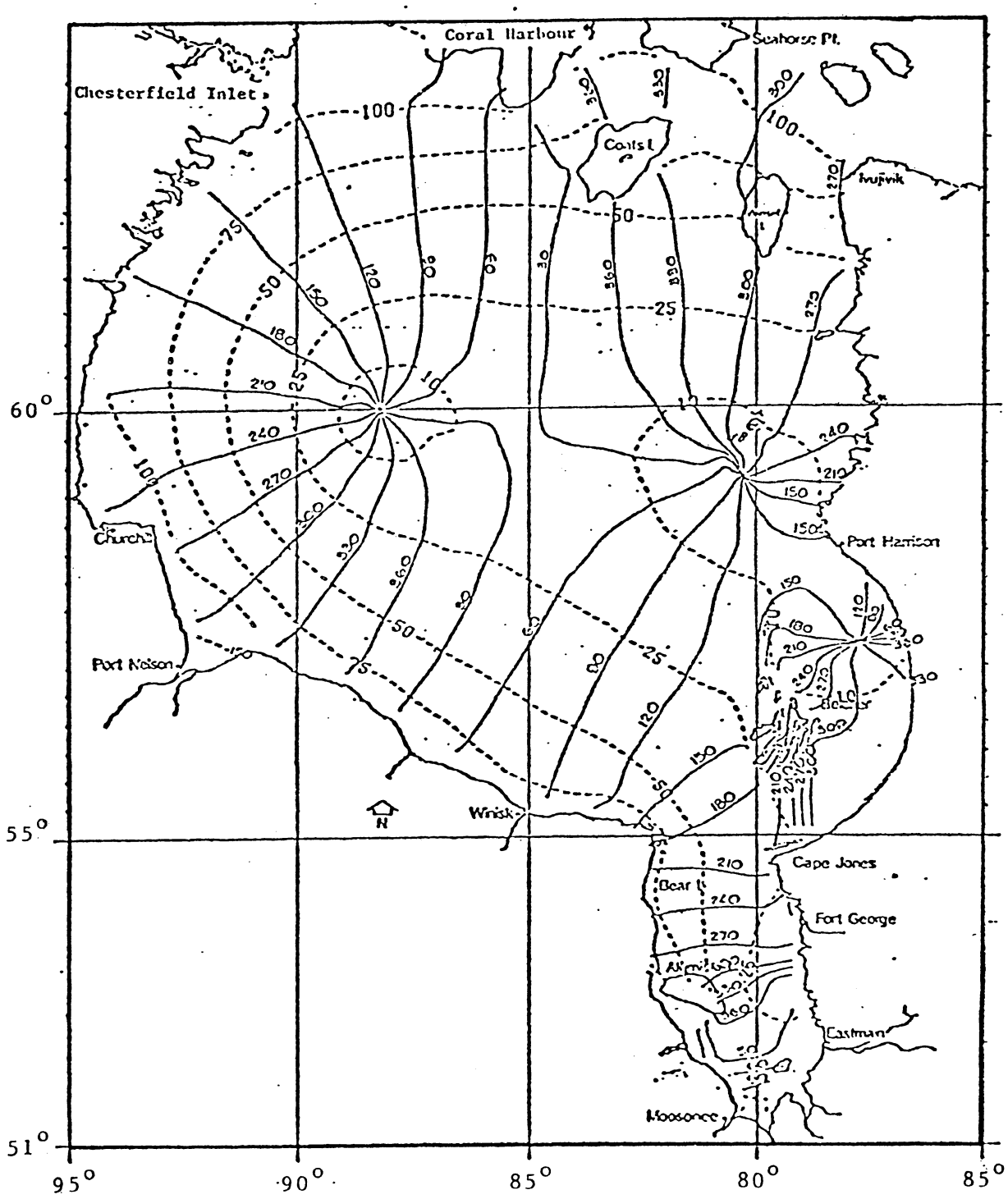

	Observed at Station*				Freeman-Murty Model*				Analytical Model			
	M_2		S_2		M_2		S_2		M_2		S_2	
STATION	H(cm)	β(°)	H(cm)	β(°)	H(cm)	β(°)	H(cm)	β(°)	H(cm)	β(°)	H(cm)	β(°)
Coral Harbour	100	358	33.7	44	105	350	40	45	116.6	349.4	40.8	45.0
Port Harrison	11	330	1.6	23	10	150	3	240	4.9	283.0	3.0	315.4
Cape Jones	64	222	20.0	281	40	210	12	285	49.2	229.9	15.5	285.6
Fort George	66	238	15.2	329	25	240	8	330	25.7	253.7	9.0	309.4
Moosonee	62	111	13.7	200	55	110	15	200	39.0	188.0	13.9	187.5
Winisk	109	83	28.6	158	110	85	28	160	102.6	83.5	27.3	168.6
Port Nelson	161	315	39.9	54	160	315	50	30	162.2	311.9	52.0	31.2
Churchill	152	239	47.0	306	145	240	48	310	125.7	236.9	43.2	309.4
Chesterfield Inlet	131	129	45.7	181	130	125	45	185	127.4	130.2	44.6	172.5

* after Freeman and Murty (1976)

Table 2.1a

Numerical Modelling of the M_2 and S_2 tide in the Hudson Bay

Comparison with Shore Station Data.

STATION	Observed at Station*				Freeman-Murty Model*				Analytical Model			
	N_2		K_1		N_2		K_1		N_2		K_1	
	H(cm)	β(°)	H(cm)	β(°)	H(cm)	β(°)	H(cm)	β(°)	H(cm)	β(°)	H(cm)	β(°)
Coral Harbour	20.8	314	7.3	144	22	325	7.5	155	22.0	324.9	9.4	151.5
Port Harrison	2.7	276	2.4	23	2	90	3.0	65	2.0	92.7	3.0	56.9
Cape Jones	20.4	191	2.3	27	8	180	2.5	60	9.6	187.7	5.0	72.4
Fort George	10.2	211	5.7	116	5	220	3.5	190	7.9	181.4	3.1	75.3
Moosonee	11.3	68	12.2	171	12	70	9.0	180	12.0	69.8	8.1	175.6
Winisk	19.2	45	5.0	322	18	50	6.5	345	18.0	50.2	7.8	302.7
Port Nelson	27.1	202			30	285			30.0	285.0		
Churchill	31.5	212			30	215			24.4	210.6		
Chesterfield Inlet	27.4	96			22	100			20.4	94.3		

Table 2.1b

Numerical Modelling of the N_2 and K_1 Tide in the Hudson Bay

Comparison with Shore Station Data

is acceptable, and in the vicinity of the degenerate amphidromic point in James Bay and the Belcher Islands where the amplitudes are very small. For comparative purposes tables 2.1a and 2.1b give the Freeman-Murthy and our analytical model results for the four tidal constituents as compared with observations from a number of shore based stations. In view of these results it was decided to use the derived set of coefficients C_j^H, C_j^β to compute the tidal effect and correct the altimetry data we had available in our altimetry data base.

2.3 On the Modelling on Non-Tidal Physical Influence on the Sea Surface

Although the sea tide effect can be a dominant term in z_t, the time varying part of the ssh's, other non-tidal varying effects including periodic and secular variations in the sea level are to be expected to contaminate the altimetry data. A further direct oceanographic factor affecting sea level in high latitudes, such as in the Hudson Bay region, is the damping influence of sea-ice upon the vertical movement of the water surface. In the present case, a study of ice condition maps produced by the Atmospheric Environment Service revealed no data overlap, with the exception of three altimetry passes, with the period of ice formations in Hudson Bay. We therefore did not concern ourselves with the influences of such effects in the present study. Nevertheless a few of the crossover points (cf. section 2.5) involving these passes, which showed gross ssh differences probably due to altimeter lock-on loss or ice accumulation, were easily detected by our pre-adjustment editing

process (cf. section 5.1) and eliminated from the computation of the mean sea surface.

An established technique for modelling some of the known physical influences on the sea level has been set out by *Vanicek (1978)*. *Anderson (1978)* has extended this approach into what might be referred to as a multiple linear regression analysis whereby a linear model based on air/water temperatures, atmospheric pressure and geostrophic wind velocities is used to portray the physical influences on the sea level.

In the context of the present study, despite the attention given to the subject, especially in view of the much suspected effect of storm surges and of piling-up water due to wind stress, which is most apparent in shallow water bodies and in the presence of land barriers such as is the case with the Hudson Bay, the lack of any relevant data precluded any attempt in modelling these effects. Discussion with BIO personnel (*Wells, personal communication*) postulated levels of these variations below the 1 m level. From available time series of barometric records $\{P_i, t_i\}$, taken at Churchill and Great Whale River (see figure 3.2) approximately every four hours during the GEOS-3 Doppler campaign, a maximum change of the order of 25 mbar was noted, i.e.

$$\delta P(t_i) = P(t_i) - \text{mean } (P) \leq 25 \text{ mbar.}$$

Taking for instance Vanicek's (1978) pressure coefficient of dependence to be in the range of -0.5 to -0.2 cm/mbar, such a change in atmospheric pressure would imply a sea level variation to be expected between 13 cm to 50 cm, which lends credence to the above postulated level. Because

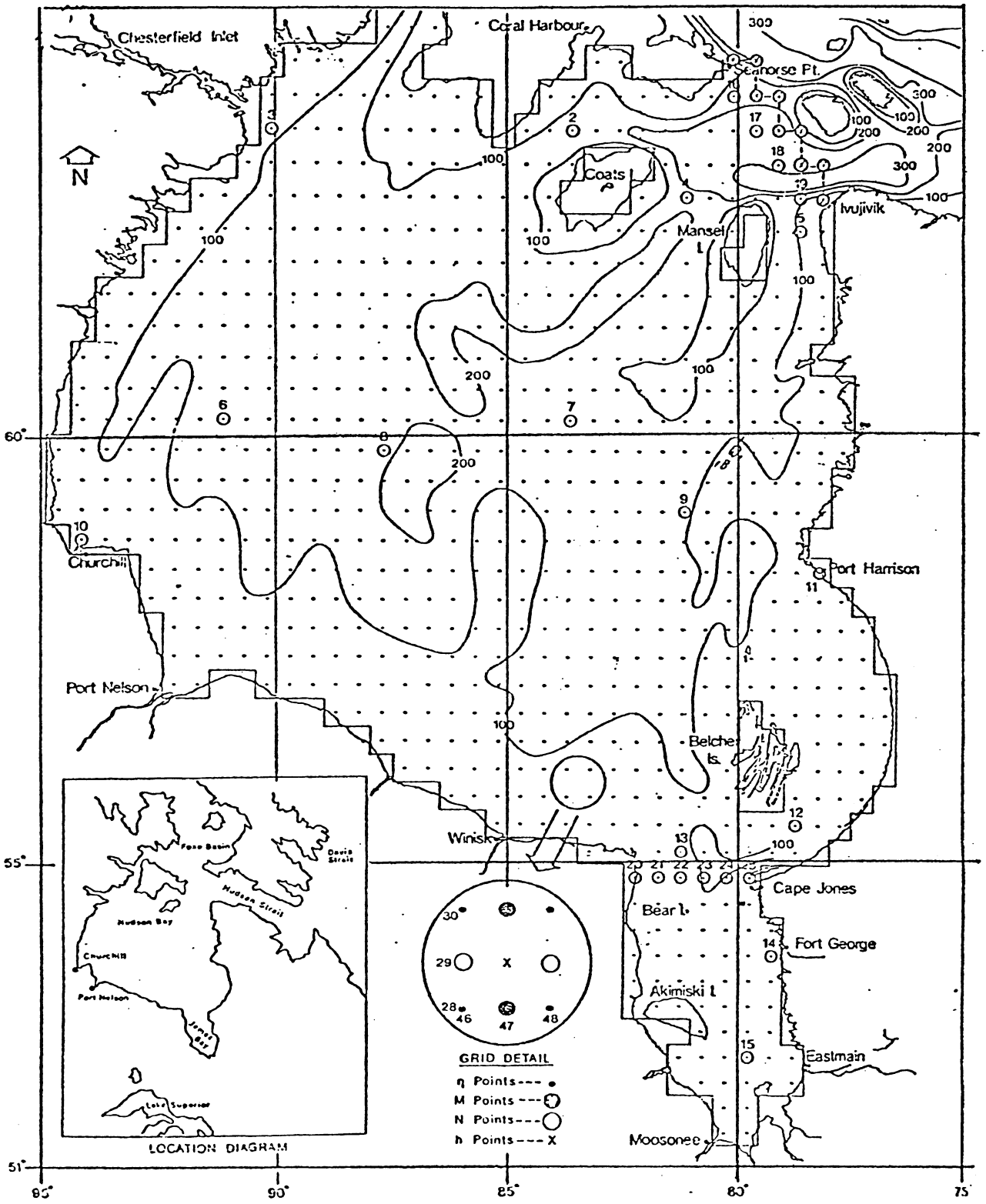

Figure 2.4 - Bathymetry in Hudson Bay (contours in m)

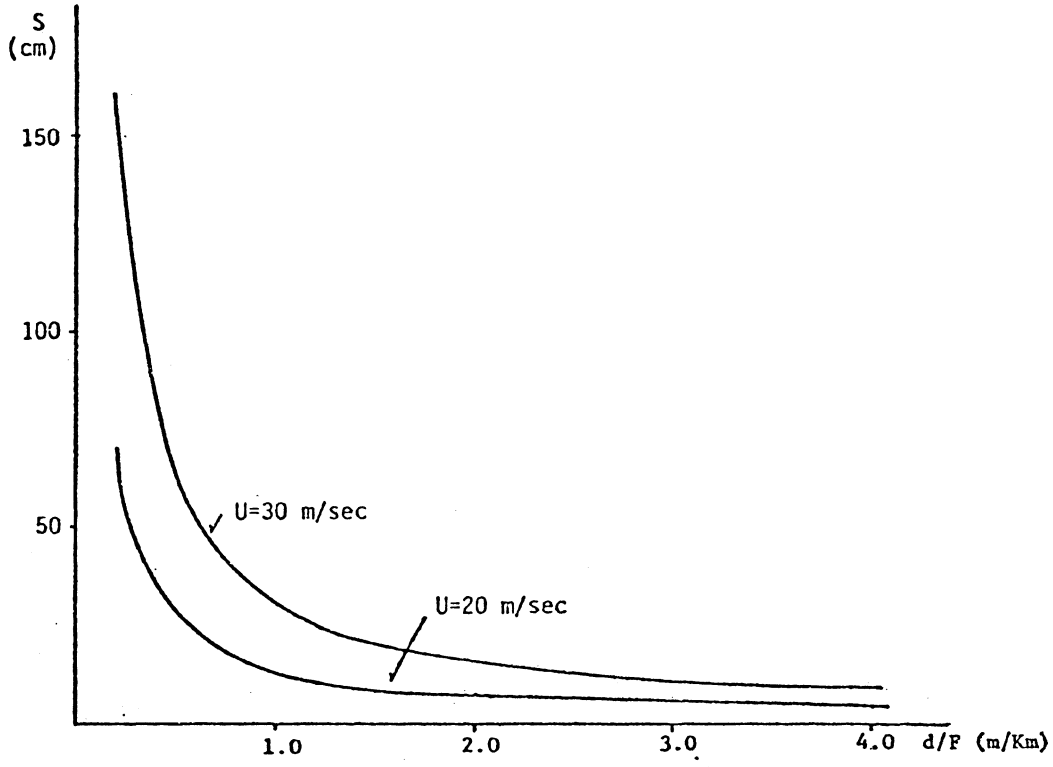

Figure 2.5 Wind pile-up effect as a function of the depth-to-fetch ratio

of certain correlation between pressure and wind effects, the variation can be expected somewhat larger under adverse wind conditions. The sea level response to the wind stress effect can be estimated from the fundamental equation of wind set-up (*Miller, 1958; Wilson, 1960; Hamon, 1966*)

$$\frac{S}{L} \simeq k \cdot \frac{U^2}{gd}$$

where S is the pile-up of water induced by a steady wind velocity U over a fetch L of water of depth d, g is the acceleration of gravity and k is a coefficient of the order of $3.3 \cdot 10^{-6}$ (*Wilson, 1960*). From the bethymetry of the Hudson Bay (see figure 2.4) and figure 2.5 which indicates the relation between the maximum pile-up and the depth-to-fetch ratio for wind velocities 20 m/sec and 30 m/sec, it is evident that except near the coastline where shallow and more limited fetches can prevail the sea surface variation to be expected due to wind stress is unlikely to exceed 50 cm. *Forrester (1980)* for instance has found under similar wind conditions in Lake Ontario water transfers due to wind of the order of 10 cm. In view of this evidence we therefore abandoned for this investigation any attempt to model these influences choosing instead to treat their effect as noise to the altimetry measurements.

2.4 Altimetry Bias Removal

Sea surface heights as obtained from altimetry measurements and corrected for sea tide effects are still contaminated by altimeter instrument bias and residual orbit errors mainly due to the shortcomings of the adopted geopotential model used in the orbit integration.

The GEOS-3 altimeter bias has been widely discussed in the literature. There is a general agreement that the altimeter reads too

short by about 1 to 4 metres. The calibration value by *Martin and Butler (1977)* has been verified for the Western Atlantic region by a number of investigators (e.g. *Eisner, 1979*), but a global analysis of GEOS-3 passes seems to suggest a value that is in disagreement by 1 - 2 meters (*Pisacane et al, 1978*). In view of this uncertainty, in our investigation we chose, instead of assuming a constant bias which could be added to all altimetry measurements, to solve for the bias together with the orbital errors affecting the reduction of the altimetry data.

2.5 Orbit Error Modelling

There are several approaches leading to the parameterization and removal of the orbital biases affecting the altimetry data. *Rummel and Rapp (1977)* and *Rapp (1978, 1979)* have fitted the altimetry data to low order geoids using only one or two free parameters to describe the altimetry biases. *Hadgigeorge and Trotter (1978)* and *Blaha (1977a)* have been successful in solving for the state vectors of short arc orbits simultaneously with the solution of the oceanic geoid. *Blaha (1975, 1977b)* has derived a technique for combining altimetry data with gravimetry and spherical harmonic potential coefficients in uniform reductions.

In the context of present study, an approach used by numerous investigators to remove discrepancies from the altimetry data banks appears more expedient. Over short time periods, as it is the case with the altimetry arcs over the Hudson Bay, the orbit error along with the altimetry bias (if any) can be modelled as a polynomial in time t, such as

$$s = a_0 + a_1 t + a_2 t^2 + \ldots ,$$

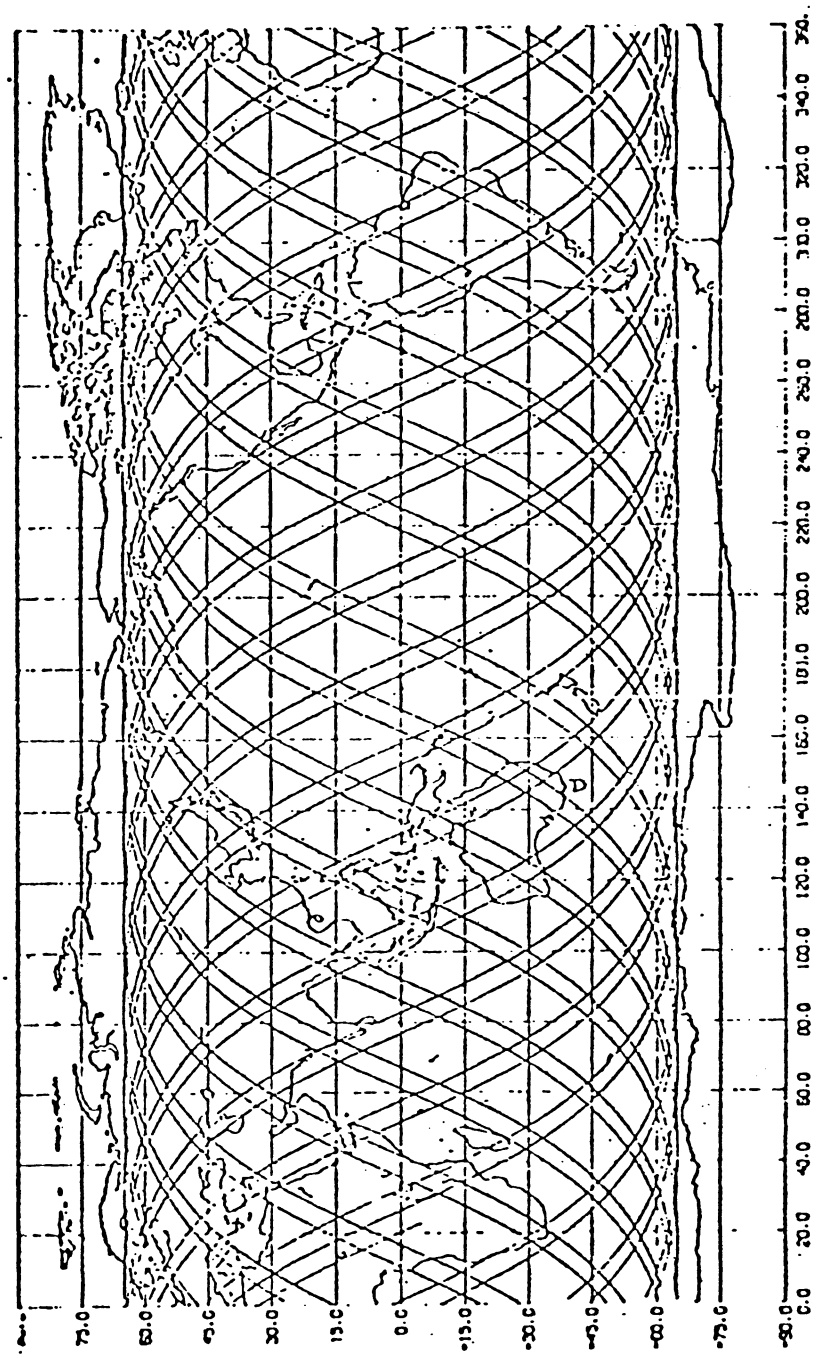

Figure 2.6 GEOS-3 Two Day Arc Ground Track

and corrections can be estimated so that the data have the best rms agreement at the crossing points of intersecting orbital arcs. By imposing intersection constraints we really assume the time invariance of the sea surface (incorrectly) and the adjustment of the regional network of orbital arcs can successfully remove the orbit errors without any loss of information about the geometry of the sea surface only if the orbit errors are assumed random from one satellite pass to the next. The extent to which these errors can be reduced in this manner depends very much on the orbital characteristics of the GEOS-3 satellite. GEOS-3 ground tracks trace out a n° x n° grid every ≈ 25/n days. This is illustrated in figure 2.6 which shows the pattern of GEOS-3 ground track for a two day arc. It can be deduced from this figure that in the case of long arcs orbital errors exhibit periods of one half revolution, one revolution and fourteen revolutions in addition to a resonance effect with a period of approximately 5 days and linear drifts with time (*Mather et al, 1978*). Since over a limited area orbital errors are expected to have predominately a once per revolution type of variation, a low order polynomial should serve as a satisfactory model for short arcs.

The principal difficulty in reducing these errors by means of intersection analyses seems to be an undesirably long (~500 km) correlation distance of the radial errors in the east-west direction between arcs (*Anderle, 1977*). This is a factor limiting the usefulness of densely spaced altimetry tracks in these intersection analyses, since the 500 km correlation distance implies that neighbouring orbital

arcs have nearly identical errors due to unmodelled gravity field errors in the orbit integration, which might not be detected in the intersection analysis, or might not be reduced at the rate of the reciprocal square root of the number of arcs as one would expect for random errors. *Anderle's and Hosking's (1977)* suggestion of investigating the use of a high degree function expressing the bias prompted us to model the errors for each orbital arc as absolute bias, a tilt and a second order effect (bend) which would perhaps allow a more expedient way of removing the bias.

SECTION 3

GEOS-3 ORBIT IMPROVEMENT FROM LOCAL DOPPLER TRACKING

This section deals with the treatment of GEOS-3 Doppler data from five tracking stations in the vicinity of Hudson Bay with regard to the intended local improvement of the orbits required to utilize the altimetry data. Preprocessing to correct the station time scales is described in section 3.2. Section 3.3 deals with the multistation processing required to obtain the orbit biases for the short arcs in the Hudson Bay. This discussion is developed beginning with the basic methodology considerations (section 3.1) upon which the computation of the results rests.

3.1 Methodology Considerations

As has already been pointed out, the level of orbit determination capability is a major limiting factor posed on satellite altimetry reductions. In the context of the Hudson Bay Experiment a GEOS-3 Doppler campaign conducted simultaneously with the altimetry data acquisition had resulted in a considerable amount of GEOS-3 Doppler tracking data having been collected which would promise a significant orbit improvement.

Results of previous TRANSIT network analyses in the Geodetic Survey of Canada and UNB have demonstrated that over a limited area, residual

orbit biases in a reasonably accurate orbit (e.g. the one described by a satellite ephemeris covering the data span in question) can be determined by using short spans of Doppler data in an orbit fit such as in

(i) the short arc (*Brown, 1976*),

(ii) semi short-arc (*Kouba and Wells, 1976*) or

(iii) translocation modes of computation (*Wells, 1976b*)

Loosely stated the differences between these various classes of computational modes result from two major aspects, namely the modelling of ephemeris errors with the a priori ephemeris given six degrees of freedom (short-arc methods) or less (semi short-arc methods), and the simultaneity of receiver operation (translocation modes).

In view of the long Canadian experience in processing Doppler satellite data, the approach at (ii) above currently being used in Canada as described e.g. in *Kouba (1974, 1979)* and *Kouba and Wells (1976)* naturally suggested itself as the most obvious choice for the present study. In short, in this approach orbital constraints are imposed by fitting a satellite trajectory to one pass of data at a time and allowing the orbit to relax parallel to itself. The orbit is kept parallel as a consequence of the Guier's theorem (*Guier, 1965*) underlying the two basic principles of Doppler satellite positioning that

- when the error in the satellite trajectory is small, the actual and estimated (from a satellite ephemeris) trajectories are nearly parallel; and that
- in a set of satellite Doppler observations from a single pass, the time of closest approach (i.e. the time t_{ca} at which the slope of the

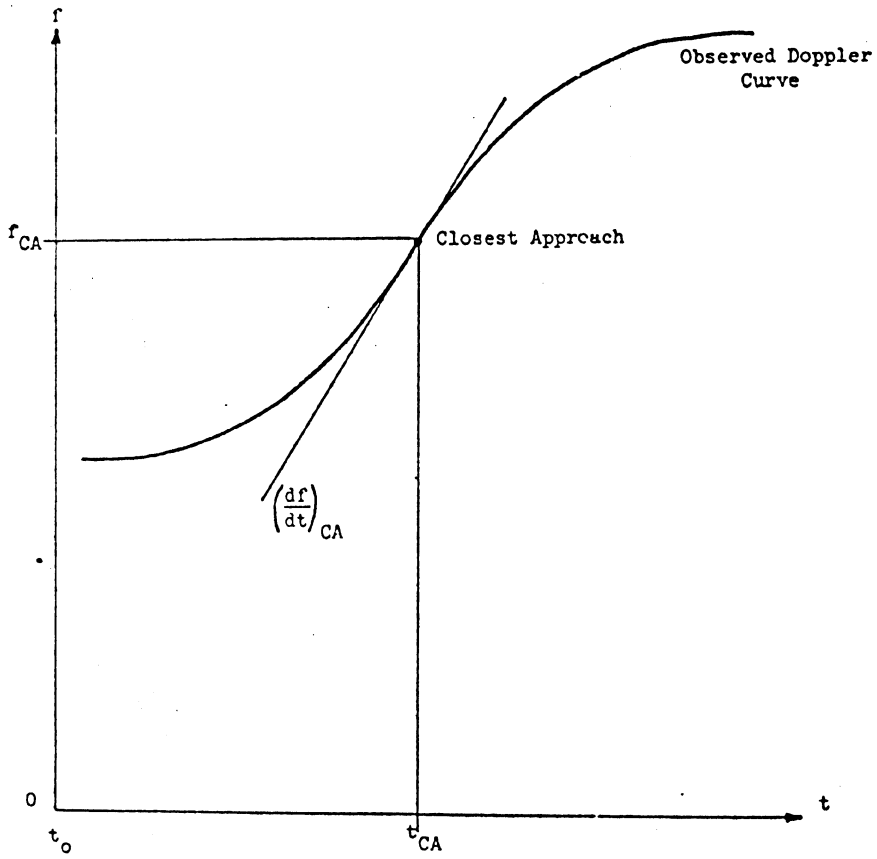

Figure 3.1a

Parameters describing a Doppler Curve

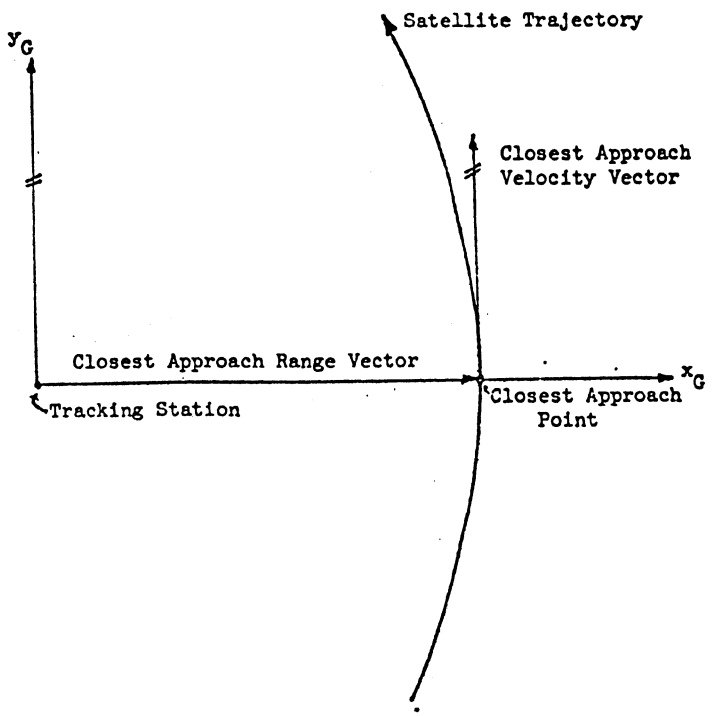

Figure 3.1b

Guier Plane Geometry

Doppler curve is maximum, cf. figure 3.1a), the receiver to satellite range at closest approach (related to the maximum value of the slope of the Doppler curve), and the frequency offset between the satellite and receiver oscillators (related to the Doppler frequency f_{ca} at maximum slope) are the most representative parameters describing the information content of these observations.

By adjusting the satellite position at closest approach in the plane defined by the closest approach range and velocity vector (Guier plane, cf. figure 3.1b), Doppler residuals can be reduced to their noise level thus making the Guier plane the optimum coordinate system in which to examine both orbit errors and measurement noise (*Wells, 1974*) - other alternative approaches such as editing in the plane of least movement (*Hetch, 1976*) also exist, which however are almost equivalent to Guier plane navigation except perhaps somewhat easier to implement in a minicomputer. Doing so essentially amounts to performing parallel translations of the satellite trajectory in the range (X_G) and along-track (Y_G) directions respectively. While the orbit is kept parallel, its orientation is determined exclusively from the available satellite ephemerides, whereas its shape is well approximated by a continuous function through the use of simple base functions (*Hatch, 1976; Nesbo and Ekmann, 1977*)

$$\Phi = \{1, \sin nt, \cos nt\} \quad , \qquad (3.1)$$

where n is the mean satellite motion and t is time, without being subject to any subsequent adjustment during the data reduction. However, the location of the orbit is determined from the data as a differential translation, the components of which are modelled as biases in the along-track, across-track and out-of-plane directions.

By using essentially the same procedure it was felt that it would be possible to improve GEOS-3 satellite ephemerides in two main steps: first, by recovering possible station uncertainties using all available short arc Doppler passes over the area; then by recovering the orbit biases for each arc in a multistation solution whereby the tracking station locations (eventually assumed known to accuracy better than that of potential data biases) are constrained to the previously determined coordinates.

3.2 Preprocessing to correct Station Time Scales

The GEOS-3 Doppler data we had initially received had already been preprocessed mainly to correct synchronization to UTC (*Kouba, 1978*). This was necessary because GEOS-3 Doppler tracking data from the stations at Churchill, Great Whale River and Fredericton (see Figure 3.2) had been acquired using CMA 725 geodetic receivers operating in conjunction with CMA 722B receivers (run from the CMA 722 oscillator), in which case synchronization to UTC was provided by the NNSS (TRANSIT) time marks (at even minute times) as recognized by the CMA 722B receivers. Although the synchronization procedure was performed during the experiment typically once a day, further corrections for propagation delays, NNSS satellite clock errors and receiver delays (of the CMA 722B) were necessary. The initial preprocessing which had been carried out was intended.

a. to compute propagation delays and frequency offsets using synchronization passes of NNSS data;
b. to compute predicted propagation delays in case the NNSS data was missing; and

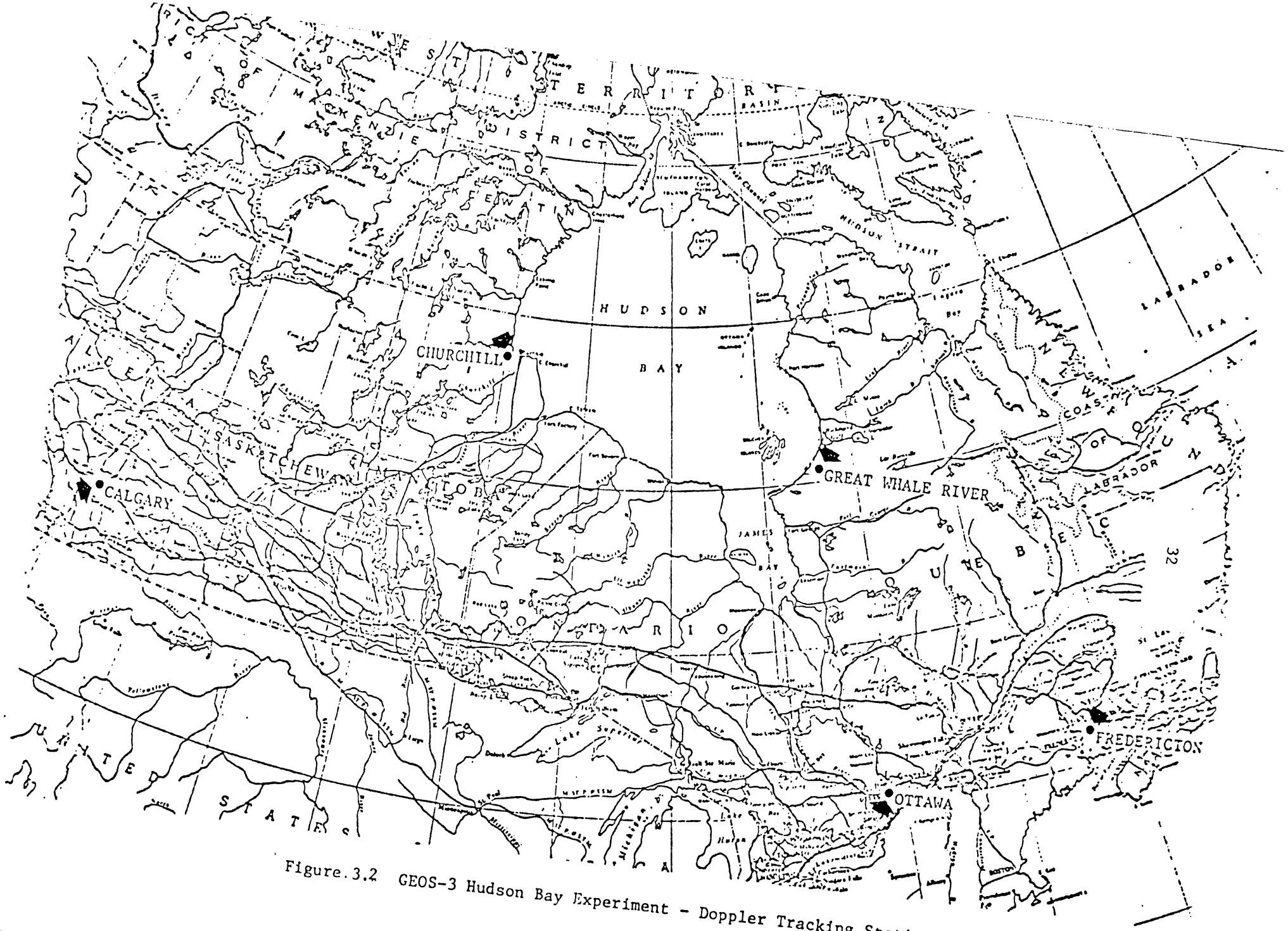

Figure 3.2 GEOS-3 Hudson Bay Experiment - Doppler Tracking Stations

c. to match computed or predicted delays and meteorological data with CMA 725 GEOS-3 Doppler data and transform the CMA 725 format to GEOCEIVER format.

For each NNSS synchronization pass which successfully passed the usual PREDOP-GEODOP screening (*Lawnikanis, 1975a; Kouba and Boal, 1975*), satellite clock errors and frequency offsets were interpolated at the synchronization time t_s using the information published regularly in the USNO TRANSIT satellite reports (Series 17) and propagation delays were computed. As a next step, a second order approximating polynomial of the form

$$\Delta f(t) = \Delta f(t_o) + a_1(t-t_o) + a_2(t-t_o)^2 \qquad (3.2)$$

where

t denotes time in days,

t_o is the synchronization day, and

Δf is the frequency offset scaled to the nominal 400 MHz,

was chosen for each station to describe the original frequency history of the receiver oscillators for the entire data aquisition period. The numerical values $\Delta f(t_o)$, t_o , and a_1 , a_2 for each station were computed as listed in table 3.1.

Table 3.1

Polynomial Approximation Parameters
for Frequency Offsets at Doppler Tracking Stations

STATION	$\Delta f(t_o)$ Hz	to Day	a_1 Hz/day	a_2 Hz/day^2
100 Churchill, Man.	-6.28	248	0.0016	$-0.2600.10^{-4}$
200 Great Whale River, Que.	-1.90	249	0.0340	$-0.1100.10^{-3}$
300 Fredericton, N.B.	0.96	249	0.0300	$-0.1125.10^{-3}$

The times t recorded by the CMA 725 receivers were then corrected for propagation delay (at the synchronization time t_s), satellite clock errors and frequency offsets in the following manner

$$\tau = t - \Delta t_s - \Delta t_p(t_s) - \Delta f(t_m) \cdot 400 \cdot 10^{-6} - \Delta t \qquad (3.3)$$

where

τ .... corrected UTC time epochs,

Δt_s .... interpolated satellite clock error at t_s

Δt_p .... propagation delay at t_s (either computed or predicted)

Δf .... clock rate due to frequency offset evaluated at epoch $t_m = (t+t_s)/2$

Δt .... receiver delay taken (according to manufacturer's supplied values) as 700 μsec for stations 100 and 200, and 600 μsec for station 300.

In turn, recorded GEOS-3 Doppler counts (corrected for ionospheric refraction effects) were corrected for frequency offset Δf to obtain

$$D^c_{\tau_i\tau_j} = D^r_{\tau_i\tau_j} - \Delta f\left(\frac{\tau_i+\tau_j}{2}\right) \cdot \frac{324}{400} \cdot (\tau_j - \tau_i) \qquad (3.4)$$

where $\tau_j - \tau_i$ is nearly 30 sec and D^c is used to distinguish the corrected Doppler counts from their recorded counterparts D^r. For a full discussion of these computations together with a detailed account of the results *Kouba (1978)* should be consulted. Here it will suffice to note that following this preprocessing the time scales of the three receivers were considered to be within 100 μsec relative to each other and with respect to UTC, which agrees with the requirements set by *NASA (1972b)*; timing errors from synchronization to sychronization

were considered to be less than 90 μsec for computed delays and up to 215 μsec for predicted delays, whereas the actual frequency was considered to be well approximated at each station by the fitted polynomial (3.2) to within 5 parts in 10^{10} which corresponds to a station receiver drift to about 50 μsec/day.

3.3 GEOS-3 Doppler Solutions

The final GEOS-3 Doppler reductions were made possible by making use of computer time and software kindly made available to us by GSC. Using a new version of the GEODOP software package (*Kouba and Boal, 1975; Kouba, 1979*) after latest modifications by *Kouba (Nov. 1979, Personal communication)* to handle some problematic Doppler data from Churchill, Great Whale River and Fredericton we were able to carry out 3 multistation solutions with the purpose of recovering a portion of the GEOS-3 orbit biases. The new GEODOP version, utilizes a number of new developments in Doppler satellite software (*Kouba, 1979*) which include.

- an improved orbit presentation by a 9th order Tchebychev polynomial fit to the precise ephemeris;
- a complete orbit orbit error model for six orbital biases (corrections to Keplerian elements);
- an improved tropospheric refraction model with a ray bending correction according to *Black (1978)*; and
- an additional station bias for short term receiver frequency drift.

The actual computations were subdivided into three time spans: day 246-280, 281-310, and 311-346, 1976. Since GEOS-3 Doppler

data was available consistently, their distribution in time posed no constraints in selecting these intervals. However, severe problems with the Doppler data from the Calgary station limited our ability to achieve the desired optimum station configuration which would promise a strong solution as it has been shown by extensive simulations at UNB (*Nesbo, 1976a*) prior to the Doppler campaign.

3.3.1 Summary of Assumptions and Decisions

With only four remaining stations participating in our solutions we proceeded to recover the orbit biases for each satellite pass. The decisions relevant to these computations were:

(a) to compute, for each time span, the position vector for each tracking station using the precise ephemeris and all GEOS-3 Doppler data at this stations the NNSS station coordinates available for each station were used as initial coordinates in these computations (Table 3-2);
(b) to combine into one multistation solution for each time span all data from each station (after data rejections resulting from the Guier navigations at each station); station positions of the Doppler sites were held to their previously determined values (mean position from the three time spans) by being subject to weighted constraints with standard deviations of 0.5 metres assigned to all three coordinates;
(c) in combining the data from all stations the orbit was relaxed by translocating between all pairs of stations and merging the results of all translocations into one multistation solution;
(d) the orbit parameters (Keplerian elements derived from the precise ephemeris state vectors) were assumed to be subject to a priori weighted constraints with standard deviations of 5.0 metres.

3.3.2 Multistation Processing Results for Orbit Biases

Corrections to the adopted station positions (cf. table 3.2) were obtained from each multistation solution as shown in table 3.3. Table 3.4 gives an insight into the results obtained for the weekly span of days 311-317, 1976 from the recovery of orbital biases for each pass, where a conversion to distance has been made to each Kepler element to allow for easier comparison.

The results for the semi-major axis δa, the eccentricity δe, and the eccentric anomaly δE (and hence the mean anomaly δM) errors, which predominantly affect the satellite height, have been combined into the satellite height error δh using the relationship between the appropriate Keplerian elements (*Kozai, 1959*):

$$\frac{\delta r}{a} = \frac{e}{\sqrt{1-e^2}} \sin f \, \delta M + \frac{r}{a} \cdot \frac{\delta a}{a} - \cos f \, \delta E \qquad (3.5)$$

and assuming that small periodic pertubations δr in the satellite radius vector r will be directly absorbed into the satellite height, i.e. by taking

$$\delta h \doteq \delta r \quad .$$

All terms have already been defined except f which denotes the true anomaly. In turn δa, δe, δE, and δh have been plotted and shown in figures 3.3a to 3.3d.

With the understanding that these errors provide only a partial indication of the extent of orbit improvement gained by the utilization of the Doppler tracking data we proceeded to generate a

TABLE 3.2

Initial Coordinates of GEOS-3 Doppler

Tracking Stations in Hudson Bay

	Station	ϕ			λ			H(m)	X(m)	Y(m)	Z(m)
028	Ottawa, Ont.	45°	23'	39".034	284°	17'	10".501	50.6	1107130	-4347803	4518259
100	Churchill, Man.	58	45	32.837	265	54	40.754	-21.7	-236436	-3307616	5430056
200	Great Whale River, Que.	55	16	52.280	282	14	52.370	-21.4	772386	-3558029	5219264
300	Fredericton N.B.	45	57	0.680	293	21	29.086	50.6	1761274	-4078248	4561416

Ref. Ellipsoid: a = 6378145 m, f = 1/298.255

A priori variances: $\sigma_X^2 = \sigma_Y^2 = \sigma_Z^2 = 0.5^2$ metres^2

TABLE 3.3

GEOS-3 Doppler Multistation Results

Periods Day 246-280, 281-310, 311-346, 1976

Station	# of passes	# Dopplers	Δx(m)	Δy(m)	Δz(m)
028	52	584	-0.14	-0.07	0.41
	16	117	-0.99	-2.32	-0.16
	2	17	0.47	-0.58	0.35
100	132	2384	0.44	-0.14	-0.38
	117	2192	-3.25	-1.00	-0.70
	187	3485	-2.60	-1.68	-1.41
200	190	2984	-1.21	0.26	-0.85
	167	2522	-0.63	1.53	2.20
	206	3173	-0.02	1.22	1.75
300	196	3390	0.30	0.18	0.23
	169	2837	-0.89	0.42	-0.64
	199	3348	-1.13	-0.66	-0.18

Table 3.4

GEOS-3 Orbit Determination Results

Days 311-317, 1976

DAY	Time h	Time m	δa (m)	$R_o\delta E$ (m)	$R_o\delta i$ (m)	$R_o\delta\Omega$ (m)	$R_o\delta\omega$ (m)	$R_o\delta e$ (m)	δh (m)
311	18	18	4.4	2.3	-3.5	5.6	5.2	2.5	2.21
	19	57	-0.2	-2.0	3.9	-4.3	-2.7	-0.2	-0.04
	21	35	-0.9	1.5	2.7	-2.1	2.2	-0.1	-0.85
	23	13	-4.3	10.1	7.9	-5.9	-1.8	-3.6	-0.81
312	0	52	-0.1	-0.4	-0.3	-0.4	0.5	0.8	-0.93
	2	32	1.7	2.0	2.7	-1.9	-1.7	4.5	-2.79
	16	25	1.9	9.4	-2.3	-4.6	-0.4	-0.5	2.35
	18	4	1.5	5.4	-2.9	-1.4	3.3	-0.2	1.63
	19	43	-2.0	-8.6	0.1	5.0	2.1	1.4	-3.28
	21	21	-0.7	-10.3	3.4	3.4	1.3	-1.8	0.93
	22	59	-2.5	-0.7	-1.0	-1.5	10.0	2.7	-5.13
313	0	37	1.5	-1.5	0.8	-2.4	-0.1	2.9	-1.43
	2	17	3.3	-2.2	3.4	-0.1	-1.2	4.9	-1.57
	16	11	-2.1	-5.2	-4.5	-3.2	-0.2	4.0	-5.20
	17	49	-2.0	-2.7	-2.3	5.7	2.1	2.7	-4.43
	19	28	7.0	-0.5	-1.0	8.8	10.6	-0.7	7.71
	21	7	1.2	-5.8	-3.0	3.1	-1.8	-5.5	6.39
	22	45	-1.8	-5.8	0.0	1.9	0.7	-3.5	1.51
314	0	23	-6.6	-3.1	1.1	3.3	-7.4	-1.4	-5.22
	2	2	2.2	-6.3	0.2	2.1	1.3	1.4	1.15
	15	57	-0.1	3.0	-2.2	-4.5	-2.4	6.4	-4.74
	17	35	2.8	14.7	0.8	1.7	1.7	2.8	0.39
	19	14	-5.9	-1.3	3.9	-6.7	-6.1	0.8	-6.58
	20	52	-1.0	2.4	1.4	-1.4	0.4	0.3	-1.29
	22	30	-0.6	6.9	4.9	-5.8	-4.3	-6.7	5.75
315	0	8	-2.3	5.2	4.1	-6.8	-0.3	-3.3	0.94
	1	48	0.9	2.6	0.5	-0.5	-2.5	-0.2	1.08
	3	29	-0.4	0.2	-1.7	-1.8	-1.9	2.0	-1.82
	17	21	3.2	11.0	5.1	1.1	-0.3	0.6	2.65
	18	59	1.1	4.9	-1.2	1.9	3.6	2.6	-1.29
	20	38	1.6	4.8	0.9	-0.9	2.1	-0.9	2.41
	22	16	-1.2	4.2	3.4	-3.6	-2.3	-3.7	2.32
	23	54	1.3	2.1	5.3	-3.3	-0.6	-4.4	3.03
316	1	33	-2.9	6.9	1.6	-0.8	-2.1	0.0	2.88
	17	6	0.6	1.4	2.0	1.1	2.5	4.5	-3.21
	18	45	3.5	3.1	-5.4	14.2	5.1	3.9	-0.07
	20	24	0.1	-1.5	-1.3	1.2	1.4	1.3	-1.13
	22	2	-2.7	-4.7	0.1	1.9	-2.8	-0.6	-2.09
	23	40	-5.6	9.5	-1.3	-2.7	-6.8	-2.0	-3.73
317	1	18	0.0	6.1	1.1	-7.5	-2.6	0.5	-0.44
	16	52	-1.8	3.8	-0.8	-0.9	2.0	2.0	-2.34
	18	31	-2.4	-6.8	10.1	-8.9	3.2	-3.5	0.66
	20	9	-5.1	-3.4	2.9	-1.2	2.6	-1.0	-4.21
	23	26	6.6	4.3	0.8	-5.9	22.8	1.5	5.20

$R_o \simeq$ satellite radius r, used for scale only

Figure 3.3a

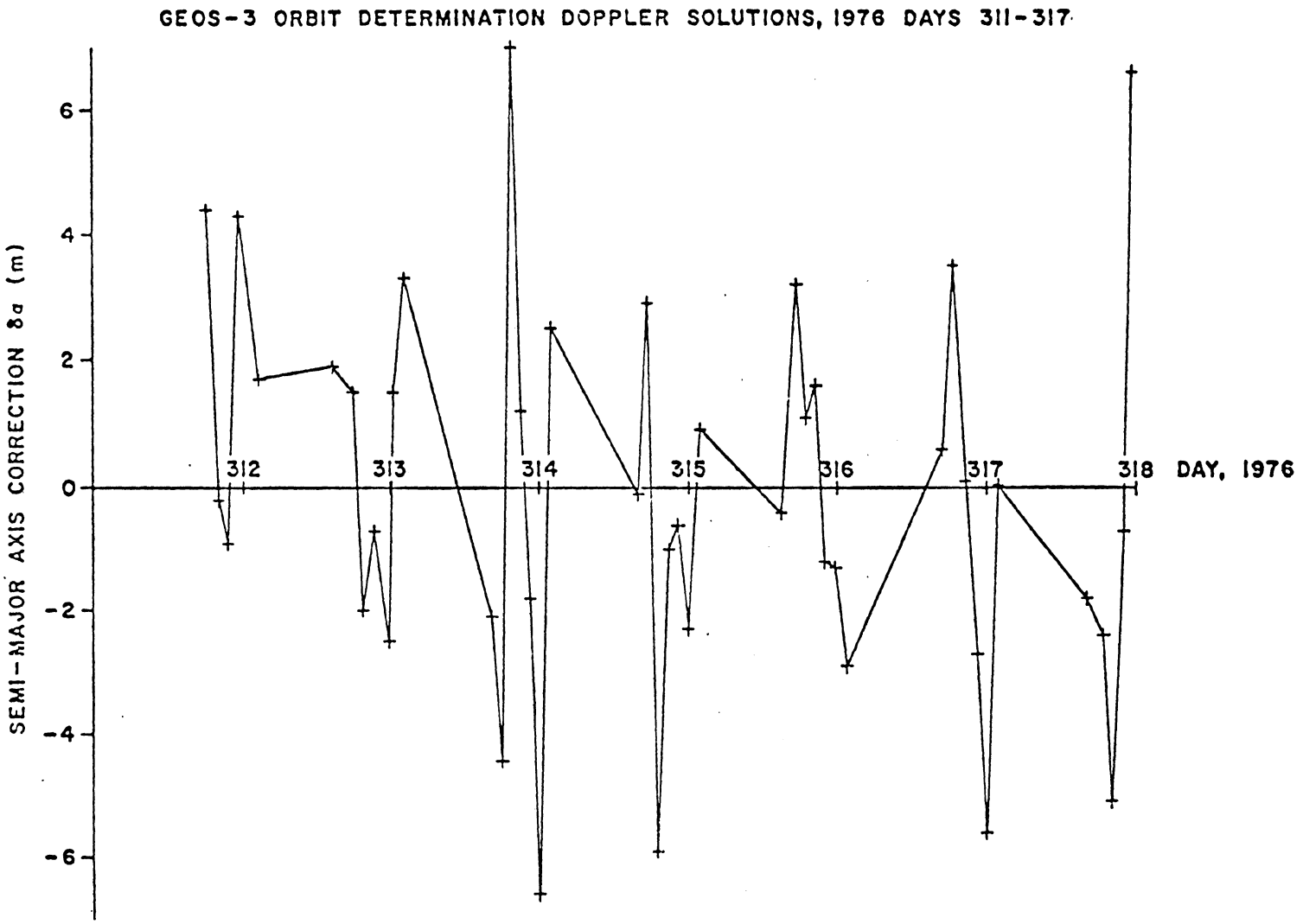
GEOS-3 ORBIT DETERMINATION DOPPLER SOLUTIONS, 1976 DAYS 311-317
SEMI-MAJOR AXIS CORRECTION δa (m)
6
4
2
0
-2
-4
-6
312
313
314
315
316
317
318
DAY, 1976

Figure 3.3b

GEOS-3 ORBIT DETERMINATION DOPPLER SOLUTIONS, 1976 DAYS 311-317

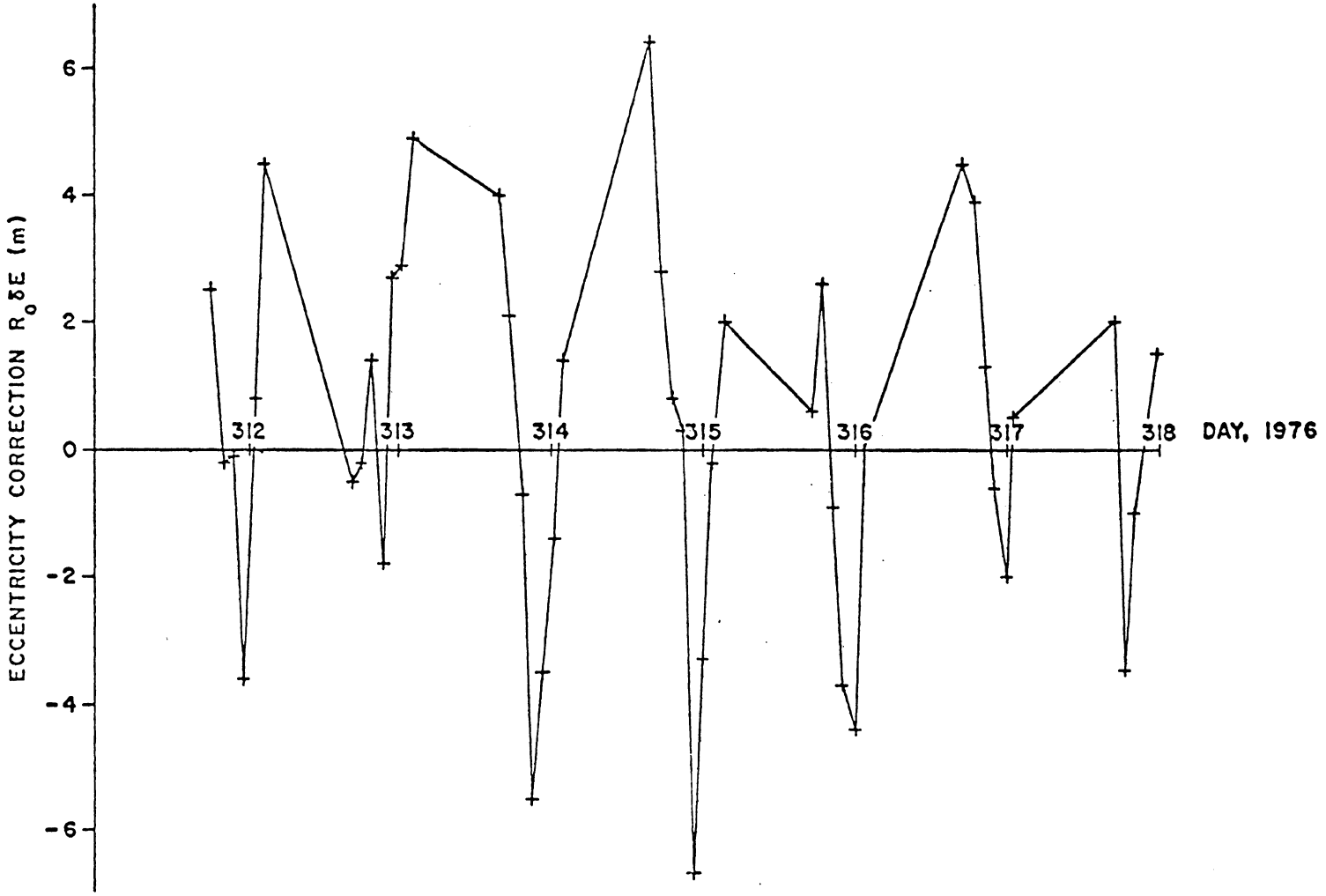

Figure 3.3c

GEOS-3 ORBIT DETERMINATION DOPPLER SOLUTIONS, 1976 DAYS 311-317

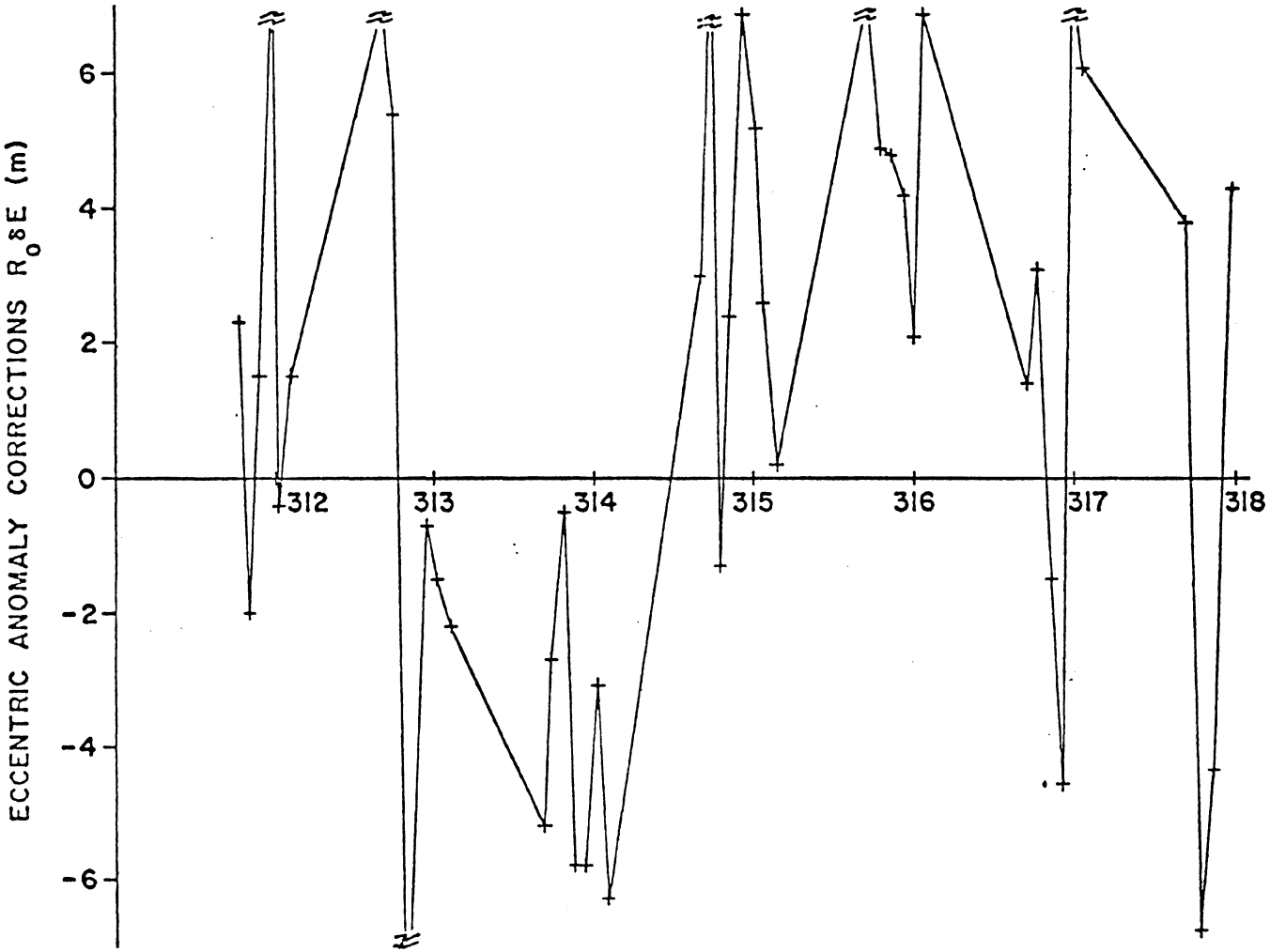

Figure 3.3d

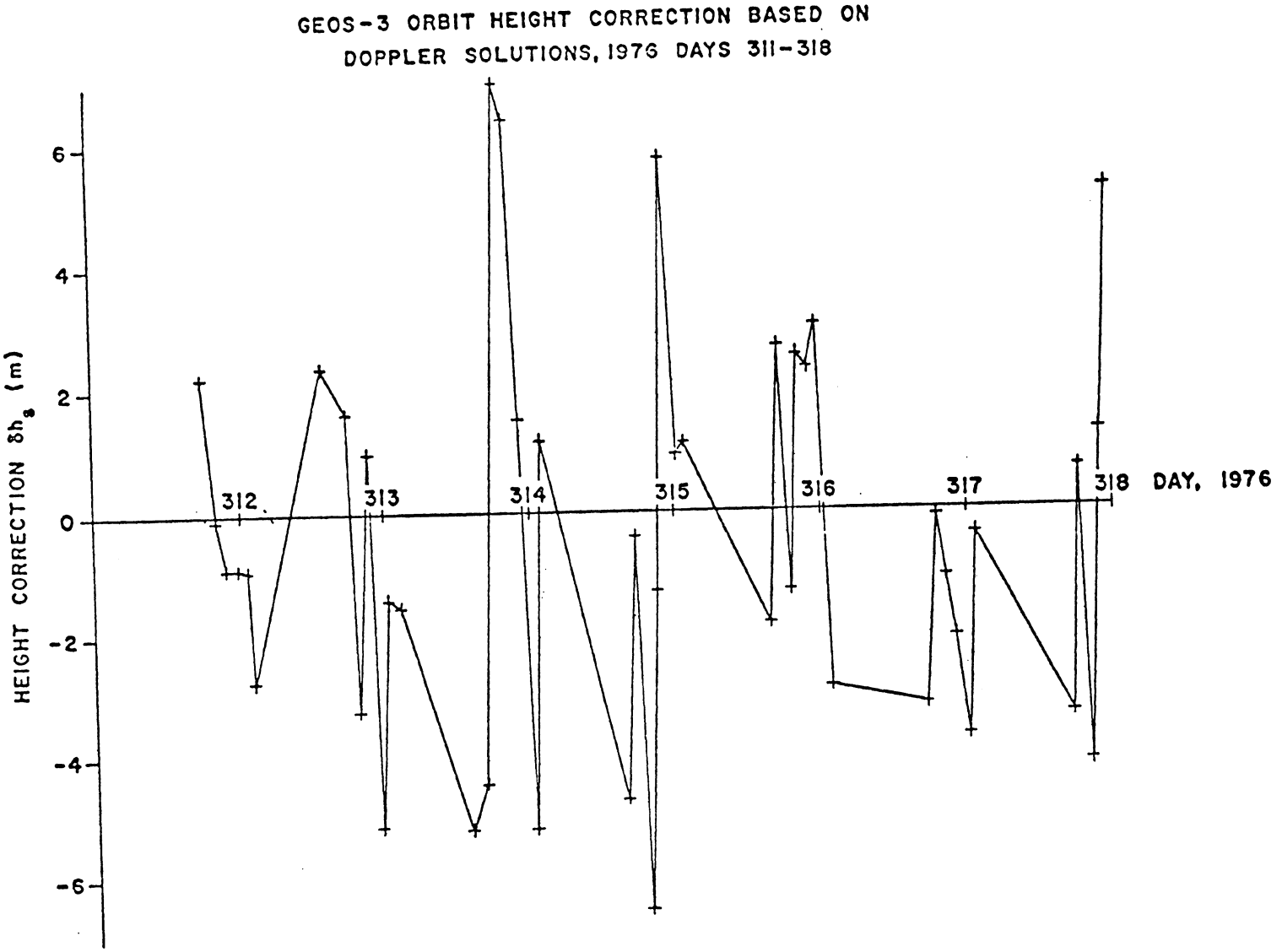
GEOS-3 ORBIT HEIGHT CORRECTION BASED ON
DOPPLER SOLUTIONS, 1976 DAYS 311-318
HEIGHT CORRECTION δh_s (m)
6
4
2
0
-2
-4
-6
312
313
314
315
316
317
318
DAY, 1976

set of updated precise ephemerides of the GEOS-3 orbits by using these computed orbital biases. The necessary expressions for the Keplerian orbit on which so recovered orbital biases (resolved as already explained into along-track δE, across track δa, and out-of-plane $\delta\eta$ components) are superimposed have been derived in *Wells (1974)*. The transformation to cartesian coordinates (average terrestrial) is

$$X_T = R_3(-\Omega + GAST)\ R_1(-i)\ R_3(\omega) \begin{vmatrix} (a+\delta a)(\cos(E+\delta E) - e) \\ (a+\delta a)\sqrt{1-e^2}\ \sin(E+\delta E) \\ \delta\eta \end{vmatrix} \qquad (3.6)$$

where

X_T ... vector of satellite position coordinates (X,Y,Z), here evaluated at every minute of each ephemeris pass;

Ω ... right ascension of the ascending node;

ω ... argument of the perigee;

i ... satellite inclination angle;

GAST .. Greenwich Apparent Sidereal Time;

R_i ... 3 x 3 rotation matrices *(Krakiwsky and Wells, 1971)*.

All other terms have already been defined except the expression of the out-of-plane bias $\delta\eta$ given in the new GEODOP version in terms of the corrections to the inclination angle δi and the right ascension of the ascending node $\delta\Omega$ as *(Kouba, 1979)*

$$\delta\eta = -r\ [\delta i \sin(f + \omega) - \delta\Omega \cos(f + \omega) \sin i] .$$

At a later stage these ephemerides, kept in the standard precise ephemeris format, were merged with the available altimetry data, using GEODOP software (*Lawnikanis, 1975a*) duly modified for our specific purposes, and served as "base" ephemerides to reduce the altimetry ranges. It was the orbits computed from these base ephemerides against which we were able to assess the available altimetry data and also gain a further insight into the extent of orbit improvement by comparing results of the adjustment of ssh's of crossing points prior to the availability of these orbits.

SECTION 4

LEAST SQUARES ADJUSTMENT OF INTERSECTING SATELLITE ALTIMETRY ARCS

The relationship of the altimetry ranges and the satellite height to the sea surface height above a reference ellipsoid has already been pointed out in the early part of section 2. It has been noted also that since the accuracy of the computed satellite orbits is generally poorer than the precision of the radar altimeter (except in calibration areas), bias corrections to the satellite positions can be obtained by means of intersection analyses of the ssh's at the crossing points of satellite sub-tracks on different orbital arcs over the same area. Then a refinement of the altimetry derived sea surface heights is possible by applying these corrections to the data. The major task set forth in this section is to discuss the basic mathematical model leading to such an analysis and to outline the estimation process upon which the adjustment of altimetry ranges is based. Eventually we shall follow the same route in using the available GEOS-3 altimetry (cf. section 5) for the estimation of the sea surface in the Hudson Bay.

We begin this development by discussing first the problem of determining the needed location and time of intersection between different satellite sub-tracks.

4.1 Determination of Intersection Points

While the altimetry is not observed, generally, at these intersection points, the location and time of intersection between ascending (S/N) and descending (N/S) passes can be determined from the following relationship between the appropriate Keplerian elements (*Kaula, 1968*):

$$\sin (\lambda + \theta - \Omega) = \tan \phi \cot i \qquad (4.1a)$$

where

ϕ .... geocentric latitude,

λ .... longitude,

θ .... Greenwich Sidereal time,

Ω .... right ascension of the ascending node,

i .... satellite inclination.

Considering the time varying elements, equation (4.1a) can be rewritten as

$$\sin [(\lambda+\theta_o-\lambda_o) + (\dot{\theta} - \dot{\Omega})t] = \tan \phi \cot i \qquad (4.1b)$$

where $\dot{\theta}$ and $\dot{\Omega}$ are the rates of change θ and Ω, and θ_o, Ω_o are the initial values of θ and Ω at some reference time t=0. In practice obtaining each intersection point from eqn. (4.1b) involves two equations, one for each arc, solved iteratively for a common latitude and longitude, whereas the time of intersection and the ssh's at this point within each arc are found by interpolation, cf. section 5.1.

4.2 Mathematical Formulation of Least Squares Adjustment

Let us consider the sea surface height (ssh) z_i as derived at the epoch of an individual altimetry observation of the i-th arc and corrected for atmospheric influences and the sea tide effect. The actual ssh z_i' may generally be related to z_i through an equation of the form

$$z_i' = z_i + s_i + \varepsilon_i \tag{4.2}$$

where

s_i is the error of the ssh due to orbital errors, and any altimeter instrument bias; and

ε_i is the error of the ssh due to altimeter noise and any unmodelled (or improperly modelled) temporal sea surface variations.

The quantity ε_i is considered to be random with zero expected value (i.e. zero mean), so that

$$E\{\varepsilon_i\} = 0$$

where E denotes the mathematical expectation operator.

According to the discussion in section 2.5, for short arcs s_i can be expressed as a polynomial in time as

$$s_i = [a_o + a_1(t - t_o) + a_2(t - t_o)^2]_i \tag{4.3}$$

where

t is the time epoch of the observation

t_o is a reference time (may be chosen conveniently as the time at mid-arc), and

a_o, a_1, a_2 are coefficients to be estimated, representing the absolute bias, tilt and a bend (second order effect) of the i-th arc.

Where two ground tracks of altimetry arcs i and j intersect at a point P, cf. figure 2.1, estimates of z'_p from two values z_{Pi} and z_{Pj} occur and equation (4.2) gives an observation equation of the form

$$(z_{Pi} - z_{Pj}) + (s_{Pi} - s_{Pj}) + (\varepsilon_{Pi} - \varepsilon_{Pj}) = 0 . \qquad (4.4a)$$

Expressing s_i in (4.3) as

$$s_i = A_i \bar{X}_i$$

where $\bar{X}_i$ is the vector of error model parameters for the i-th arc and A_i is the corresponding design matrix of the error model, equation (4.4a) may be written as

$$(z_{Pi} - z_{Pj}) + (A_{Pi} \bar{X}_i - A_{Pj} \bar{X}_j) + (\varepsilon_{Pi} - \varepsilon_{Pj}) = 0$$

or after dropping the point identifier

$$(z_i - z_j) + (A_i \bar{X}_i - A_j \bar{X}_j) + (\varepsilon_i - \varepsilon_j) = 0 \qquad (4.4b)$$

Expanding equations (4.4b) to include several observations one may write a single equation in matrix form as

$$z + A\bar{X} + \varepsilon = 0 \qquad (4.5)$$

where

- z is the vector of the ssh differences at the crossing points of two arcs;
- A is the design matrix pertaining to the error model s;
- $\bar{X}$ is the vector of the error model parameters to be estimated; and

ε is the vector of observational errors.

Denoting the least squares estimates of $\bar{X}$ and ε by X and V respectively, eqn. (4.5) may be written in the form of the general explicit least squares model in (*Krakiwsky, 1975*)

$$AX + BV + W = 0 \tag{4.6a}$$

where

$$W \equiv Z$$

$$V \equiv \varepsilon$$

$$B \equiv I \qquad (I = \text{unit matrix}).$$

The minimization of the variation function (*Krakiwsky, 1975*)

$$\phi = V^T PV + 2K^T (AX + BV + W) \tag{4.6b}$$

where K is a vector of unknown Lagrange multipliers, and $P \equiv C_z^{-1}$ is the weight matrix of the crossover observations, leads to the well-known system of normal equations

$$NX + U = 0 \tag{4.7a}$$

where

$$N = A^T PA \tag{4.7b}$$

$$U = A^T PW \tag{4.7c}$$

In the present context, the minimum of the quadratic form in equation (4.6b) is chosen to reflect the time invariance of the (stationary) sea surface heights and therefore account for the stochastic properties, such as variation and correlation, of all observations. The degree to which such observations are uncorrelated depends primarily upon the orbital modelling, as well as the correlation between temporal sea surface variations. Herein, altimetry observations are assumed uncorrelated since correlation information is not available anyway and their variance is used to weigh the intersection observations, so that the weight

matrix P assumes a diagonal form

$$P = \text{diag}\ (p_1\ p_2\ p_3\ \ldots)$$

where

p = weight of the intersection observation (S/N ssh minus N/S ssh) between two arcs i and j

$= 1/\ E\ \{\varepsilon_i - \varepsilon_j\}^2$

($\varepsilon_i, \varepsilon_j$ = error of the ssh at the intersection point within the i and j arc)

The solution of eqn. (4.7a) for X gives

$$X = -(A^T P A)^{-1}\ A^T P W$$

$$= -N^{-1}\ U \qquad (4.8a)$$

from which returning to equation (4.6a) we may deduce the vector of residuals after the adjustment as

$$V = -(AX + W) \qquad (4.8b)$$

In turn, it follows readily from (4.4b) that the adjusted ssh's at the crossing point P of two arcs i and j may be obtained as

$$\hat{z}_i = A_i\ X_i + v_i \doteq A_j\ X_j + v_j = \hat{z}_j \qquad (4.9a)$$

with

$$v_i = -v_j = \frac{1}{2}\ v_{ij} \qquad (4.9b)$$

where v_{ij} is the element of the vector V in (4.8b) which corresponds to the crossover observation at P, and the symbol "^" is used to distinguish the ssh estimates at P from their observed counterparts.

4.3 Weighting of Orbit Error Parameters

There exists an alternative approach to the problem discussed thus far which uses a priori knowledge of the error model parameters. If such knowledge exists, it is desirable to have it reflected on the previous solution. From the geometrical/physical point of view such a situation arises for instance when a set of reference orbits are selected to provide the overall orientation of the adjusted sea surface. This has been applied in several global GEOS-3 altimetry adjustments (e.g. *Marsh et al, 1978*) whereby precise laser reference orbits were selected in areas such as the Northwestern Atlantic, the Northeast Pacific off the coast of California and the Indian Ocean to provide the overall orientation of the estimated sea surface relative to the center of mass of the earth. From the estimation point of view, the additional information available can be understood as either

(a) adding constraints to the main mathematical model (4.5); that is, formulating an additional mathematical model containing only the unknown model parameters (i.e. absolute constraints), or

(b) constraining the latter by means of some finite weights associated with them.

The first situation will not be treated here and the interested reader is referred to e.g. *Mikhail (1976)* or *Vanicek and Krakiwsky (in prep.)*. The second situation can be treated in exactly the same manner as previously described, i.e. one can just substitute appropriate matrices and vectors in the earlier results with all the properties of the least squares adjustment remaining valid. The implications of applying

weighted constraints in the estimation process can also be related to the inherent rank deficiency or ill-conditioning of the problem. Since eqn. (4.5) is expressed in terms of ssh differences, a constraint must be used to anchor the solution (much the same way as in a free levelling network). For three parameter solution for s, cf. eqn. (4.3), one needs to constrain three orbital arcs. All other orbital arcs are then adjusted such that the differences in the ssh's between these and the constrained arcs is minimized.

In practical terms, by replacing the weight matrix P of the crossover observations by

$$\tilde{P} = \begin{vmatrix} P & 0 \\ 0 & P_{X_2} \end{vmatrix} = \begin{vmatrix} C_z^{-1} & 0 \\ 0 & C_{X_2}^{-1} \end{vmatrix} \tag{4.10}$$

where X_2 denotes the subset of weighted parameters in X and $C_{X_2}^{-1}$ is its associated covariance matrix, we obtain similar to the equations (4.7)

$$\tilde{N}X + \tilde{U} = 0 \tag{4.11a}$$

$$\tilde{N} = \tilde{A}^T\tilde{P}\tilde{A} \equiv \begin{vmatrix} A_1^TPA_1 & A_1^TPA_2 \\ (A_1^TPA_2)^T & A_2^TPA_2 + P_{X_2} \end{vmatrix} \tag{4.11b}$$

$$\tilde{U} = \tilde{A}^TPW \equiv \begin{vmatrix} A_1^TPW \\ A_2^TPW \end{vmatrix} \tag{4.11c}$$

where the design matrices A_1, A_2 pertain to the non-weighted and weighted parameters respectively, i.e.

$$A \equiv [A_1 \quad A_2] \quad .$$

The final solution for X can be written in much the same way as in equation (4.8a) with the exception of matrix $P_X (\equiv P_{X_2})$, namely

$$(N + P_X)\, X + U = 0 \qquad (4.12)$$

where N and U are given by (4.7b, c). When no parameters are weighted then $P_X \equiv 0$ and (4.8a) is reduced as a special case; when all parameters are weighted $X_2 \equiv X$ in which case the parameters assume the role of "quasi-observations" (*Krakiwsky, 1975; Blaha, 1976*).

4.4 Solution of Normal Equations

In the present context of altimetry reductions, the development of the normal equations (4.8) or (4.12) can generally lead to a system of equations which grows in dimensions with both the number of orbital arcs and the number of error parameters expressing the bias for each arc. In practical applications although the size of the normal equations can be large, the coefficient matrix of the normal equations have or can be made to have a useful pattern of zero and non-zero submatrices (*Allen and Martin, 1977*).

By partitioning the orbital arcs into groups of S/N (ascending) and N/S (descending) passes the original normal equations (4.8) can be reduced to have a banded structure

$$\begin{vmatrix} N_{11} & & & & N_{1n} \\ & N_{22} & & & N_{2n} \\ & & N_{33} & & N_{3n} \\ & & & \ddots & \vdots \\ N_{1n}^T & N_{2n}^T & N_{3n}^T & \cdots & N_{nn} \end{vmatrix} \begin{vmatrix} X_1 \\ X_2 \\ X_3 \\ \vdots \\ X_n \end{vmatrix} + \begin{vmatrix} U_1 \\ U_2 \\ U_3 \\ \vdots \\ U_n \end{vmatrix} = 0 \qquad (4.13)$$

where the coefficient matrix N can be expressed schematically as

$$N \sim \searrow\!\downarrow .$$

The sense of this scheme is that the horizontal and vertical arrows represent row and column blocks of non-zero submatrices, whereas the diagonal arrow represents a diagonal array of non-zero submatrices. The arrows indicate that the normal equation matrix N can extend theoretically without limit keeping the structure as depicted above.

In appendix A we have developed the details of a practical algorithm which takes advantage of the "banded-diagonal" structure of the normal equation matrix. Here it will suffice to give a brief summary.

Arranging the orbital arcs into groups of S/N and N/S passes essentially amounts to partitioning the original vector of the unknown parameters X into two vectors X' and X" (corresponding to each group of passes) so that

$$X = \begin{vmatrix} X' \\ X'' \end{vmatrix}$$

Partitioning the original normal equations (4.7) to be conformable with the partitioning of X yields

$$\begin{vmatrix} N' & \bar{N} \\ \bar{N}^T & N'' \end{vmatrix} \begin{vmatrix} X' \\ X'' \end{vmatrix} + \begin{vmatrix} U' \\ U'' \end{vmatrix} = 0 \qquad (4.14b)$$

By virtue of the fact that crossover altimetry observations preclude two S/N or two N/S passes to appear simultaneously in an observation equation, one can assume without any loss of generality that the vector X" is "common" to most, if not all, of the original observation equations, whereas X' is composed of (possibly) a large number of subvectors X_1', X_2', X_3', ..., X_n' each of which appears only in a subgroup of observation equations with corresponding subvectors of X". Under these circumstances the observation equations (4.5) may be ordered into groups corresponding to various subvectors X_i' so that

$$\begin{vmatrix} A_1' & & & & A_1'' \\ & A_2' & & & A_2'' \\ & & A_3' & & A_3'' \\ & & & \ddots & \vdots \\ & & & A_n' & A_n'' \end{vmatrix} \begin{vmatrix} X_1' \\ X_2' \\ X_3' \\ \vdots \\ X_n' \\ X'' \end{vmatrix} + \begin{vmatrix} V_1 \\ V_2 \\ V_3 \\ \vdots \\ V_n \end{vmatrix} + \begin{vmatrix} W_1 \\ W_2 \\ W_3 \\ \vdots \\ W_n \end{vmatrix} = 0 \qquad (4.15)$$

The direct evaluation of the normal equations of the system of observation equations (4.15), under the assumption of uncorrelated observations, i.e. $P = \text{diag}\,(P_1\ P_2\ P_3\ \ldots\ P_n)$, leads to a system

$$\begin{vmatrix} N'_1 & & & & & \bar{N}_1 \\ & N'_2 & & & & \bar{N}_2 \\ & & N'_3 & & & \bar{N}_3 \\ & & & \ddots & & \vdots \\ & & & & N'_n & \bar{N}_n \\ \bar{N}_1^T & \bar{N}_2^T & \bar{N}_3^T & \cdots & \bar{N}_n^T & N'' \end{vmatrix} \begin{vmatrix} X'_1 \\ X'_2 \\ X'_3 \\ \vdots \\ X'_n \\ X'' \end{vmatrix} + \begin{vmatrix} U'_1 \\ U'_2 \\ U'_3 \\ \vdots \\ U'_n \\ \end{vmatrix} = 0 \qquad (4.14b)$$

where

$$N'' = \sum_{k=1}^{n} N''_k = \sum_{k=1}^{n} A''^T_k P_k A''_k \qquad (4.15a)$$

$$U'' = \sum_{k=1}^{n} U''_k = \sum_{k=1}^{n} A''^T_k P_k W_k \qquad (4.15b)$$

$$N'_k = A'^T_k P_k A'_k \tag{4.15c}$$

$$\bar{N}_k = A'^T_k P_k A''_k \tag{4.15d}$$

$$U'_k = A'^T_k P_k W_k \tag{4.15e}$$

In view of the block diagonal structure of the N' portion of the normal equations matrix the solution of (4.14b) for $X = [X' \; X'']^T$ can be obtained via partitioning and successive summations of the form

$$X'' = M''(U'' - \bar{N}^T N'^{-1} U') \tag{4.16a}$$

$$= M'' \sum_{k=1}^{n} [A''^T_k P_k W_k - A''^T_k P_k A'_k (A'^T_k P_k A'_k)^{-1} A'^T_k P_k W_k]$$

and for each X'_i vector

$$X'_i = N'^{-1}_i U'_i - N'^{-1}_i \bar{N}_i X'' \tag{4.16b}$$

$$= (A'^T_i P_i A'_i)^{-1} A'^T_i P_i W_i - (A'^T_i P_i A'_i)^{-1} A'^T_i P_i A''_i X'' .$$

where

$$M'' = (N'' - \bar{N}^T N''^{-1} \bar{N})^{-1} \tag{4.17}$$

$$= \sum_{k=1}^{n} [A''^T_k P_k A''_k - A''^T_k P_k A'_k (A'^T_k P_k A'_k)^{-1} A''^T_k P_k A'_k].$$

Finally, in order to introduce a priori weighted constraints to the i-th arc, one may treat the situation much the same way, the only difference being in the appropriate formulae the replacement of the matrix N_i' (or N_i'') by $N_i' + P_{X_i'}$ (or $N_i'' + P_{X_i''}$).

As a concluding remark on the solution of the normal equations in the foregoing manner we note the similarity of the computational flow in this development with the first order partitioned regression of *Brown and Trotter [1969]*. We also note that the main attraction of this solution is that orbital biases can be recovered for one group of arcs (i.e. S/N arcs) once the orbital errors of the other group (i.e. N/S arcs) have been obtained. This virtually allows (theoretically) any number of S/N passes to be processed simultaneously. Simply to increase the number of S/N passes one has to increase the summation limit in eqn. (4.16a) and (4.17). To increase the number of the N/S passes, which provide the "common" error parameter set, one has to increase respectively the size of the vector X" and the matrix M", which generally poses theonly limitation as to the maximum number of passes which can be reduced in this manner.

4.5 Covariance Estimation

It is appropriate to conclude this section by deriving corresponding covariance matrices for both the recovered error parameters and the adjusted observations. These covariances are indispensable to any statistical evaluation of the results (*Vanicek and Krakiwsky, in prep.*).

First, in as much as the inverse of the coefficient matrix of the normal equations provides (up to a scale) the covariance matrix of the adjusted parameters, it follows immediately from (4.16a) that the covariance matrix of X'' can be readily obtained as

$$\hat{C}_{X''} = M'' \tag{4.18a}$$

without additional computational effort since M'' has to be computed in order to obtain the solution for X''.

In the case of vector X' the situation is slightly different. Although it can be shown (cf. appendix A) that the covariance matrix of X' is given by an expression of the form

$$\hat{C}_{X'} = N'^{-1} + N'^{-1} \bar{N} M'' \bar{N}^T N'^{-1} = M'$$

it is possible to by-pass the need of computing M' by exploiting once again the block diagonal structure of N'. Applying the covariance law to eqn. (4.16b) the covariance matrix of a subvector X'_i can be obtained as

$$\begin{aligned} \hat{C}_{X'_i} &= N'^{-1}_i + N'^{-1}_i \bar{N}_i M'' \bar{N}^T_i N'^{-1}_i \\ &= N'^{-1}_i + Q_i M'' Q^T_i \end{aligned} \tag{4.18b}$$

and respectively the cross-covariance of an arbitrary pair of vectors X'_i, X'_j can be obtained as

$$\hat{C}_{X'_i X'_j} = Q_i M'' Q^T_j , \quad i \neq j \tag{4.18c}$$

where

$$Q_k = N_k^{-1} \bar{N}_k , \quad k = i \text{ or } j.$$

Finally, the covariance matrix of the adjusted observations can be shown [*Krakiwsky, 1975; Vanicek and Krakiwsky, in prep.*] to be equivalent to

$$\begin{aligned} \hat{C}_z &= C_z - \hat{C}_V \\ &= \sigma_o^2 P^{-1} - \hat{C}_V \end{aligned} \tag{4.19}$$

which also reflects the improvement gained in the variance-covariance properties of the original observations through the adjustment. In case that only the relative scale of the covariance matrix of the observations is known, i.e. the a priori variance factor σ_o^2 is not known, σ_o^2 can be replaced by the estimated variance factor given by

$$\hat{\sigma}_o^2 = \frac{V^T P V + X^T P_X X}{df} \tag{4.20}$$

where df is the degrees of freedom associated with $\hat{\sigma}_o^2$. Similarly, the covariance matrices for the parameters can be properly scaled so that

$$\hat{C}_{X''} = \hat{\sigma}_o^2 M'' \tag{4.18d}$$

$$\hat{C}_{X'} = \hat{\sigma}_o^2 M' \tag{4.18e}$$

Direct evaluation of $\hat{C}_z$ requires that $\hat{C}_V$ (= $A\hat{C}_X A^T$) is available which is impractical when V is large. However, even if it is impractical to compute the entire matrix $\hat{C}_V$, it is still possible to do it for different subvectors of V in much the same way as we did

with $\hat{C}_X$. Furthermore, if there is no direct use of $\hat{C}_{\hat{z}}$ and the only purpose of requiring $\hat{C}_V$ is for the statistical assessment of the observations further simplifications can be made. *Vanicek and Krakiwsky (in prep.)* point out that when testing each individual component of the residual vector V for outliers within the observational series, the covariances need not be considered, but the knowledge of the respective variances is essential. Investigating the general properties of the matrix $\hat{C}_V$ *Pope (1976)* has shown that an expedient compromise can be reached in the computation of these variances, which otherwise would be extracted from $\hat{C}_V$, even if $\hat{C}_V$ is not available. For a parametric adjustment, such as in this case, the variance of the k-th residual in vector V can be approximated by

$$\hat{\sigma}^2_{v_k} = \left(\frac{df}{n}\right) \left(\frac{\hat{\sigma}_o^2}{p_k}\right) \qquad (4.19b)$$

where p_k is the a priori weight of the k-th observation and n is the number of elements in the vector V.

SECTION 5

RESULTS OF THE ANALYSIS OF GEOS-3 ALTIMETRY IN HUDSON BAY

To test the methodology discussed in the preceeding sections we performed an analysis of the GEOS-3 altimetry in Hudson Bay for the estimation of the mean sea surface associated with the period from September to December, 1976. The results of this analysis have been based on the adjustment of a regional network of 71 GEOS-3 orbital arcs intersecting at nearly 700 crossing points in the Hudson Bay with a distribution as shown in figure 5.1. Our approach in eliminating orbital errors from the estimation of the sea surface has been to model the altimetry arc biases as a polynomial in time and solve for corrections to each arc to make the data have the best rms agreement at the crossover points. In the results reported immediately below such corrections were obtained with respect to orbits generated from the "base" ephemerides we had computed from the Doppler solutions described in section 3. Results with regard to reductions carried out with the original NASA orbits are also reported at the end of this section.

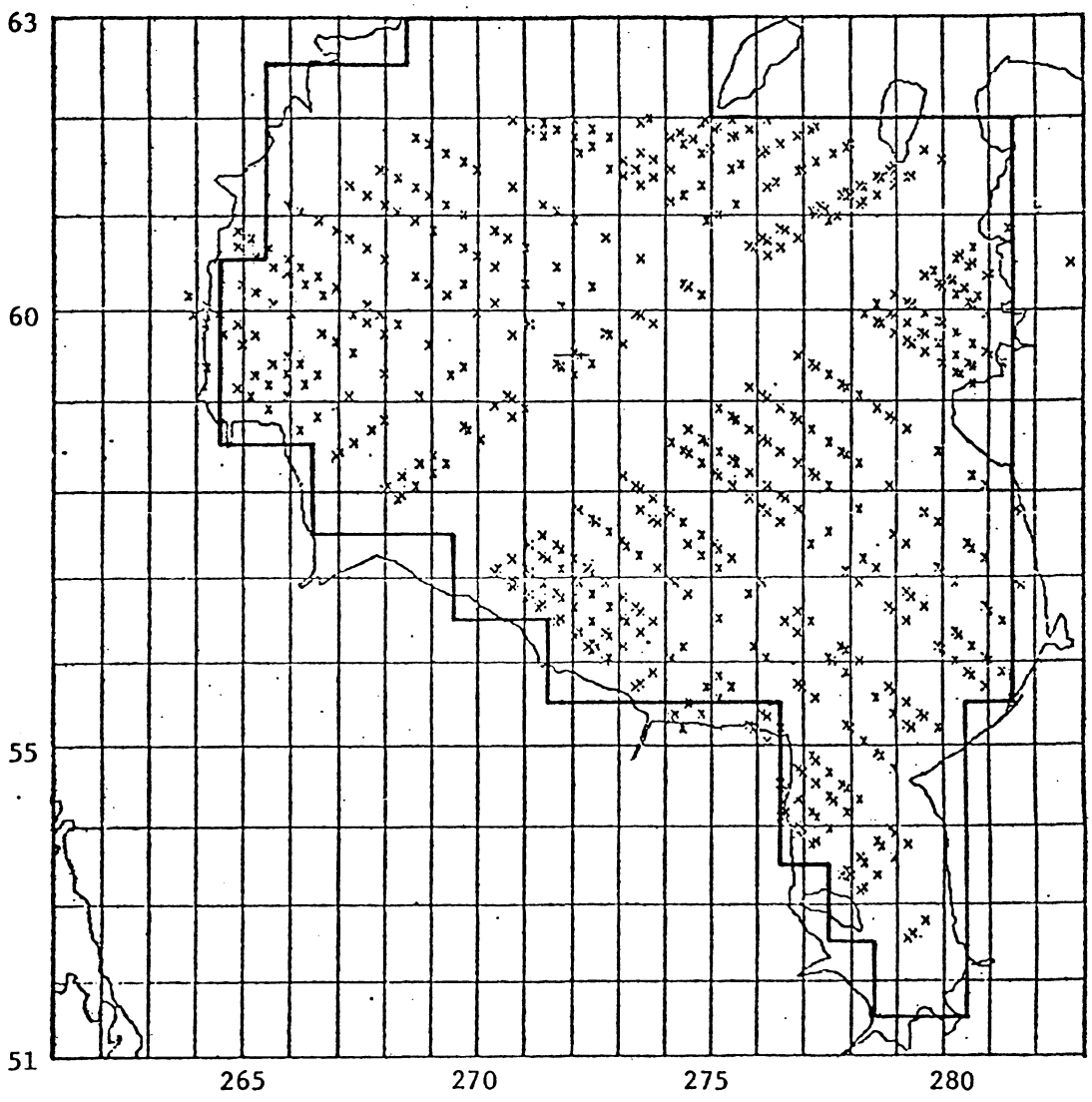

Figure 5.1

Distribution of Crossover Points of
GEOS-3 Altimetry Arcs in the Hudson Bay

5.1 Outline of Treatment

5.1.1 Data Selection

During the initial stage of preprocessing certain characteristics of the altimetry data were identified for editing criteria. Using essentially four editing criteria which have also appeared in *Rapp (1978)*, we subjected the original data to an automatic editing procedure which examined the data to identify gross errors induced by either the instrumentation or the data handling process, *(Delikaraoglou and Vanicek, 1979)*. As already explained in section 1.2 the supplied GEOS-3 data contained information which represent averages of measurements grouped into variable 2.048 sec or 3.477 sec frames. For a frame measurement to be accepted for further processing it had to meet the following conditions:

1. The altitude measurement standard deviation parameter in the data record should be within the range: $0.25 < \sigma_{ALT} < 8.00$ metres; this could identify noisy data.
2. The absolute sea surface height parameter should be less than 170 metres, thus eliminating points with unreasonable ssh because of overland data, very bad orbits or time tag errors.
3. The Automatic Gain Control Voltage (AGCV) parameter, which is a measure of the received signal level, should be within the range: $-78 <$ AGCV < -62 dbm, with its standard deviation determined from the individual AGCV measurements within the frame required to be less than 2 dbm.

4. The $H_{1/3}$ parameter, which is a measure of the sea state, should be less than 88 metres.

A second level of editing involved a smoothing operation to derive one representative altitude per major frame. Using appropriate algorithms and timing parameters described in *Leitao et al (1975)* to properly time tag parameters on the data record, we chose to use a cubic spline fit rather than a first degree polynomial fit on which the frame value given in the original data is based.

To create the crossover data set required for the intersection analysis we developed a procedure that takes the edited passes on the data base and identifies all crossover points within given meridians and parallels (for the present study selected as 51° to 62° latitude and 262° to 283° longitude east). This procedure initially involved finding the location and time of intersection between ascending and descending passes. In turn a cubic spline interpolation through each altimetry arc was used to obtain the exact sea surface height at the crossing point. The sea tide effect, computed from the analytical tidal model described in section 2.2, was then applied to the interpolated ssh at this point. Sea surface height differences at the intersection points (S/N ssh minus N/S ssh) which disagreed by more than an input edit level were flagged for rejection and were not used in the final adjustment. Such discrepancies in the ssh differences so deleted can be attributed mainly to time tag errors. The times of the altimeter ranges are correlated with the GEOS-3 ephemerides to define z, cf eq. (2.1). The accuracy with which this correlation is performed is critical as the rate of change of the altimeter range can be as large as 20 m/sec. In those terms cutoff edit levels of the order of 10 m to 20 m seem to be common practice with GEOS-3 data (e.g. *Mather et al, 1978; Masters et al, 1979*).

A measure of the accuracy of the orbits has been provided by the ssh differences at the crossing points. The statistical distribution of the noted crossover discrepancies in the above data set has been plotted on a histogram shown in figure 5.2a, where the mean and rms differences are also indicated. It is noted that the rms discrepancy at a 20 m cutoff edit level is $\pm$ 5.51 m which is about the level of the expected radial discrepancies in the satellite ephemerides used for this reduction.

5.1.2 Unknowns and Constraints Used in the Reductions

In adjusting the regional network of crossover points shown in figure 5.1 we carried out an adjustment whereby an absolute bias and a tilt were first computed for each arc. To investigate furthermore the use of a high order function expressing the bias, a test adjustment including the recovery of a bend (second order effect) correction for each arc was also carried out. In either case weighted constraints were exercised on these parameters thus allowing the reference orbits generated by the "base" ephemerides to provide the overall orientation of the adjusted sea surface.

The orbit error parameters were assumed subject to a priori constraints of 10.0 m and 0.02 m/sec respectively. These values were considered to be relaxed enough to accommodate expected errors in the computed orbits. The a priori standard error for all altimetry measurements was assumed to be 0.7 m (so that each crossing point altimetry difference had a standard error of 1.0 m). The crossover discrepancy cutoff was chosen at the 20 m level. The final set of points included in the adjustment were checked to ascertain that they were within the specified coastline boundaries shown in figure 5.1 and also

examined to test (based on an input sigma criterion) the compatibility of each observation "within-the-context" of the entire observational series (*Vanicek and Krakiwsky, in prep.*).

5.1.3 Results of the Least Squares Adjustment

The final reduction of GEOS-3 altimetry over the Hudson Bay included data from 68 passes and 544 intersection points. Biases and tilts for each pass were computed in a least squares adjustment process with the results shown in table 5.1. In turn, these biases and tilts were applied to the data and adjusted ssh differences at the crossing points were estimated together with respective mean and rms difference values. Any crossover differences whose magnitude was greater than a test level based on a max-tau criterion (*Pope, 1976*) were flagged for rejection and the above correction procedure was repeated. This warranted that a small number of intersection points which showed unacceptably large crossover differences after the adjustment were not included in the final set of adjusted ssh's.

The mean sea surface, taken as the average ssh at each intersection point, was determined in this manner with an estimated accuracy of $\pm$ 0.98 m (on the first iteration). When a stringent input cutoff level of 10 m was applied on the ssh differences and the adjustment was repeated, the estimated accuracy of the mean sea surface was $\pm$ 0.63 m which compares favourably with the postulated precision of the GEOS-3 radar altimeter in the short pulse mode.

An indication about the improvement gained through the adjustment process is obtained by comparing the discrepancies in the crossover points before and after the adjustment. From the

statistics listed in table 5.2a it can be seen that the rms difference at a 10 m cutoff discrepancy level has been reduced to 1.11 m.

When the above adjustment process was repeated with the altimetry data set reduced with respect to the originally supplied NASA (WFC) orbits, the results showed little change in the statistics of the two regional solutions, cf. tables 5.2. However, randomly checked adjusted ssh's at the same crossover points were found different by as much as 1 to 2 metres. A definite assessment of the role of the Doppler improved orbits in the altimetry adjustment was therefore decided to be put off until after a comparison of the estimated sea surface in each case was made against known geoidal features.

As a closing remark on the results of the least squares adjustment it should be noted in this connection that when the above estimation process was repeated with a second order effect (bend) for each arc included in the solution little change was noticed in the results (bend effects of the order of 10^{-5} to 10^{-7} m/min^2 were found). This can be attributed to the fact that in the present case we are dealing with a limited area and short arcs of length which at best reach only one tenth of a full revolution, in which case an absolute bias and a tilt can adequately express the bias for each orbital arc.

5.2 Surface Fitting of the Adjusted Sea Surface Heights

At this stage we have a set of adjusted ssh's referred to the NWL 9D system ellipsoid (a = 6378145 m, f = 1/298.255) which has been the reference system of the orbits used to reduce the altimetry

Table 5.1

ORBITAL BIASES SOLUTION

N/S REV.	ABS. BIAS (m)	TILT (m/min)	SECOND ORDER EFFECT (m/min^2)
7918	-4.595	0.042	
7862	9.408	-0.598	
7932	-2.816	-0.087	
7662	-1.638	-0.420	
7464	9.994	0.435	
7620	0.365	-0.276	
7634	-1.404	0.438	
7663	2.129	-0.243	
7335	-2.470	-0.339	
7791	1.051	-0.095	
7307	-2.143	0.264	
7876	-1.904	-0.242	
7606	-0.215	-0.050	
7520	0.642	-0.591	
7534	-3.942	-0.027	
7406	-4.793	-0.077	
7378	1.020	0.284	
7605	-5.834	-0.103	
7591	-1.490	0.268	
7407	3.346	-0.017	
7449	-0.577	0.376	
7421	-0.194	0.182	
7833	-6.179	0.172	
7847	-5.726	-0.367	
7592	6.563	-0.144	
7577	-2.915	0.495	
7861	-0.410	-0.071	
7393	7.229	-0.312	
7463	2.526	0.248	
7392	-1.439	0.053	
7734	0.579	0.163	
7720	16.370*	0.089*	
7705	-1.548	0.065	
7506	-1.522	0.443	
7961	-2.598	-0.087	
7762	-1.388	0.068	
7989	-1.378	0.444	
7904	-0.328	-0.163	
7947	0.792	0.176	
7435	2.787	-0.316	
7478	3.798	-0.088	
7676	3.736	-0.084	

* Pass rejected in second iteration

Table 5.1 Cont'd

S/N REV	ABS. BIAS (m)	TILT (m/min)	SECOND ORDER EFFECT (m/min^2)
7680	-0.443	0.076	
7481	-1.156	0.800	
7637	-3.371	-1.085	
7495	-2.794	-0.943	
7509	-2.005	1.474	
7779	-4.082	-0.252	
7765	7.531	-1.367	
7865	-1.501	0.656	
7467	0.529	1.376	
8561	-1.976	-0.289	
7552	-0.092	-0.357	
7424	0.251	-0.310	
7850	-4.964	-0.056	
7381	-0.989	-0.987	
7396	3.507	0.809	
7580	57.820**	-11.440 **	
7452	-1.680	-0.213	
7438	-0.396	-0.319	
7794	0.462	1.160	
7595	-9.767	2.608	
7922	3.673	2.467	
7907	-0.238	-1.374	
7978	-2.011	-0.399	
7410	2.741	0.658	
7737	-0.315	0.510	
7651	-3.041	-0.733	

** Readjusted in second iteration to 11.950 and -2.639 respectively

TABLE 5.2a

Altimetry Crossover Differences
For Doppler Fitted Reference Orbits

	Before adjustment (1)	After adjustment (2a)	(2b)
Mean Difference (m)	0.83	0.07	0.01
RMS Difference (m)	5.51	1.49	1.11
No. of Crossing Points	611	544*	510**
Cutoff Discrepancy (m)	20	20	10

* Differences between cols. (1) and (2a) are due to max-tau rejections and points outside specified coastline boundaries.

** Differences between cols. (2a) and (2b) are due to cutoff discrepancy level only.

TABLE 5.2b

Altimetry Crossover Differences
For Reference Orbits Supplied by NASA

	Before adjustment (1)	After adjustment (2)
Mean Difference (m)	1.42	0.02
RMS Difference (m)	5.07	1.31
No. of Crossing Points	601	543
Cutoff Discrepancy (m)	20	20

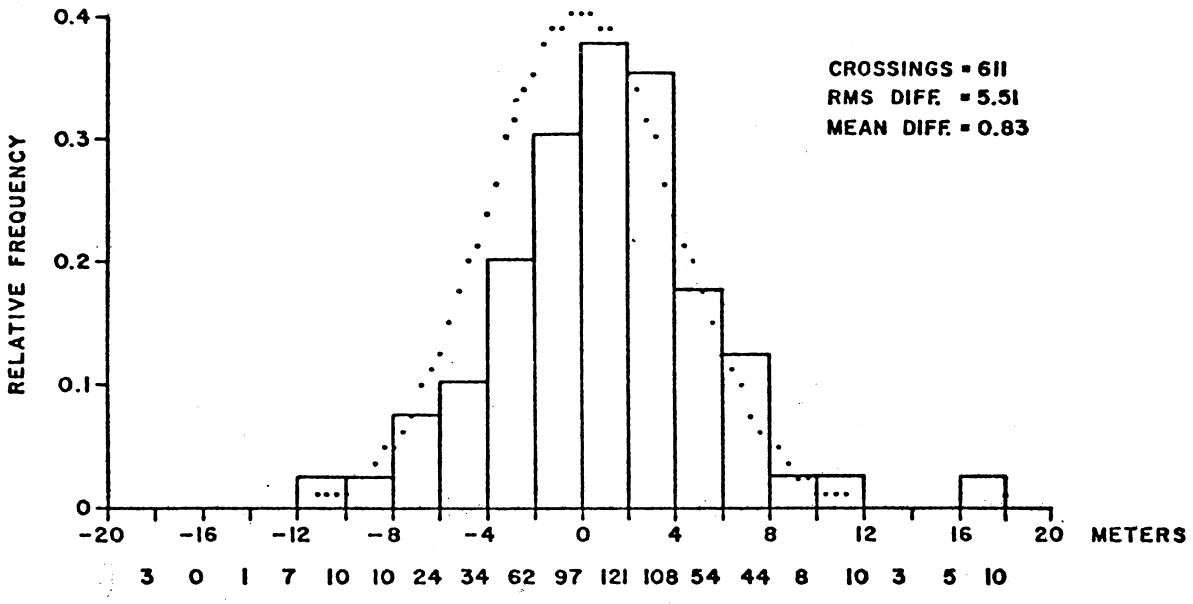

Figure 5.2a
HISTOGRAM OF CROSSOVER SEA SURFACE HEIGHT DIFFERENCES BEFORE ADJUSTMENT

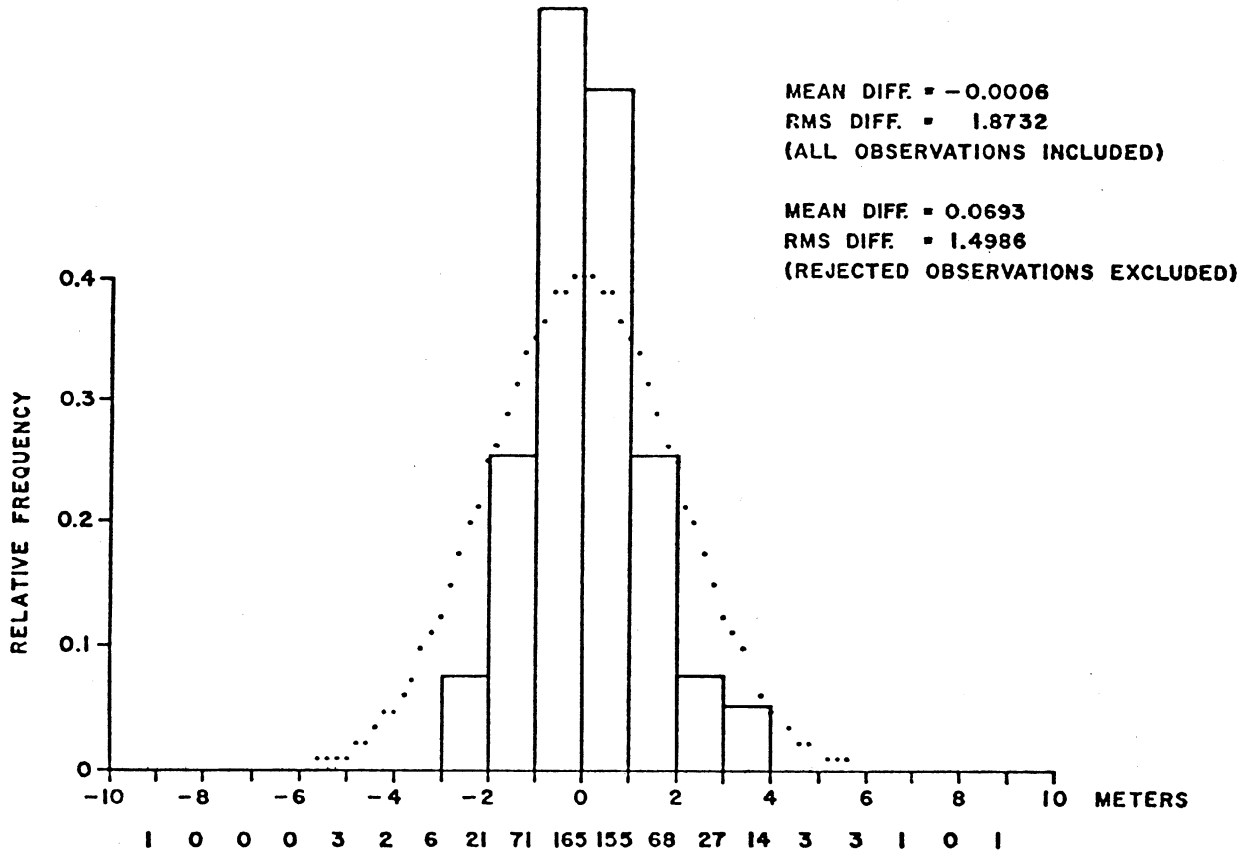

Figure 5.2b
HISTOGRAM OF ADJUSTED CROSSOVER SEA SURFACE HEIGHT DIFFERENCES

data. Using this set of ssh's one can produce the usual maps of the sea surface for the time period of the data acquisition.

To construct such maps directly from the data is impractical due to the density of points involved. The common approach is then to predict a set of grid values generally determined from irregularly spaced data by methods developed in the "model" or "operational" approach described in (*Moritz, 1978; Tscherning, 1979*).

The problem in hand clearly parallels the task commonly faced by geodesists of prediction whereby a solution $\{a_i\}$ is sought to a system of equations

$$D_i = \sum_{i=1}^{n} a_i L_j h_i = \{a_i\}^T \{L_j h_i\} \qquad (5.1)$$

relating D_i known, as well as predicted, gravity field quantities through linear functionals L_j of functions h_i.

The different methods often employed to attack this problem vary mostly according to the base functions h_i which are used. In a similar context *Kearsley (1977)* has demonstrated the use of both a simple deterministic approach (i.e. using a $(\text{distance})^{-4}$ weight function) and a least squares collocation procedure. For our specific purpose we considered different possible approaches including such functions as bicubic splines (*Sunkel, 1977*), multi-quadratic functions (*Hadgigeorge and Trotter, 1978; Hardy, 1979*) and algebraic polynomials (*Vanicek and Merry, 1973; Merry, 1975*) which can also be chosen, so that they are well suited for local detailed gravity field representation. Of these approaches, we found that least squares approximation using

high order approximating polynomials offers the advantage of little computational complexity and is well suited within the context of the intended application.

Adapted to the situation, this approach reduces to a simple regression such that eq. (5.1) becomes

$$D(\phi, \lambda) = \Phi^T (\phi, \lambda)\, a \tag{5.2}$$

where $D(\phi, \lambda)$ denotes the known, as well as predicted, gravity field quantities, $\Phi(\phi, \lambda)$ is the well-known Vandermonde's matrix composed of functional values of selected base functions (algebraic or other), and a is a vector of coefficients to be determined. The base functions can be selected arbitrarily. For the present purpose the simplest choice is to approximate the ssh $z(x, y)$ at a point (x, y) by a mixed algebraic polynomial P_n of order n, such that

$$P_n(x, y) = \sum_{i,j=0}^{n} a_{ij}\, x^i y^j \doteq z(x, y) \tag{5.3}$$

with x, y indicating the local cartesian coordinates of the point given by

$$x = R\,(\phi - \phi_o) \tag{5.4a}$$

$$y = R\,(\lambda - \lambda_o)\cos\phi \tag{5.4b}$$

where R is the mean radius of the earth and (ϕ_o, λ_o) is an arbitrary origin preferably chosen near the centroid of the area of interest.

In this case the coefficients a_{ij} of the polynomial P_n are determined in such a way as to minimize the weighted sum of the squares of the discrepancies between the height of this mathematical surface and the height of the sea surface of k mesh points covering the area of interest.

Using the above surface fitting procedure and ordinary least squares methodology (*Vanicek and Wells, 1972*) we obtained very satisfactory results using as low an order of the approximating polynomials as three (sixteen coefficients). The prediction errors using these polynomials were found to be well below the 1σ estimated accuracy of the data. The larger prediction errors occurred at the edges of the sea surface area (where it is to be expected that the solution is weak), or at the areas where the surface is very convoluted due to the presence of islands. By increasing the order of the polynomials it was found that the model fits the observations better. At the present, indications are that for an area of the size of Hudson Bay and the given number and distribution of data points, the optimum order of the polynomial to use is about five although this may be increased with an increasing number of observations.

5.3 Comparison Between Sea Surface and Geoid in Hudson Bay

5.3.1 Data Used in the Comparison

To verify the results of the estimated sea surface in Hudson Bay a number of comparisons were made with two combined geoids independently computed at UNB and GSC respectively, and a GEOS-3 altimetry derived sea surface computed by DMA and supplied to us by GSC.

The DMA GEOS-3 sea surface, which was given on a 1° x 1° grid, consisted of point heights derived from about 150 GEOS-3 altimetry arcs on the Hudson Bay reduced and adjusted in conjunction with NSWL precise GEOS-3 orbits (*Lachapelle and Brace, 1979*). This data set was referenced to the World Geodetic System 1972 (WGS 72) ellipsoid having an equatorial radius a = 6378135 m and flattening f = 1/298.26. (*Seppelin, 1974*).

The GSC combined geoid consisted of a set of geoid heights on a 0°.5 x 1° grid computed from a combination of GEM-10B potential coefficients (*Lerch et al, 1978*) and 1° x 1°, 15' x 15' and 5' x 5' mean gravity anomalies used in a combined integral formulae and collocation approach as described in *Lachapelle (1977, 1979)*.

The UNB combined geoid consisted of 20' x 20' geoid undulations computed from a combination of GEM-10 potential coefficients (*Lerch et al, 1977*) and 1° x 1° and 20' x 20' mean gravity anomalies in an approach whereby the total undulation at a point (ϕ , λ) was obtained as (*John , 1980*)

$$N = N_s + N_R$$

with

$$N_s = N_o + R \sum_{n=2}^{\ell_{max}} \sum_{m=0}^{n} [\bar{J}^*_{nm} \cos m\lambda + \bar{K}_{nm} \sin m\lambda] \bar{P}_{nm}(\sin \phi)$$

$$(\bar{J}^*_{nm} = \bar{J}_{nm} - J'_{nm})$$

$$N_R = \frac{R}{4\pi G} \iint_{\sigma_1} S^*(\psi)(\Delta g_1 - \Delta g_s)\, d\sigma + \frac{R}{4\pi G} \iint_{\sigma_2} S^*(\psi)\ (\Delta g_2 - \Delta g_s)\, d\sigma$$

where

$$S^*(\psi) = S(\psi) - \sum_{n=2}^{\ell_{max}} \frac{2n+1}{n-1} P_n (\sin \phi) \quad \text{.... modified Stokes functions}$$

Δg_s ... gravity anomaly component implied by the GEM-10 potential coefficients

Δg_1 ... set of 20' x 20' mean gravity anomalies

Δg_2 ... set of 1° x 1° mean gravity anomalies

σ_1 ... inner zone of surrounding cap area (set of all points at a spherical distance $\psi \leq 1°$)

σ_2 ... outer zone of surrounding cap area (set of all points for which $1° < \psi \leq 10°$)

R ... mean radius of the earth

G ... mean value of gravity

$\bar{J}_{nm}, \bar{K}_{nm}$ .. GEM-10 potential coefficients up to degree $\ell_{max} = 30$

J'_{nm} ... potential coefficients of the normal field

$\bar{P}_{nm}$ ... fully normalized associated Legendre functions

N_o ... zero order undulation of the geoid.

Both geoids above were referred to a geocentric ellipsoid of adopted equatorial radius a = 6378135 m and implied flattening f = 1/298.257.

5.3.2 Some Basic Relations

As already stated, the ssh's obtained from the least squares adjustment referred to the ellipsoid adopted with the NWL 9D system. To compare these ssh's with corresponding gravimetric geoid heights the following formula (*Heiskanen and Moritz, 1967; Schaab and Groten, 1979*)

$$N^*_{ALT} - N_G = \Delta X \cos\phi \cos\lambda + \Delta Y \cos\phi \sin\lambda + \Delta Z \sin\phi + N_o$$

has been applied, where

$\Delta X, \Delta Y, \Delta Z$ are the coordinates of the origin of the altimetry reference ellipsoid,

N_G is the known gravimetric geoid undulation,

N^*_{ALT} is the altimetry derived ssh after transformation to a common reference ellipsoid, and

N_o has been defined above.

For the present comparisons we chose to use the WGS 72 ellipsoid, whose equatorial radius and flattening are the same as those used for the gravimetric undulations (the difference of 0.003 in f^{-1} can only contribute $\simeq$ 15 cm in the undulation difference at the latitude of Hudson Bay).

Using 16 polynomial coefficients resulting from the surface fitting of the adjusted ssh's, cf. section 5.2, we predicted several surface grid points by sampling corresponding ssh's in a 20' x 20' and a 0°.5 x 1° grid. A correction was then applied to these values to transform them from the NWL 9D to the WGS 72 by using *(Seppelin, 1974)*

$$N^{*}_{ALT}\ (\phi,\ \lambda) = N_{ALT}\ (\phi,\ \lambda) + a\ \Delta f \sin \phi - \Delta a + \Delta r$$

with

Δr = -5.27 metres

Δa = -10.0 metres

Δf = $-0.112415 \cdot 10^{-6}$

a = 6378135 metres.

Comparisons between N^{*}_{ALT} values and the two geoids were carried out by taking the differences $N^{*}_{ALT} - N_G$ at corresponding grid points under the assumptions of

(a) no origin shift between the two systems, i.e. constraining ΔX, ΔY, ΔZ to zero; and

(b) constraining ΔX,ΔY, ΔZ to the values recently reported in *Grappo and Huber (1979)*.

In such comparisons, the mean difference

$$\overline{\Delta N} = \frac{\sum_{i=1}^{n} (N^*_{ALT} - N_G)}{n}$$

from n points provides a measure of the zero order term of the geoid. Respectively, the rms difference between corresponding N^*_{ALT} and N_G values

$$\sigma_{\overline{\Delta N}} = \left\{ \frac{\sum_{i=1}^{n} (N^*_{ALT} - N_G - \overline{\Delta N})^2}{n-1} \right\}^{1/2}$$

provides a measure of the fit of the geoid model used to evaluate the N_G values to the altimetry derived sea surface represented by the N^*_{ALT} values.

5.3.3 Comparison of Results

Table 5.3a summarizes the results of the comparison between our altimetry derived sea surface in the Hudson Bay and the GSC and UNB gravimetric geoids, as well as the DMS GEOS-3 sea surface.

With the understanding that smaller rms difference values are indicative of a closer fit between compared surfaces, the closer agreement is readily noticeable, as it is to be anticipated, between the two altimetry data sets. The noted rms difference of $\pm$ 0.98 m may well be attributed both to the presence of unmodelled time varying effects in the sea surface and anticipated differences induced by the different reduction procedures used to obtain the adjusted altimetry data. Nevertheless, it provides a strong external indication of the consistency of our estimated

sea surface, and hence our estimation process. The comparisons with the GSC and UNB geoids suggest an equally satisfactory agreement, especially in view of the fact that N^*_{ALT} still contains short wavelength noise (due to residual instrumental effects and unmodelled sea surface variations), and it is an estimate of the sea surface rather than the geoid. The noted rms differences can be related to several causes including errors in the combined geoids, or short-period orbit errors affecting the radial component of the GEOS-3 orbital arcs (and hence the ssh structure) through wavelengths which cannot be absorbed into bias and tilt corrections. Errors of the first type may result from such sources as the terrestrial gravity data, the geopotential coefficients, the neglect of the presence of the atmosphere, truncation errors, etc. In the present case, the estimated accuracy of the GSC geoid is of the order of 1 m (*Lachapelle, 1979*), whereas error estimates due to the gravity data used in the computation of the UNB geoid undulations have been found (*John, 1980*) to be in the range from 0.3 m in the most of the southern part of Hudson Bay up to 1.8 m in the northern areas where gravity coverage is sparse (see figure 5.4c). Errors of the second type may occur, for instance, because of possible biases in the Doppler station coordinates and the Doppler orbit adjustment. Generally, the magnitude of such errors is unlikely to exceed a few decimeters (*Mather et al, 1977*), however, some level of spurious structure can be expected to be introduced into the sea surface and possibly be present in the given results.

The different mean offset (-0.33 m vs. -0.08 m) of the GEOS-3 sea surface with respect to the UNB and GSC geoids is likely to be related to a scale difference in the two geoids due to the use of different geopotential models. However, the rather large systematic offsets readily seen in the results using non-zero ΔX, ΔY, ΔZ can only be attributed

Table 5.3a

Comparisons of Gravimetric and Altimetry Derived Undulations (ssh's)

reduced with respect to Doppler Fitted Reference Orbits

	$N_{ALT,DMS}-N^*_{ALT}$	$N_{UNB}-N^*_{ALT}$	$N_{GSC}-N^*_{ALT}$
Mean Difference (metres)	-0.97	-0.33	-0.08
RMS Difference (metres)	(1.37) 0.98	(1.33)1.28	(1.26)1.26
Number of Comparisons	115	1141	244

N^*_{ALT} - UNB Altimetry Undulations (ssh's) after transformation from NWL 9D to WGS 72

$N_{ALT,DMA}$ - DMA Altimetry Undulations of 1° x 1° grid. Reference ellipsoid WGS 72 with a = 6378135 m, f = 1/298.26.

N_{UNB} - UNB Gravimetric Geoid (GEM-10 $+\Delta g$) on 20' x 20' grid. Reference ellipsoid with a = 6378135 m, f = 1/298.257.

N_{GSC} - GSC Gravimetric Geoid (GEM-10B$+\Delta g$) on 0.5 x 1° grid. Reference ellipsoid with a = 6378135 m, f = 1/298.257.

- Values in parentheses indicate RMS differences prior to removing the corresponding mean difference value

Table 5.3a Cont'd

Comparison of Gravimetric and Altimetry derived Undulations (N_{GSC}-N^{*}_{ALT}) assuming a shift of the altimetry system origin with respect to the center of mass of the earth

	(1)	(2)
Mean Difference (metres)	-3.67	-2.38
RMS Difference (metres)	(3.87) 1.24	(2.70) 1.26
Number of Comparisons	244	244

(1) - ΔX = 0.5, ΔY = 0.4, ΔZ = 4.4 metres (Grappo and Huber, 1979, investigation No. 1)

(2) - ΔX = 1.3, ΔY = 0.3, ΔZ = 2.8 metres (Grappo and Huber, 1979, investigation No. 2)

to the large ΔZ shift assumed between the origins of the ellipsoids of reference for the altimetry sea surface and the GSC geoid respectively. Presently these systematic offsets are considered with caution, especially in view of more recent results (*West, 1980*) which, in clear disagreement with *Grappo and Huber (1979)*, reveal nearly zero origin shifts lending by extent credence to the previous results using zero ΔX, ΔY, ΔZ.

The mean differences listed in table 5.3a also provide an insight into the implied equatorial radius of the best fitting ellipsoid to the sea surface in the Hudson Bay. If the weighted average of the mean differences $N^*_{ALT} - N^*_{UNB}$ set equal to δa and added to the adopted semi-major axis of the reference ellipsoid (a = 6378135 m) a value of the equatorial radius of the best fitting ellipsoid equal to 6378135.2 m would be obtained. This is 0.7 m greater than the value of 6378134.5 for the mean earth ellipsoid reported by *Lachapelle (1979)* as a result of a comparison of gravimetric geoid heights from GEM-10B potential coefficients and mean gravity anomaly data, and Canadian Doppler - derived geoid undulation sets. On the other hand, it is 1.8 m less than the value of 6378137 m recently reported by several investigators (*Rapp, 1979; Grappo and Huber, 1979; Mather and Rizos 1979*) and 3.8 m less than the value of 6378139 m obtained in the course of the development of GEM-10B (*Lerch et al, 1978*)"... from an altimeter range bias which was recovered from all GEOS-3 altimeter data orbitally reduced to GEM-10B". Such estimates are based on the analysis of geocentric tracking station coordinates along with estimates of the mean sea level

(MSL) obtained from levelling data sampled at coastal tide gauges. On the other hand the ellipsoid obtained from GEOS-3 data is the one that best fits MSL as sampled over the oceans. This can be expected to be somewhat lower than one which fits MSL in coastal areas due to the positive contribution by the topography and its isostatic compensation to the shape of the geoid in such areas (*Mather, 1978; Mather and Rizos, 1979*). In that sense, the value reported here of 6378135.2 m (which also agrees exactly with *West's (1980)* value), although determined from a single regional set of data, seems to corroborate this fact.

5.3.4 Mapping of Altimetry Derived Sea Surface

To gain a further insight on the sea surface features depicted by the GEOS-3 altimeter, the sea surface and the combined geoids used in the previous comparisons were contoured and plotted with the results shown in figures 5.3 through 5.5. As already pointed out due to the density of data involved the sea surface was sampled at grid points whose ssh's were predicted using the surface fitting technique described in section 5.2. The contour maps provided here have been plotted using grid points spaced at 1° and thereby reflect wavelengths greater than 200 km. The land features and coastline boundaries have been superimposed on the contours using a Cartographic Automatic Mapping program (*CAM, 1970*) available at UNB.

From figures 5.4b and 5.5b, which indicate the existing differences between the corresponding UNB and GSC geoids and the sea surface, it is evident that the largest differences occur in the edges

GEOS-3 ALTIMETRY SEA SURFACE
IN THE HUDSON BAY REGION
(Ref. Ell.: a = 6378135.00 m , f = 1 / 298.26·)

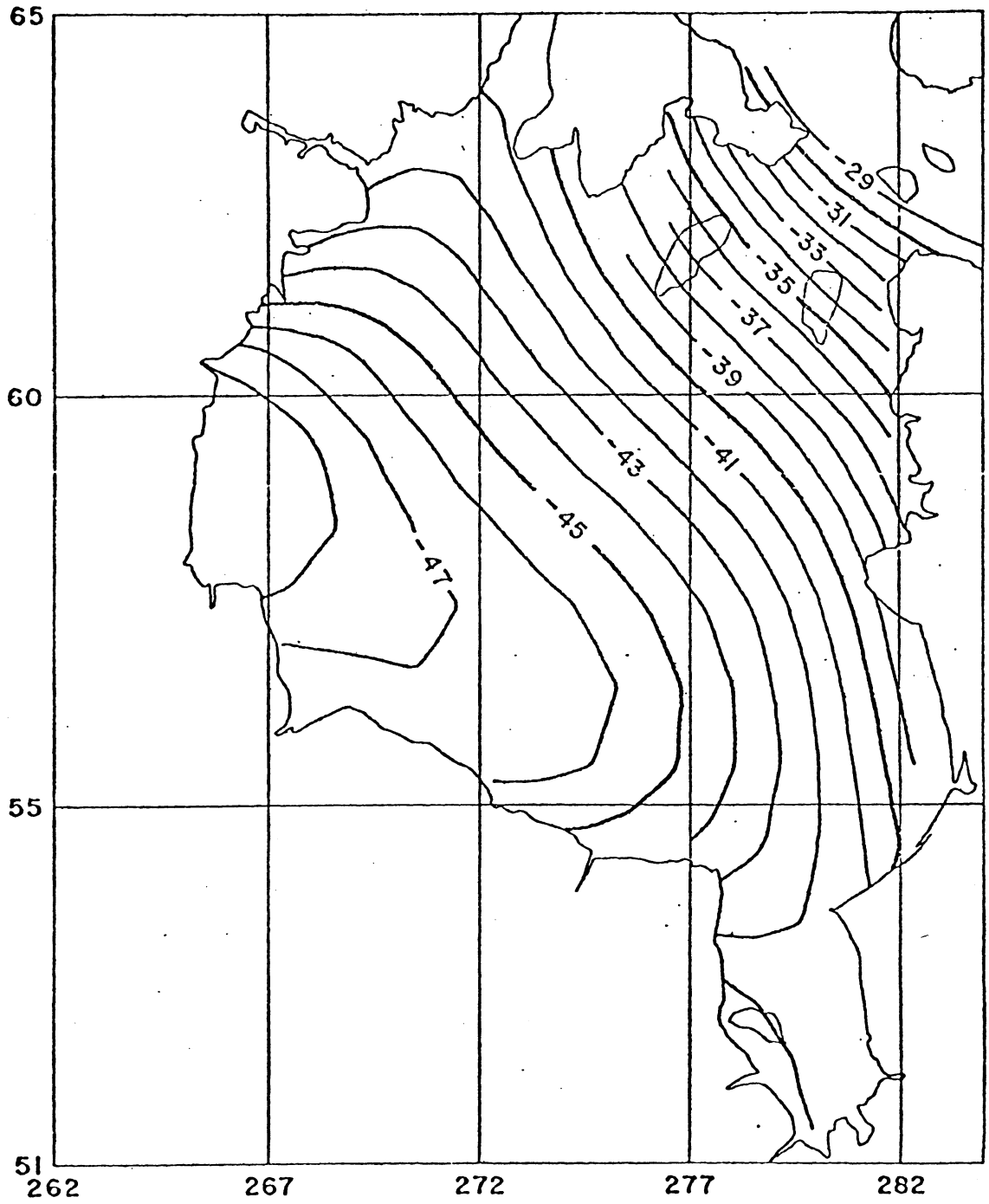

Figure 5.3

UNB GEOID FROM GEM-10 AND GRAVITY
IN THE HUDSON BAY REGION
(Ref. Ell. a = 6378135.00 m , f = 1/298.26·)

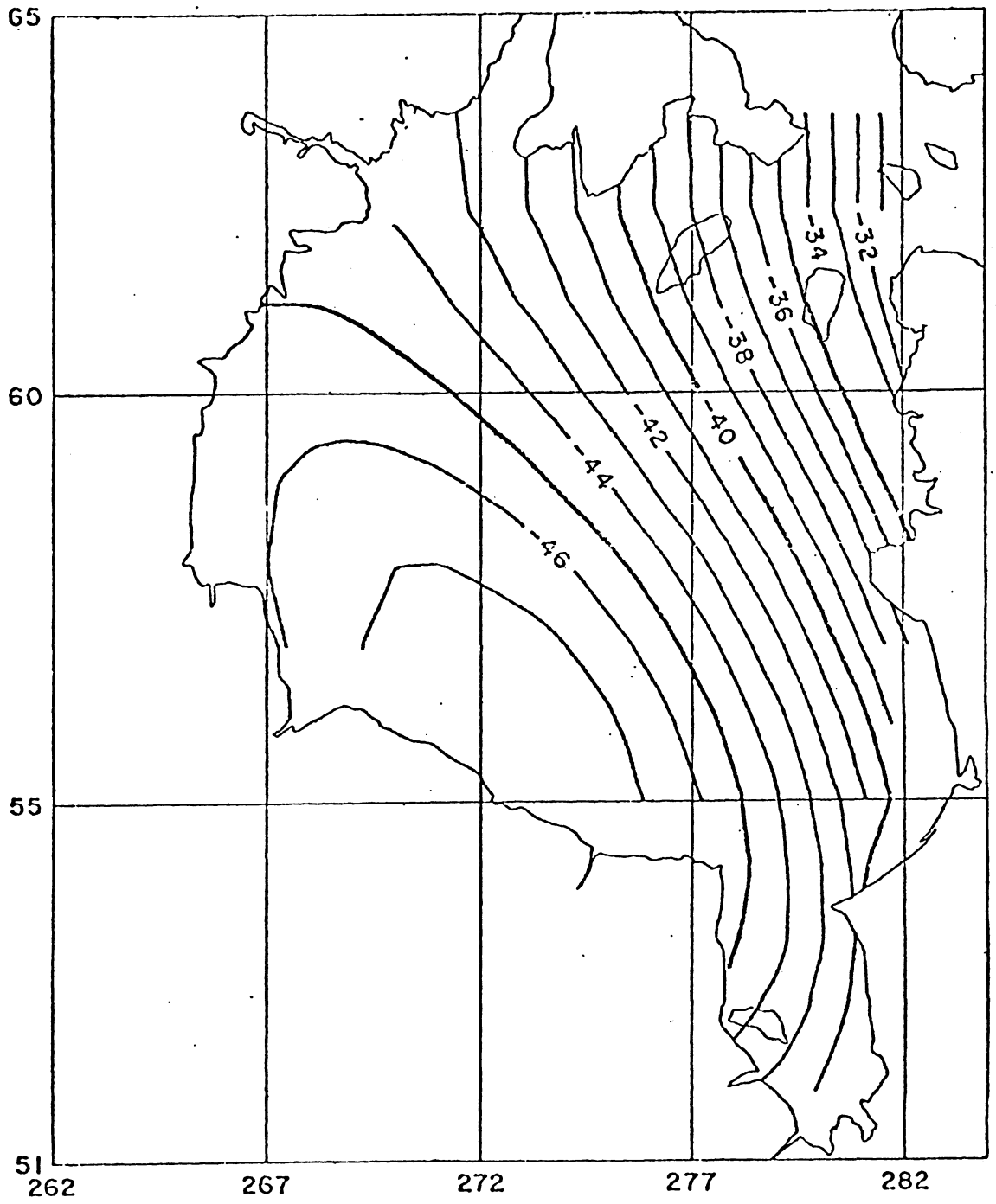

Figure 5.4a

HUDSON BAY REGION

UNB GEOID - GEOS-3 SEA SURFACE

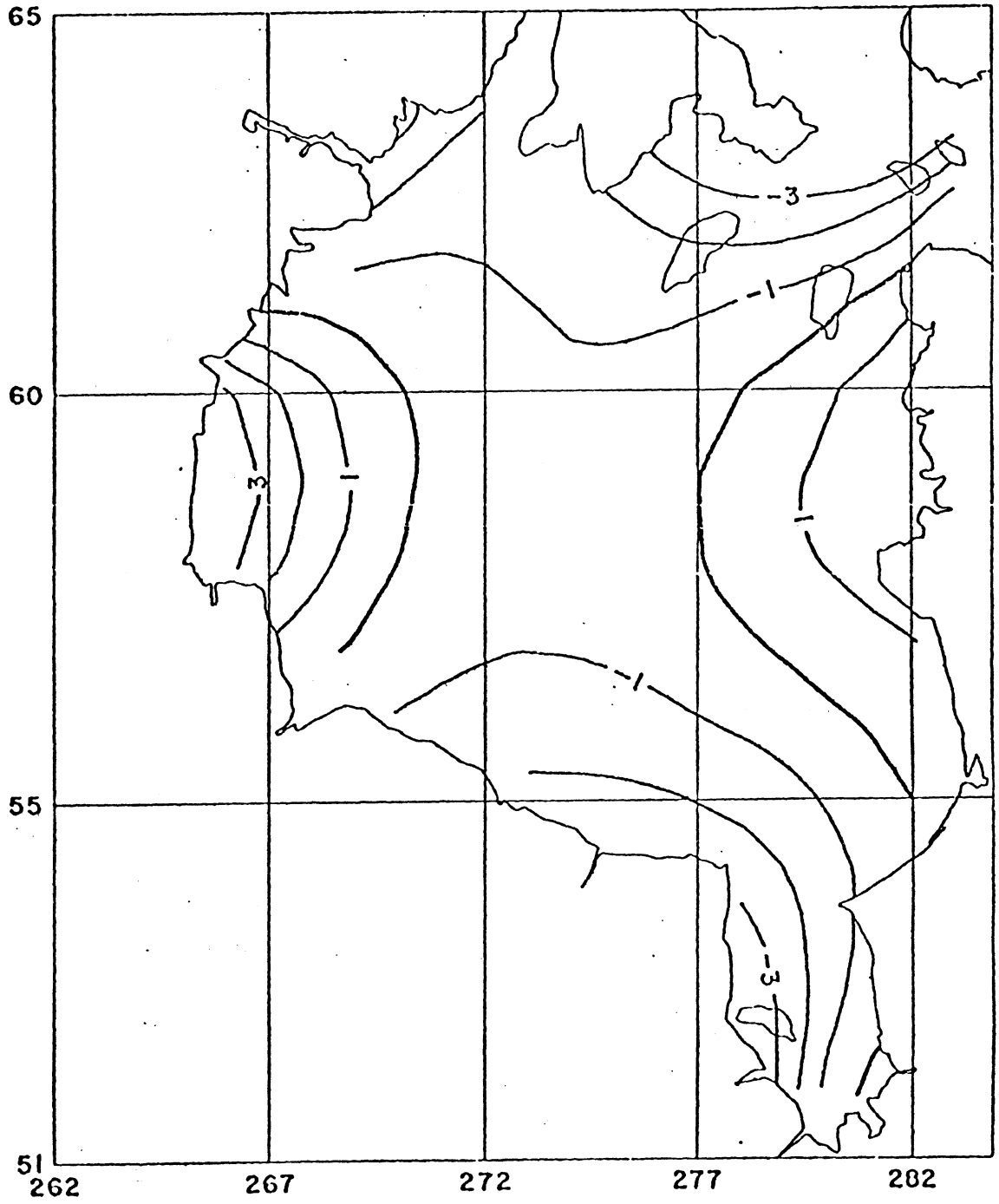

Figure 5.4b

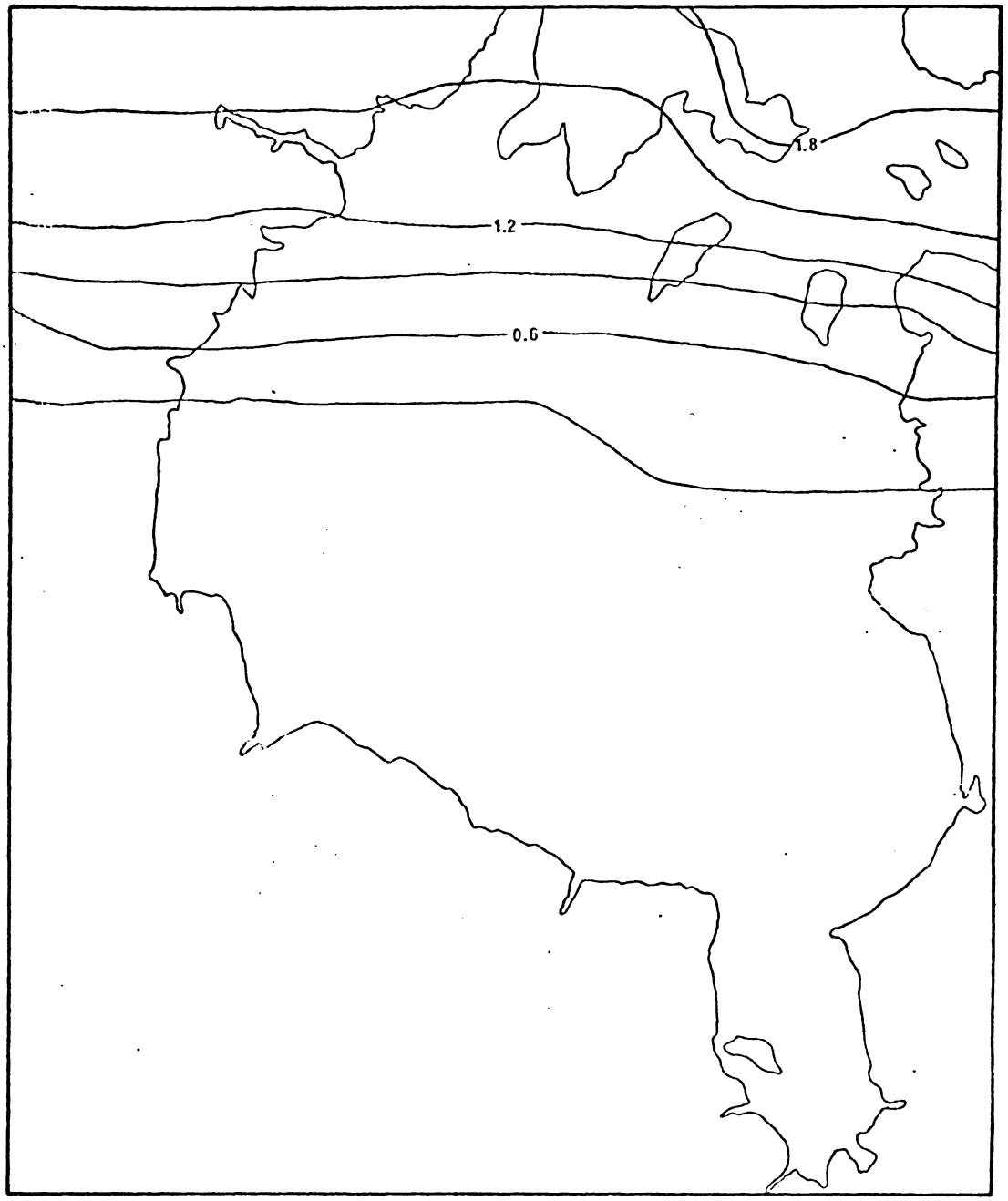

Figure 5.4c

ESTIMATED ERRORS IN THE HUDSON BAY GEOID (m)
(After John , 1980)

GSC GEOID FROM GEM-10B AND GRAVITY
IN THE HUDSON BAY REGION
(Ref. Ell.: a = 6378135.00 m , f = 1/298.26·)

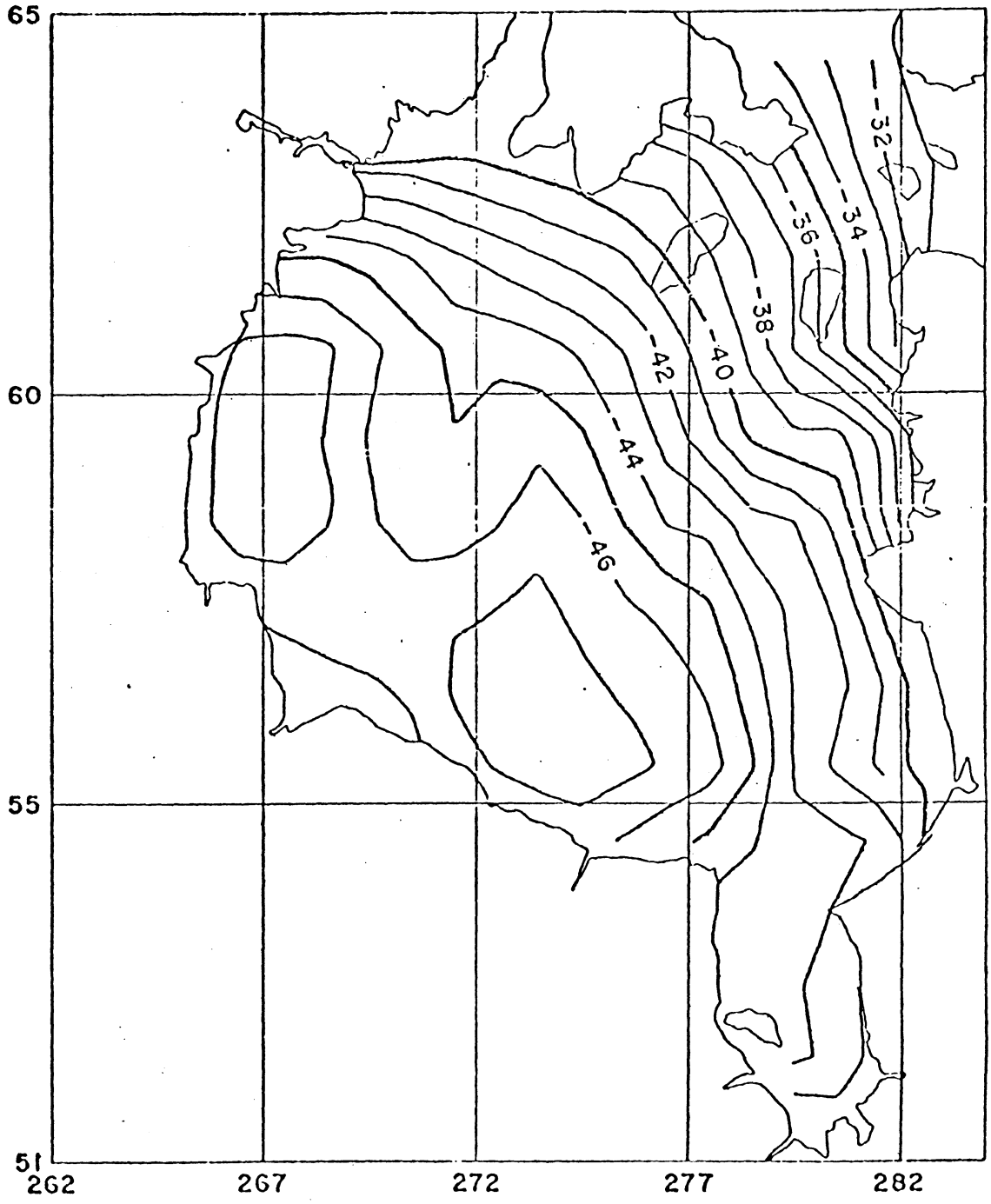

Figure 5.5a

HUDSON BAY REGION

GSC GEOID - GEOS-3 SEA SURFACE

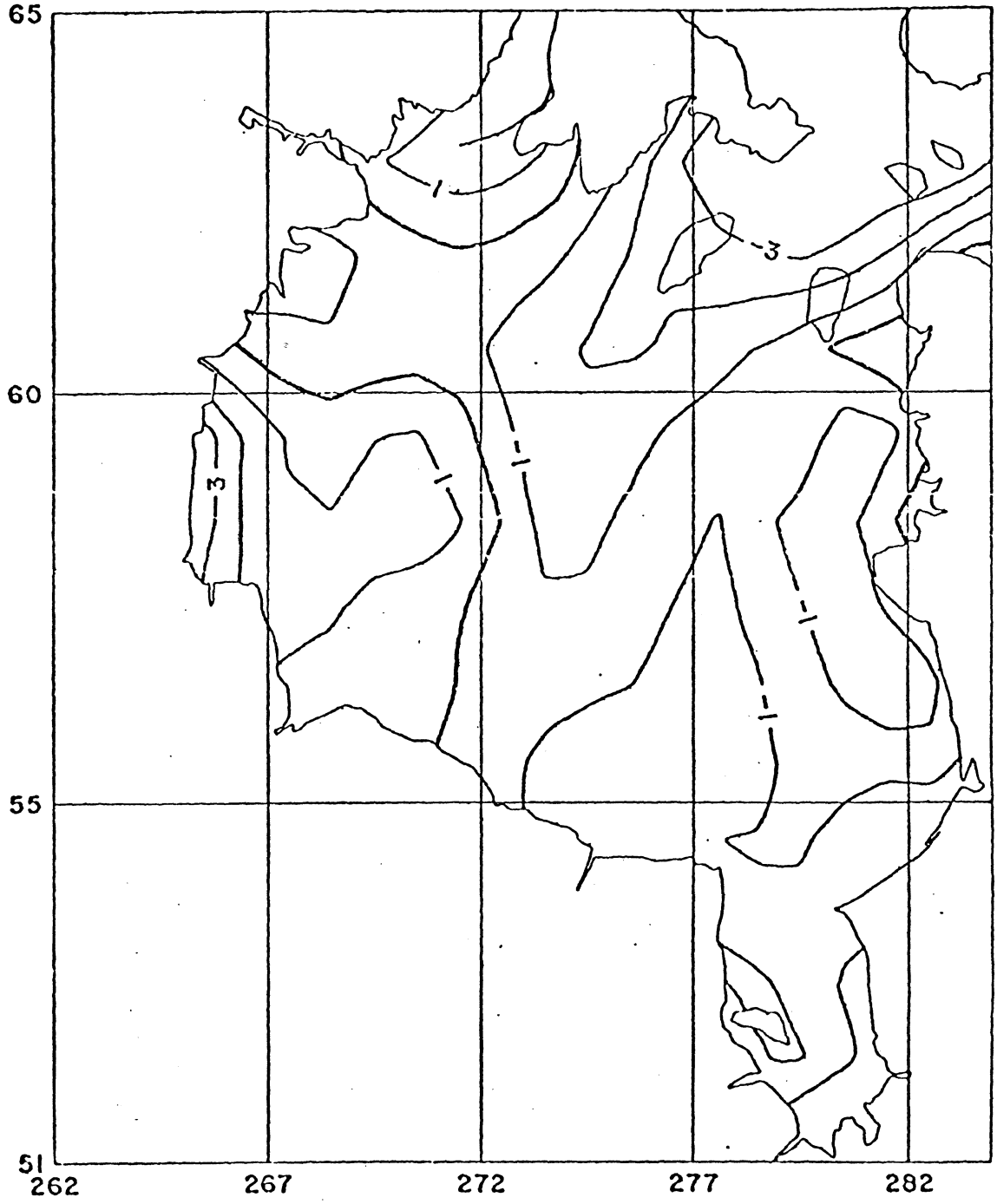

Figure 5.5b

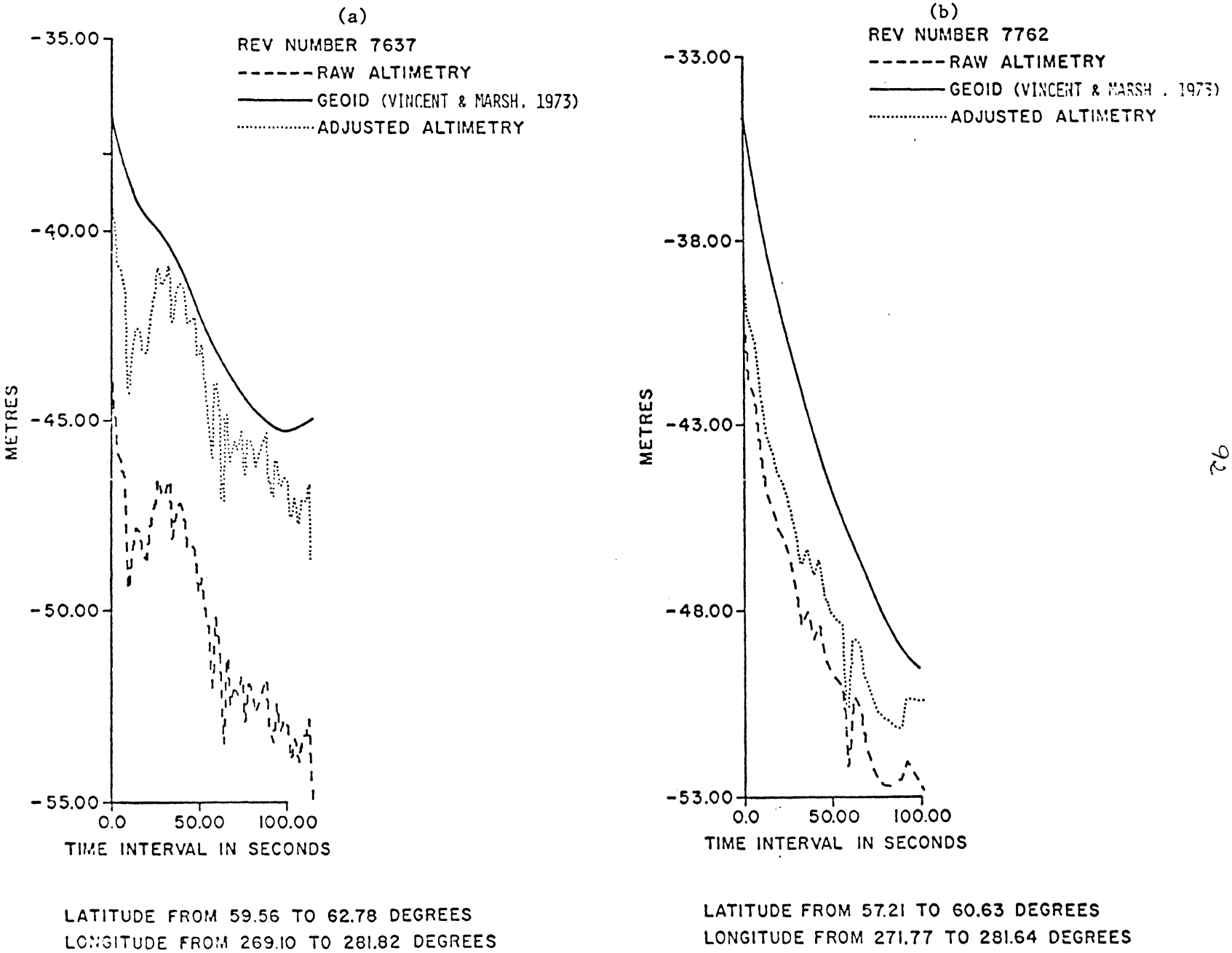

Figure 5.6 Example of GEOS-3 Sea Surface Profiles in Different Stages of Processing

of the sea surface, where moreover the accuracy of prediction is small, and in the areas of steepest gradient of the geoid heights such as for instance at the northeast areas of Coats and Mansel islands. However, all known geoidal features of the geoid, such as the slope from northeast to southwest with the lowest value of about -48 metres occuring at approximately 60° N latitude and 262° E longitude, are very well depicted.

Completely independent tests were also made by comparing geoidal profiles with ssh profiles obtained from the GEOS-3 altimetry data. Such profiles are more appropriate to detect any time varying components in the sea surface and resolve the shortest wavelengths of the ssh structure, which otherwise tend to be smoothed out by the surface fitting procedure or tacitly ignored by choosing to use only the mean of the two ssh's at each crossover point after the adjustment. Figures 5.6a, b are examples of such comparisons showing two arbitrarily chosen data profiles along rev. 7637 (mean epoch - YYMMDD: 760930, HHMMSS: 190821 UTC) and rev. 7762 (mean epoch - YYMMDD: 761009, HHMMSS: 151850 UTC) in their different stages of processing. In either case short wavelength features, sometimes as small as 1 metre, are shown by the altimeter measurements. To identify these variations as actual geoid height fluctuations is difficult to accomplish at this stage. Such a task would only be possible if additional oceanographic information, repeated altimetry and precise sea gravimetric measurements or a combination of all become available.

5.4 Some Additional Results

It is appropriate to conclude this discussion of the comparison of our estimated sea surface and the geoid by looking into the results obtained from similar comparisons when the altimetry data was reduced with respect to the originally supplied NASA (WFC) orbits. Table 5.3b summarizes the results from these comparisons. The mean and rms

Table 5.3b

Comparisons of Gravimetric and Altimetry Derived Undulations (ssh's)

reduced with respect to NASA supplied Reference Orbits

	$N_{ALT,DMA}-N^*_{ALT}$		$N_{UNB}-N^*_{ALT}$		$N_{GSC}-N^*_{ALT}$	
Mean Difference (metres)		-2.00		1.41		-1.11
RMS Difference (metres)	(2.25)	1.03	(2.05)	1.48	(1.62)	1.18
Number of Comparisons		115		128		244

N^*_{ALT} - UNB Altimetry Undulations (ssh's) after transformation from NWL 9D to WGS 72

$N_{ALT,DMA}$ - DMA Altimetry Undulations on 1° x 1° grid. Reference ellipsoid WGS 72 with a = 6378135 m, f = 1/298.26.

N_{UNB} - UNB Gravimetric Geoid (GEM-10+Δg) on 1° x 1° grid. Reference ellipsoid with a = 6378135 m, f = 1/298.257.

N_{GSC} - GSC Gravimetric Geoid (GEM-10B+Δg) on 0.5 x 1° grid. Reference ellipsoid with a = 6378135 m, f = 1/298.257.

- Values in parentheses indicate RMS differences prior to removing the corresponding mean difference value

Table 5.3b Cont'd

Comparison of Gravimetric and Altimetry derived Undulations

$(N_{GSC}-N^{*}_{ALT})$ assuming a shift of the altimetry system orign

with respect to the center of mass of the earth

		(1)		(2)
Mean Difference (metres)		4.70		-3.71
RMS Difference (metres)	(4.84)	1.16	(3.62)	1.21
Number of Comparisons		244		244

(1) - $\Delta X = 0.5$, $\Delta Y = 0.4$, $\Delta Z = 4.4$ metres (Grappo and Huber, 1979, investigation No. 1)

(2) - $\Delta X = 1.3$, $\Delta Y = 0.3$, $\Delta Z = 2.8$ metres (Grappo and Huber, 1979, investigation No. 2)

differences indicated should be viewed in connection with the results listed on table 5.2b and should be compared with the corresponding values given in table 5.3a.

Differences taken between our estimated ssh's and those corresponding to the DMA GEOS-3 geoid showed a mean difference of -2.00 m, with a rms difference of $\pm$ 2.25 m prior to removing the above mean difference. In doing so a value of $\pm$ 1.03 m was obtained.

A comparison of these results with those listed in table 5.3a suggests no significant difference in the fit (implied by the rms values) of our estimated sea surface with the DMA GEOS-3 version when going from the altimetry data set reduced with the Doppler fitted orbits to the data set reduced with the originally supplied WFC orbits. There is, however, a noticeable mean offset of 1.03 m suggesting an equal radial shift in the sea surface when going from one set of orbits to the other. There is a number of factors which could account for these differences, namely the presence in the WFC orbits of significant radial biases between ascending and descending passes in areas such as the Hudson Bay (attributed mainly to the global tracking station complement used by NASA in computing these long arc orbits), which were partially removed by using short spans of Doppler data in the present solution (the noted (table 5.2b) mean crossover difference of 1.41 m seems to corroborate this fact).

A comparison of the GSC geoid with the same sea surface solution showed a mean difference of -1.11 m as compared to -0.08 m obtained from the sea surface solution oriented using the short arc Doppler fitted orbits. The better fit, implied by the noted rms difference of 1.18 m as compared to 1.26 m, shown between the GSC geoid and the sea surface oriented using the WFC orbits can be regarded as a positive indication that indeed some spurious

structure (at the decimeter level) was introduced into the sea surface as a result of the Doppler orbit adjustment. However, at the noise level of the altimetry data this difference in the fit between the two surfaces is not considered to be significant. Similar results were obtained from the comparison with the UNB gravimetric geoid. In view of this evidence, it can be reasonably concluded that the short arc Doppler fitted orbits were accurate enough to provide a reliable regional orientation of the estimated sea surface on the Hudson Bay.

SECTION 6

SUMMARY AND CONCLUSIONS

In the preceeding sections a procedure for determining the sea surface in the Hudson Bay from GEOS-3 satellite altimetry data has been described. An analysis of a set of altimetry data collected from September to December 1976 has indicated the data's utility to the determination of the sea surface to an estimated accuracy better than one metre. While the results presented here have been based on assumptions and decisions pertaining to the intended application of the Hudson Bay Experiment, the following summary will serve to highlight the strengths and weaknesses of the estimation process used in this study and hence usefully direct further investigations towards future applications.

(1) A regional improvement of the orbits required to reduce the altimetry data seems to be possible from supplementary Doppler tracking in the area of interest. Evidence supporting this agrument has been provided in the context of the present study from the comparison of the estimated sea surface against the best available geoids in the Hudson Bay. This facility may be further enhanced in future study areas by making an effort in attaining maximum geometric strength of the

tracking network/satellite orbits configuration. From the Canadian viewpoint, since most of the future potential users of the altimetry system have already indicated the main areas of interest (*Hodgson, 1973; Wells, 1976*) it should be relatively easy to determine the optimum network configuration by means of simulations conducted for these areas.

(2) The need of modelling the various effects due to the dynamics of the sea surface has been emphasized in several instances. Of these, the sea tide effect is relatively easy to account for if a suitable tidal model is used. This was done in the context of the present study using a specially developed analytical tidal model based on the work of *Freeman and Murty (1976)*. A test adjustment for the purpose of examining the appropriateness of the developed tidal model, while it produced no significant changes on the statistics of the regional solution for the sea surface when the tide correction was suppressed, it resulted in the tide effects being absorbed into the recovered orbital biases, which in turn caused changes in the adjusted ssh's up to ~1.5 m relative to their previously determined values. This suggests that the possibility still exists that the results can be further refined if a more accurate tidal model is used. In this context, the newly developed global tidal model by *Schwiderski (1978)*, which is claimed to be accurate to 10 cm anywhere in the world oceans, should be considered as an obvious candidate. Modelling of other physical influences on the sea level, other than tide, should also be considered. Although in the present study lack of pertinent information

precluded any such effort, in future studies it is important that at least some of the known physical influences on the sea surface be removed from the data by means of the best currently available models (e.g. *Vanicek, 1978; Anderson, 1978*). This would require modelling of storm surges coupled with synoptic information and readily available long-term data, such as air/water temperatures, atmospheric pressure, geostrophic and/or local wind velocities, etc., collected on a regular basis. This is a critical factor inherent in this approach.

(3) The modelling process of residual orbit biases by a simple polynomial in time, together with crossover constraints of the intersections of satellite sub-tracks of different satellite passes contributes significantly to the removal of orbit errors due possibly to unmodelled gravity field effects. For the short arcs in Hudson Bay the modelling of orbit errors for each arc by an absolute bias and a tilt (bias rate) produced satisfactory results. The inclusion of a second order effect marginally affected the results, as was to be expected. This, however, may be usefully pursued in the case of longer arcs.

(4) When the above approach was taken, the orbit relaxation was also restricted in the sense that a priori weights were assigned to each of the orbit bias components. Aside from the intention of making use of all available information about the orbit biases, applying weighted constraints in the estimation process would also be

related to the inherent rank deficiency or ill-conditioning of the problem. This is because an adjustment set up only in terms of crossover ssh differences, much the same way as a free network, can define the shape of the estimated sea surface; however, it does not provide any information on the orientation and position of the entire surface. To alleviate this problem the approach of weighted constraints was used here to improve the condition of the normal equations which otherwise would be unsolvable in the domain of ordinary matrix algebra. The alternatives would be an "inner constraints" approach (*Vanicek and Krakiwsky, in prep.*) or a generalized inverses approach (*Rao, 1973; Bjerhammar, 1973*). There seems to be no compelling reason to choose one of these alternatives. It is noted, however, that if the first approach is taken, strictly speaking it would require a full covariance matrix reflecting the a priori distribution of the error parameters used. In rare circumstances such a full matrix will be available from a previous solution (primary adjustment on a global basis perhaps) which may be used, in turn, in the new (regional) adjustment to anchor the solution with respect to some well defined control orbits. If, however, only a diagonal weight matrix is used (as it was done here) derived from assumed standard deviations of the a priori estimates of the parameters, then the estimated parameters are not unbiased any longer, since the arbitrary diagonalization of the covariance marrix has changed the a priori distribution of the parameters from the one normally reflected by the full matrix. The implications and risks involved in this practice are obvious. The

application of "poor" or "over-weighted" constraints may very well result on unreasonable distortion of the results or occasionally even indicate non-existant inconsistencies in the observations. At present the best alternative seems that the a priori information available about the parameters be used in the post-estimation analysis of these parameters. The confidence interval associated with the resulting error parameters must be in agreement with the prior distributions assumed in the estimation procedure [*Vanicek and Krakiwsky, ch. 13, in prep.*]. Otherwise, a revision of the assumptions becomes necessary. These should be considered if the already developed software for this study is modified.

(5) The complete set of adjusted altimetric profiles (section 5.3) should be examined in more detail. As already has been pointed out such profiles are more appropriate to detect any time varying components on the sea surface and resolve the shortest wavelengths of the ssh structure. These data would therefore be used to address the inverse problem, i.e. whether one can learn anything about the non-tidal sea surface effects from the detailed differences between the reference geoid and the complete altimetric profiles. This task would require a finer resolution geoid portraying wavelengths shorter than those resolved by averaging gravity values over 1° squares. This is a critical factor inherent in this approach. A possible alternative would be to perform an analysis on the data as a time series (i.e. data sampled uniformly on time) and interpret the results in terms of physical wavelengths in a manner similar to Wagner's (1979) or Brammer's (1979) analysis.

APPENDIX A

OUTLINE OF A PRACTICAL SOLUTION OF THE NORMAL EQUATIONS IN A LEAST SQUARES ADJUSTMENT OF ALTIMETRY INTERSECTING ARCS BY PARTITIONING AND SUCCESSIVE SUMMATION OF NORMAL EQUATIONS.

As already pointed out in section 4.3, the partitioning of altimetry intersecting arcs into groups of ascending (S/N) and descending (N/S) passes, leads to a system of normal equations with a coefficient matrix assuming a bordered, block-diagonal structure, which can be conveniently exploited to allow a computationally efficient solution. The task of this section is to provide a concise computational outline of this solution.

To begin with, let us return to the system of the normal equations having the particular structure of eqn. (4.14b)

$$\begin{vmatrix} N'_1 & & & & & \bar{N}_1 \\ & N'_2 & & & & \bar{N}_2 \\ & & N'_3 & & & \bar{N}_3 \\ & & & \ddots & & \vdots \\ & & & & N'_n & \bar{N}_n \\ \bar{N}_1^T & \bar{N}_2^T & \bar{N}_3^T & \cdots & \bar{N}_n^T & N'' \end{vmatrix} \begin{vmatrix} X'_1 \\ X'_2 \\ X'_3 \\ \vdots \\ X'_n \\ X'' \end{vmatrix} + \begin{vmatrix} U'_1 \\ U'_2 \\ U'_3 \\ \vdots \\ U'_n \end{vmatrix} = 0 \qquad \text{(A-1a)}$$

where

$$N'' = \sum_{k=1}^{n} N''_k = \sum_{k=1}^{n} A''^T_k \, P_k \, A''_k \qquad \text{(A-2a)}$$

$$U'' = \sum_{k=1}^{n} U_k'' = \sum_{k=1}^{n} A_k''^T P_k W_k \qquad \text{(A-2b)}$$

$$N_k' = A_k'^T P_k A_k' \qquad \text{(A-2c)}$$

$$\bar{N}_k = A_k'^T P_k A_k'' \qquad \text{(A-2d)}$$

$$U_k' = A_k'^T P_k W_k \qquad \text{(A-2e)}$$

with all notations being the same as those encountered in the early part of section 4.3.

In a more compact form, the coefficient matrix in the above normal equations can be written as

$$N \equiv \begin{vmatrix} N' & \bar{N} \\ \bar{N}^T & N'' \end{vmatrix} . \qquad \text{(A-1b)}$$

Next, let the inverse of N be

$$M = N^{-1} = \begin{vmatrix} M' & \bar{M} \\ \bar{M}^T & M'' \end{vmatrix} \qquad \text{(A-3)}$$

where M', M'', $\bar{M}$ are each of the same order as their respective counterparts N', N'', $\bar{N}$, in N. From the basic definition of the inverse we have $NN^{-1} = NM = I$, or in partitioned form

$$\begin{vmatrix} N' & \bar{N} \\ \bar{N}^T & N'' \end{vmatrix} \begin{vmatrix} M' & \bar{M} \\ \bar{M}^T & M'' \end{vmatrix} = \begin{vmatrix} I & 0 \\ 0 & I \end{vmatrix}$$

which leads to

$$N'M' + \bar{N}\bar{M}^T = I \qquad \text{(A-4a)}$$

$$N'\bar{M} + \bar{N}M'' = 0 \qquad \text{(A-4b)}$$

$$\bar{N}^T M' + N''\bar{M}^T = 0 \qquad \text{(A-4c)}$$

$$\bar{N}^T\bar{M} + N''M'' = I \qquad \text{(A-4d)}$$

Solving (A-4b) for $\bar{M}$ in terms of M'' yields

$$\bar{M} = -N'^{-1}\,\bar{N}\,M'' \qquad \text{(A-5a)}$$

and upon substituting into (A-4d)

$$M'' = (N'' - \bar{N}^T N'^{-1}\,\bar{N})^{-1} \qquad \text{(A-5b)}$$

Once M'' has been obtained, the result can be substituted in (A-5a) to obtain $\bar{M}$ and in turn in (A-4a) to obtain M' as

$$M' = N'^{-1} + N'^{-1}\,\bar{N}\,M''\,\bar{N}^T N'^{-1} \qquad \text{(A-5c)}$$

Thereafter the formal solution of the original normal equations (4.14b) may be readily written as

$$X \equiv \begin{vmatrix} X' \\ X'' \end{vmatrix} = \begin{vmatrix} N' & \bar{N} \\ \bar{N}^T & N'' \end{vmatrix} \begin{vmatrix} U' \\ U'' \end{vmatrix} = \begin{vmatrix} M' & \bar{M} \\ \bar{M}^T & M'' \end{vmatrix} \begin{vmatrix} U' \\ U'' \end{vmatrix} \qquad \text{(A-6)}$$

or

$$X' = M'U' + \bar{M}\,U'' \qquad \text{(A-7a)}$$

$$X'' = \bar{M}^T\,U' + M''U'' \qquad \text{(A-7b)}$$

and upon utilizing the expressions (A-5) for M', M'', and $\bar{M}$, eqn. (A-7a) becomes

$$X' = N'^{-1} U' + N'^{-1} \bar{N} M'' \bar{N}^T N'^{-1} U' - N'^{-1} \bar{N} M'' U''$$

$$= N'^{-1} U' + N'^{-1} \bar{N} \underbrace{M'' (\bar{N}^T N'^{-1} U' - U'')}_{X''} \qquad \text{(A-8a)}$$

and eqn. (A-7b) becomes

$$X'' = - M'' \bar{N}^T N'^{-1} U' + M'' U''$$

$$= M'' (U'' - \bar{N}^T N'^{-1} U') \; . \qquad \text{(A-8b)}$$

Taking advantage of the block diagonal structure of N' in eqn. (A-1a), N'^{-1} is readily obtained as

$$N'^{-1} = \text{diag} \; (N_1'^{-1} \; N_2'^{-1} \; N_3'^{-1} \; \ldots \; N_n'^{-1}) \; . \qquad \text{(A-9)}$$

Furthermore since $\bar{N}$ is of the form

$$\bar{N} = (\bar{N}_1 \; \bar{N}_2 \; \bar{N}_3 \; \ldots \; \bar{N}_n) \qquad \text{(A-10)}$$

the expression $Q \equiv \bar{N}^T N'^{-1}$ becomes

$$Q = [\bar{N}_1^T N_1'^{-1} \; \bar{N}_2^T N_2'^{-1} \; \bar{N}_3^T N_3'^{-1} \; \ldots \; \bar{N}_n^T N_n'^{-1}]^T$$

$$= [Q_1 \; Q_2 \; Q_3 \; \ldots \; Q_n]^T \qquad \text{(A-11)}$$

and the expression $R \equiv \bar{N}^T N'^{-1} N = Q\bar{N}$ becomes

$$\bar{R} = \bar{N}_1^T N_1'^{-1} \bar{N}_1 + \bar{N}_2^T N_2'^{-1} \bar{N}_2 + \ldots + \bar{N}_n^T N_n'^{-1} \bar{N}_n$$

$$= Q_1 \bar{N}_1 + Q_2 \bar{N}_2 + \ldots + Q_n \bar{N}_n$$

$$= R_1 + R_2 + \ldots + R_n = \sum_{k=1}^{n} R_k \qquad \text{(A-12)}$$

Recalling eqn. (A-2a), (A-2b), M'' can be written by virtue of eqn. (A-12) as

$$M'' = N_1'' + N_2'' + \ldots + N_n'' - (R_1 + R_2 + \ldots + R_n)$$

$$= (N_1'' - R_1) + (N_2'' - R_2) + \ldots + (N_n'' - R_n)$$

$$= S_1 + S_2 + \ldots + S_n = \sum_{k=1}^{n} S_k \qquad \text{(A-13)}$$

So that the expression in parenthesis in eqn. (A-8b) becomes

$$U'' - \bar{N}^T N'^{-1} U' = (U_1'' + U_2'' + \ldots + U_n'') - (Q_1 U_1' + Q_2 U_2' + \ldots + Q_n U_n')$$

$$= (U_1'' - Q_1 U_1') + (U_2'' - Q_2 U_2') + \ldots + (U_n'' - Q_n U_n')$$

$$= \tilde{U}_1 + \tilde{U}_2 + \ldots + \tilde{U}_n = \sum_{k=1}^{n} \tilde{U} \qquad \text{(A-14)}$$

where

$$\tilde{U}_k = U_k'' - Q_k U_k' \quad , \qquad \text{(A-15)}$$

leading eventually to the solution for X''

$$X'' = M'' \sum_{k=1}^{n} [A_k''^T P_k W_k - A_k''^T P_k A' (A_k'^T P_k A_k')^{-1} A_k'^T P_k W_k] \qquad \text{(A-16)}$$

which is the same as eqn. (4-16a).

Similarly as a consequence of the block diagonal structure of N' it can easily be seen that the expression (A-8a) for X' can be written as

$$X' = \begin{vmatrix} X'_1 \\ X'_2 \\ \cdot \\ \cdot \\ \cdot \\ X'_n \end{vmatrix} = \begin{vmatrix} N'_1 & 0 & & & 0 \\ 0 & N'_2 & & & 0 \\ & & \cdot & & \cdot \\ & & & \cdot & \cdot \\ & & & & \cdot \\ 0 & 0 & \cdots & \cdot & N'_n \end{vmatrix} \begin{vmatrix} U'_1 \\ U'_2 \\ \cdot \\ \cdot \\ \cdot \\ U'_n \end{vmatrix} - \begin{vmatrix} Q_1 \\ Q_2 \\ \cdot \\ \cdot \\ \cdot \\ Q_n \end{vmatrix} X''$$

from which it follows that every vector X'_k can be determined independently as

$$X'_k = N'^{-1}_k U'_k - Q_k X''$$

$$= (A'^T_k P_k A'_k)^{-1} A'^T_k P_k W_k - (A'^T_k P_k A'_k)^{-1} A'^T_k P_k A''_k X''$$

the same as eqn. (4-16b) once the vector X'' has been obtained.

The computational flow of the entire process is easy to visualize: For the k-th group of observations the set of the following arrays is available: A'_k, A''_k, P_k, W_k.

Starting with k = 1, the following arrays can be computed

$$N'_k = A'^T_k P_k A'_k$$

$$N''_k = A''^T_k P_k A''_k$$

$$\overline{N}_k = A'^T_k P_k A''_k$$

$$U'_k = A'^T_k P_k W_k$$

$$U''_k = A''^T_k P_k W_k .$$

In turn the following auxiliary arrays are computed:

$$Q_k = \bar{N}_k^T \, N_k'^{-1}$$

$$R_k = Q_k \, \bar{N}_k$$

$$S_k = N_k'' - R_k$$

$$\tilde{U}_k = U_k'' - Q_k \, U_k'$$

As S_k, $\tilde{U}_k$ are computed, they are added to the sum of their predecessors and culmulative sum is retained. Repeating the process sequentially for n groups of observations the final values of

$$S = \sum_{k=1}^{n} S_k$$

and

$$\tilde{U} = \sum_{k=1}^{n} \tilde{U}_k$$

are obtained.

The solution for X'' follows immediately from

$$X'' = M'' \, \tilde{U}$$

in which $M'' = S^{-1}$ is also the covariance matrix of X''. The solution for each subvector X_k' is then obtained as

$$X_k' = N_k'^{-1} \, U_k' - Q_k \, X''$$

with the corresponding covariance matrix computed from, cf. section 4.4

$$\hat{C}_{X_k'} = N'^{-1} + Q_k \, M'' Q_k^t \quad .$$

This completes the derivational development of the practical solution of the system of normal equations having the particular block-diagonal structure of eqn. (A-1a) or (4.14b) resulting from

appropriate partitioning of a set of altimetry arcs in a crossover least squares adjustment into groups of S/N and N/S arcs.

APPENDIX B

DESCRIPTION OF BIO SUBSETS OF GEOS-3 ALTIMETRY DATA

GEOS-3 radar altimeter data are recorded in either of two formats, the low data rate (LDR) or high data rate (HDR), each of which is defined here in detail for the altimeter data user. All altimeter related measurements, calculated parameter and various indicators included in the BIO subsets used in this study are indicated in table B.1. Parameters included in the original NASA records, but not in the BIO subsets, are also indicated for completeness. Samples of the BIO LDR and HDR records are given in tables B.2 and B.3. Further information can be obtained by referencing the appropriate GEOS-3 preprocessing report by *Leitao et al* [1975].

Table B.1

Description of GEOS-3 radar altimetry data records

PARAMETER NAME	LOW DATA RATE SAMPLE SIZE	LOW DATA RATE INDEX	HIGH DATA RATE SAMPLE SIZE	HIGH DATA RATE INDEX	VALUE RANGE	DESCRIPTION (UNITS)
RECSIZ	1	1	1	1	538,15190	BYTES/REC ON NASA TAPE
SATID	1	2	1	2	always 7502701	SATELLITE ID
MTYPE	1	3	1	3	40 or 41	MEASUREMENT TYPE (40=Long Pulse, 41=Short Pulse)
TSIND	1	4	1	4	always 23	UTC, GROUND TRANSMITTED
STNUMB	1	5	1	5	always 0	STATION
PREPIN	1	6	1	6	13101,23101	TROPO/IONO CORRECTION UNAPPLIED
MJDATE	1	7	1	7	43028-43117	MODIFIED JULIAN DATE
FODAY	1	8	1	8		μsec PAST MIDNIGHT
SMOALT	1	9	1	9		ALT @ FODAY (Linear Fit to CALT) (cm)
LAT	1	10	1	10		SATELLITE LATITUDE (Degrees x 10^4)
LONG	1	11	1	11		" LONGITUDE (Degrees x 10^4)
ASIGMA	1	12	1	12		STD. DEV. OF SMOALT (Linear Fit) (cm)
ABIAS	1	13	1	13	always 0	ALTIMETER BIAS
TREF	1	14	1	14		TROPOSPHERIC CORRECTION (cm)
IREF	1	15	1	15	always 0	IONOSPHERIC CORRECTION (cm)
GHITE	1	16	1	16		GEOID HEIGHT @ FODAY (cm)
THITE	1	17	1	17		TIDE HEIGHT @ FODAY (cm)
FRAMTI	1	18	1	18		START OF FRAME TIME (μsec)
DOY	1	19	1	19	251-340	DAY OF YEAR
YEAR	1	20	1	20	always 76	YEAR
CALT	20	21-40	32	21-52		CUMULATIVE ALTITUDE (cm)
SAT	20	41-60	32	53-84		SATELLITE HEIGHT (cm)
CSIGH	1	61	1	85	always 1000	STD. DEV. OF SATHT (cm)
AS	20	62-81	64	86-149		ALTIMETER STATUS
* ARS	16		16			RADAR ALTIMETER AVERAGE RETURN SAMPLES (mv)
RSE	20	82-101	32	150-181		RANGE SERVO ERROR (cm)

Table B.1 Cont'd

RAGC	20	102-121	32	181-213	RADAR ALTIMETER AUTOMATIC GAIN CONTROL VOLTAGE (dbm x 10^2)
* IPG	20		320		INSTANTENEOUS PLATEAU GATE POWER (mv)
RTP	4	122-125	8	214-221	RADAR ALTIMETER TRANSMITTER OUTPUT POWER (dbm x 10^2)
ANG	4	126-129	8	222-229	RADAR ALTIMETER AVERAGE NOISE GATE (mv)
ARG	4	130-133	8	230-237	RADAR ALTIMETER AVERAGE RAMP GATE (mv)
APG	4	134-137	8	238-245	RADAR ALTIMETER AVERAGE PLATEAU GATE (mv)
AASG	4	138-141	8	246-253	RADAR ALTIMETER AVERAGE ALTITUDE/ SPECULAR GATE (mv)
* BCT	1		1		RADAR ALTIMETER BIT/CAL TEMPERATURE ^{o}C x 10
* RTT	1		1		RADAR ALTIMETER TRANSMITTER TEMPERATURE ^{o}C x 10
* RRT	1		1		RADAR ALTIMETER RECEIVER TEMPERATURE ^{o}C x 10
* GTT	1		1		RADAR ALTIMETER GLOBAL TRACKER TEMPERATURE ^{o}C x 10
* ITT	1		1		RADAR ALTIMETER INTENSIVE TRACKER TEMPERATURE ^{o}C x 10
* WST	1		1		RADAR ALTIMETER WAVEFORM SAMPLER TEMPERATURE ^{o}C x 10
* IFTA	1		1		RADAR ALTIMETER IF TEST SIGNAL AMPLITUDE (mv)
* RSA	1		1		RADAR ALTIMETER REFERENCE SIGNAL AMPLITUDE (mv)
* VTA	1		1		RADAR ALTIMETER VIDEO TEST SIGNAL AMPLITUDE (mv)
* RMI	1		1		RADAR ALTIMETER RECEIVER MIXER CURRENT (mv)
SSHITE	20	142-161	32	254-285	SEA SURFACE HEIGHT (cm)
* IRS(i)	0		5120		INSTANTANEOUS RETURN SAMPLES No. 1-16 (mv)
* AW(i)	0		16		CALCULATED AVERAGE WAVEFORMS No. 1-16 (mv)
* SAW(i)	0		16		CALCULATED SIGMAS ON AW(i) (mv)
RAGCHI	1	162	1	286	RADAR ALTIMETER AVERAGE GAIN CONTROL VOLTAGE (mv)
AVRAGC	1	163	1	287	MEAN OF RAGC (mv)
H 1/3	1	164	1	288	SIGNIFICANT WAVEHEIGHT (cm)
SMOSSH	1	165	1	289	SATHT-SMOALT-ABIAS-TREF @ FODAY (cm)

Note: '*" indicates an altimetry record parameter included in the original NASA records but not in the BIO subsets.

538.	7502701.	41.	23.	.	13101.	43041.	59306244745.	86934619.	526925
3183757.	118.	.	232.	.	4140.	3.	59305321479.	264.	76
86932966.	86933010.	86933209.	86933427.	86933555.	86933900.	86934064.	86934109.	86934287.	86934466
86934574.	86934766.	86935059.	86933427.	86935395.	86935493.	86935818.	86936284.	86936444.	86936357
86937204.	86937383	86937560.	86937738.	86937916.	86938093.	86938272.	86938450.	86938628.	86938806
86938985.	86939163.	86939339.	86939519.	86939695.	86939873.	86940052.	86940230.	86940406.	86940583
1000.	79.	79.	79.	79.	79.	79.	79.	79.	79
79.	79.	79.	79.	79.	79.	79.	79.	79.	79
79.	23.	47.	23.	70.	70.	.	.	.	23
23.	23.	70.	-47.	-23.	-23.	70.	70.	-23.	23.
.	-7217.	-7217	-7217.	-7317.	-7213.	-7194.	-7239.	-7307.	-7330.
-7353.	-7375.	-7375	-7330.	-7307.	-7307.	-7307.	-7262.	-7262.	-7285.
-7330.	6201.	6201.	6201.	6201.	2.	- 2.	2.	2.	50.
47.	44.	44.	96.	99.	93.	93.	53.	52.	56.
56.	4470.	4605.	4584.	4543.	4592.	4425.	4440.	4573.	4573.
4572	4643.	4628.	4512.	4558.	4533.	4613.	4466.	4177.	4195.
4458.	-7197.	-7282.	506.	4509.					

Table B.2

Sample of Low Data Rate Record in the BIO subsets

(165 parameters as in table B.1)

15190.	7502701.	41.	23.	.	23101.	43037.	39345563253.	86978991.	575651.
2985205.	33.	.	229.	.	-676.	.	39344025556.	260.	76.
-8888.	86982834.	86982609.	86982302.	86980316.	86882040.	86981848.	86981598.	86981441.	-8888.
86981030.	86980906.	86980670.	-8888.	-8888.	86980134.	86980026.	86979817.	86979681.	86979468.
-8888.	86979045.	86978890.	86978634.	86980316.	86978372.	86978082.	86977895.	86977752.	-8888.
86977384.	86977203.	86981284.	86981099.	-8888.	86980731.	86980548.	86980362.	86980177.	86979993.
86979809.	86979624.	86979438.	86979254.	86980916.	86978884.	86978700.	86978516.	86978331.	86978146.
86977963.	86977777.	86977591.	86977405.	86977221.	86977037.	86976852.	86976664.	86976480.	86976295.
86976109.	86975923.	86975738.	86975553.	1000.	.	79.	79.	79.	79.
79.	79.	79.	79.	.	79.	79.	79.	79.	79.
79.	79.	79.	.	79.	79.	79.	79.	79.	79.
79.	79.	.	79.	79.	79.	79.	79.	79.	79.
79.	79.	79.	79.	79.	.	79.	79.	79.	79.
79.	79.	79.	79.	.	79.	79.	79.	79.	79.
79.	79.	79.	.	79.	79.	79.	79.	79.	-9999.
-9999.	-9999.	-9999.	-9999.	.	-23.	-47.	.	..	23.
.	-47.	-47.	-23.	-23.	.	-23.	-94.	-94.	-23.
-47.	.	-23.	23.	-23.	-94.	-23.	.	-23.	.
-23.	-7210.	-7187.	-7187.	-7210.	-9999.	-7232.	-7232.	-7187.	-7187.
-7187.	-7187.	-7165.	-7165.	-9999.	-7165.	-7187.	-7187.	-7165.	-7165.
-7165.	-7187.	-7187.	-7210.	-7187.	-9999.	-7210.	-7210.	-7255.	-7255.
-7232.	-7232.	-7187.	6204.	-9999.	6204.	6204.	6204.	6204.	-9999.
6204.	-9999.	2.	2.	2.	2.	2.	2.	2.	47.
47.	-9999.	47.	47.	47.	50.	94.	94.	97.	97.
94.	97.	97.	94.	97.	53.	53.	53.	52.	50.
49.	50.	50.	-8888.	-1506.	-1465.	-8888.	-8888.	-1449.	-1441.
-1376.	-1403.	-8888.	-1363.	-1423.	-1372.	-1388.	-1388.	-1388.	-1466.
-1442.	-1490.	-1462.	-8888.	-1410.	-1440	-8888.	-8888.	-1479.	-1373.
-1370.	-1413.	-8888.	-1416.	-1421.	-7190.	-8888.	-8888.	-338.	

Table B.3

Sample of High Data Rate Record in the BIO subsets

(289 parameters as in table B.1)

REFERENCES

Allen, C.P. and C.F. Martin (1977) - "SEAHT - A Computer Program for the Use of Intersecting Arcs of Altimetry Data for Sea Surface Height Refinement", NASA CR-141432, Wallops Flight Center, Wallops Island, Va.

Anderle, R.J. and R.L. Hoskin (1977) - "Correlated Errors in Satellite Altimetry Geoids", EOS, Transactions of the American Geophysical Union, 58(6).

Anderle, R.J. (1977) - "Ocean Geodesy Based on GEOS-3 Satellite Altimetry Data", preprint of paper prepared for presentation at the 20th Annual COSPAR Meeting, Tel Aviv, Israel.

Anderson, E. (1978) - "Modelling of Physical Influences in Sea-Level Records for Vertical Crustal Movement Detection", Proc. of the 9th GEOP Conference, An International Symposium of the Applications of Geodesy to Geodynamics, Oct 2-5, Dept. of Geodetic Science Rep. 280, The Ohio State University, Columbus, Ohio 43210.

Bjerhammar, A. (1973) - "Generalized Matrix Inverses", Lecture Notes, International School in the Mountains, Ramsau, Austria.

Black, H.D. (1978) - "An easily-implemented Algorithm for the Tropospheric Range Correction", JGR, Vol. 83, p. 1825.

Blaha, G. (1975) - "The Combination of Gravity and Satellite Altimetry Data for determining the Geoid Surface", Rep. 75-0347, Air Force Geophysics Laboratory, Bedford, Mass. 01731.

Blaha, G. (1976) - "The Least Squares Collocation from the Adjustment Point of View and Related Topics", TR-76-0073, Air Force Geophysics Laboratory, Bedford, Mass. 01731.

Blaha, G. (1977a) - "Refinement of the Short Arc Satellite Altimetry Adjustment Model", Bulletin Geodesique, No. 51, p. 33.

Blaha, G. (1977b) - "Refinements in the Combined Adjustment of Satellite Altimetry and Gravity Anomaly Data", Rep. 77-0169, Air Force Geophysics Laboratory, Bedford, Mass. 01731.

Brown, D.C. and J. Trotter (1969) - "SAGA - A Computer Program for Short Arc Geodetic Adjustment of Satellite Observations", DBA System Inc., Melbourne, Fl. 32901.

Brown, D.C. (1976) - "Doppler Positioning by the Short Arc Method", Proc. of the International Geodetic Symposium on Satellite Doppler Positioning, Las Cruces, N.M. 88003.

CAM (1970) - "Documentation for a Cartographic Automatic Mapping Program", National Technical Information Service, Springfield, Va. 22151.

Delikaraoglou, D. and P. Vanicek (1979) - "Progress Report on the Analysis of the GEOS-3 Altimetry in Hudson Bay", Department of Surveying Engineering, University of New Brunswick, Fredericton, N.B.

Eisner, A. (1979) - "The GEOS-3 Altimeter Instrument Bias", Applied Physics Laboratory, The John Hopkins University, CP 073.

Estes, R. (1977) - "A Computer Softward System for the Generation of Global Ocean Tides Including Crustal Loading Effects", Contract NA55-20045, Business and Technology Systems TR-77-41.

Freeman, N.G. and T.S. Murty (1976) - "Numerical Modelling of Tides in Hudson Bay", Journal of Fisheries Research Board of Canada, 33, p. 2345.

Grappo, G.A. and D.N. Huber (1979) - "Determination of the Earth's Mean Equatorial Radius and Center of Gravity from Doppler - Derived and Gravimetric Geoid Heights", presented at the XVII General Assembly of the IUGG, Canberra, Australia, Dec.

Guier, W.H. (1965) - "Satellite Geodesy", APL Technical Digest, 4, No. 3, 2-13.

Hadgigeorge, G. and J. Trotter (1978) - "Short Arc Reduction of Radar Altimetry Computer Program", NASA CR-141434, Wallops Flight Center, Wallops Island, Va.

Hardy, R.L. (1979) - "Multiquadratic Representation of the Earth's Gravitational Field", preprint of paper presented at the XVII General Assembly of the IUGG, Canberra, Australia, Dec.

Hatch, R. (1976) - "New Positioning Software from Magnavox", Proc. of the International Geodetic Symposium on Satellite Doppler Positioning, Las Cruces, N.M. 88003.

Heiskanen, W.H. and H. Moritz (1967) - "Physical Geodesy", W.H. Freeman San Francisco.

Henderschott, M.C. (1972) - "Ocean Tides", presented at the First GEOP Research Conference on Tides, The Ohio State University, Columbus, Ohio, Oct. 26-27.

Henderschott, M.C. (1975) - "Global Numerical Tide Solutions with Inclusion of Ocean Self - Gravitation and Solid Earth Tidal Loading", presented at the XVI General Assembly of the IUGG, Grenoble, France.

Hodgson, J.H. (1973) - "Canadian Participation in the GEOS-C Project", Jan. 26 personal communication with C.W. Mathews, NASA Office of International Affairs, Washington, D.C.

Lawnikanis, P. (1975a) - "Program PREDOP", Publication of Surveys and Mapping Branch, Geodetic Survey of Canada, Ottawa.

Lawnikanis, P. (1975b) - "GEODOP Utilities Programs", Publication of Surveys and Mapping Branch, Geodetic Survey of Canada, Ottawa.

Leitao, C.D., C.L. Purdy, and R.L. Brooks (1975) - "Wallops GEOS-C Altimeter Preprocessing Report", NASA TM-X-69357, Wallops Flight Center, Wallops Island, Va.

Lerch, F.J., S.M. Klosko, R.E. Laubscher and C.A. Wagner (1977) - "Gravity Model Improvement Using GEOS-3 (GEM 9 & 10)", GSFC Document X-921-77-246, Goddard Space Flight Center, Greenbelt, Md.

Lerch, F.J., C.A. Wagner, S.M. Kloski and R.B. Belott (1978) - "Goddard Earth Model Development for Oceanographic Applications", presented at the Marine Geodesy Symposium, University of Miami, Virginia Key, Miami, Fl.

Marsh, J.G., T.V. Martin, J.J. McCarthy, P.S. Chovitz (1978) - "Mean Sea Surface computation using GEOS-3 Altimetry Data", presented at the International Symposium of Interaction of Marine Geodesy and Ocean Dynamics, Miami, Fl., Oct. 10-13.

Martin, C.F. and M.L. Bulter (1977) - "Calibration Results for the GEOS-3 Altimeter",NASA CR-141430, Wallops Flight Center, Wallops Island, Va.

Masters, E.G., R. Coleman and K. Bretreger (1979) - "On Orbital Errors and the Recovery of Regional Models using Satellite Altimetry", submitted to the Australian Journal of Geodesy, Photogrammetry and Surveying for publication in the Dec. 1979 issue.

Mather, R.S., F.J. Lerch, C. Rizos, E.G. Masters and B. Hirsch (1978) - "Determination of Some Dominant Parameters of the Global Dynamics Sea Surface Topography from GEOS-3 Altimetry", NASA TM-79558, Goddard Space Flight Center, Greenbelt, MD 20771.

Mather, R.S. and C. Rizos (1979) - "Global Mean Sea Level from GEOS-3 Altimetry", submitted to the Australian Journal of Geodesy, Photogrammetry and Surveying for publication in the Dec. 1979 issue.

Merry, C.L. (1975) - "Development and Evaluation of a technique for Deflection Prediction and Astrogravimetric Geoid Determination", Tech, Rep. No. 31, Dept. of Surveying Engineering, University of New Brunswick, Fredericton, N.B.

Mikhail, E.M. (1976) - "Observations and Least Squares", IEP - A Dun-Dunneley Publisher, New York.

Moritz, H. (1978) - "The Operational Approach to Physical Geodesy", Rep. No. 255, Dept. of Geodetic Science, The Ohio State University, Columbus, Ohio.

John, S. (1980) - "A Regional Gravimetric Geoid for Hudson Bay", presented at the Spring Meeting of the American Geophysical Union, Toronto, 22-26 May.

Kaula, W.M. (1968) - "An Introduction to Planetary Physics", John Wiley and Sons, Inc., New York.

Kearsley, W. (1977) - "The Prediction and Mapping of Geoidal Undulations from GEOS-3 Altimetry", Rep. No. 267, Dept. of Geodetic Science, The Ohio State University, Columbus, Ohio.

Kouba, J. and J.D. Boal (1975) - "Program GEODOP", publication of Surveys and Mapping Branch, Geodetic Survey of Canada, Ottawa.

Kouba, J. and D.E. Wells, (1976) - "Semi-Dynamical Doppler Satellite Geodesy", Bulletin Geodesique, 50, p. 27.

Kouba, J. (1974) - "Reduction of Doppler Satellite Data Observed in Canada", Canadian Surveyor, Vol. 28.

Kouba, J. (1978) - "GEOS-3 Doppler Data", unpublished paper circulated among the Investigators Group of the Hudson Bay Experiment.

Kouba, J. (1979) - "Improvement of Canadian Geodetic Doppler Programs", Proc. of the Second International Geodetic Symposium on Satellite Doppler Positioning, The University of Texas at Austin, Jan 22-26.

Kozai, Y. (1959) - "The Motion of a Close Earth Satellite", Astronomical Journal, 64, No. 1274, p. 367.

Krakiwsky, E.J. and D.E. Wells (1971) - "Coordinate Systems in Geodesy", Lecture Notes No. 16, Department of Surveying Engineering, University of New Brunswick, Fredericton, N.B.

Krakiwsky, E.J. (1975) - "A Synthesis of Recent Advances in the Method of Least Squares", Lecture Notes No. 42, Dept. of Surveying Engineering, University of New Brunswick, Fredericton, N.B.

Lachapelle, G. (1977) - "Estimation of Disturbing Potential Components using a Combined Integral Formulae and Collocation Approach", Collected papers, Geodetic Survey 1977, publication of the Surveys and Mapping Branch, Ottawa.

Lachapelle, G. (1979) - "Comparison of Doppler - Derived and Gravimetric Geoid Undulations in North America", Proc. of the Second International Symposium on Satellite Doppler Positioning, The University of Texas at Austin, Jan. 22-26.

Lachapelle, G. and K.L. Brace (1979) - "The Hudson Bay Geoid", draft of paper prepared for presentation at the Second Inter. Symp. on Problems Related to the Redefinition of North American Vertical Geodetic Networks, Ottawa, May 26-30.

Munk, W.H. and D.E. Cartwright (1966) - "Tidal Spectroscopy and Prediction", Phil. Trans., Royal Society, London, Ser. A 259, p. 533.

Munk, W.H., F. Snodgrass and M. Wimbush (1970) - "Tides Offshore; Transition from California Coastal to Deep-Sea Waters", Geoph. Fluid Dyn., 1, p. 161.

NASA (1972a) - "Project Plan for the Geodetic Earth Orbiting Satellite (GEOS-C), Wallops Station, Wallops Island, Va.

NASA (1972b) - "GEOS-C Mission - Proposal Briefing Information", NASA Wallops Station, Wallops Island, Va.

Nesbo, I. (1976) - "Simulation for the Hudson Bay Altimetry Experiment", unpublished paper, Dept. of Surveying Engineering, University of New Brunswick, Fredericton, N.B.

Okenwa, E.G. (1978) - "Automated Tidal Reduction of Soundings", Tech. Rep. No. 55, Dept. of Surveying Engineering, University of New Brunswick, Fredericton, N.B.

Pisacane, V.L., A. Eisner, S.M. Yionoulis, R.J. McConaly, H.D. Block and L.L. Dryor (1978) - "The GEOS-3 Orbit Determination Experiment", Applied Physics Laboratory, The John Hopkins University, CP 064.

Pope, A.J. (1976) - "The Statistics of Residuals and the Detection of Outliers", NOAA Tech. Rep. NOS65 NGsl.

Rao, C.R. (1973) - "Linear Statistical Inference and its Applications", 2nd Edition, John Wiley & Sons Inc., New York.

Rapp, R.H. (1978) - "Mean Gravity Anomalies and Sea Surface Heights Dereived from GEOS-3 Altimeter Data", NASA CR-156843, Wallops Flight Center, Wallops Island, Va.

Rapp, R.H. (1979) - "A Review of Anomaly and Undulation Determinations from the GEOS-3 Altimeter Data", Presented at the Spring Meeting of the American Geophysical Union, Washington, D.C.

Rummel, R. and R.H. Rapp (1977) - "Undulations and Anomaly Estimation Using GEOS-3 Altimeter Data without precise orbits", Bulletin Geodesique, No. 51, p. 73.

Schaab, H. and E. Grotten (1979) - "Comparison of Geocentric Origins of Global Systems from Uniformly distributed data", Bulletin Geodesique, No. 53, p. 11.

Schwiderski, E.W. (1978) - "Global Ocean Tides, Part I: A detailed Hydrodynamical Interpolation Model", Naval Surface Weapons Center, TR-3866, Dahlgren, Va.

Schureman, P. (1971) - "Manual of Harmonic Analysis and Prediction of Tides", U.S. Dept of Commerce Special Publ. No. 98. Reprinted Oct.

Seppelin, T.O. (1974) - "The Department of Defence World Geodetic System 1972", presented at the International Symposium on Problems Related to the Redefinition of North American Geodetic Networks, Fredericton, N.B., Canada.

Tscherning, C.C. (1979) - "Comparison of Some Methods for the detailed representation of the Earth's Gravity Field", presented at the XVII General Assembly of the IUGG, Canberra, Australia.

Vanicek, P. and D.E. Wells, (1972) - "The Least Squares Approximation and Related Topics", Lecture Notes No. 22, Dept. of Surveying Engineering, University of New Brunswick, Fredericton, N.B.

Vanicek, P. and C.L. Merry (1973) - "Determination of the Geoid from Deflections of the Vertical using a Least Squares Surface Fitting Technique", Bulletin Geodesique, No. 109, p. 261.

Vanicek, P. and E.J. Krakiwsky (in prep.) - "Geodesy: The Concepts", to be published.

Vanicek, P. (1978) - "To the Problem of Noise Reduction on Sea Level Records used in Vertical Crustal Movement Detection", Physics of the Earth and Planetary Interiors, 17, p. 265.

Vincent, S. and Marsh, J.G. (1973) - "Global Detailed Gravimetric Geoid", NASA TM-X-70492, Goddard Space Flight Center, Greenbelt, Md.

Wells, D.E. (1974) - "Doppler Satellite Control", Techn. Rep. No. 29, Dept. of Surveying Engineering, University of New Brunswick, Fredericton, N.B.

Wells, D.E. (1976) - "Canadian GOES-3 Investigations", presented at the GEOS-3 Principal Investigators Meeting, NASA Wallops Flight Center, Wallops Island, Va.

White, H.K., D.N. Huber and J.L. Taylor (1975) - "Comparison between Naval Surface Weapons Center and Navy Astronautics Group Ephemerides for Geoceiver Positioning", Rep. No. TR-75-001, Defence Mapping Agency Aerospace Center, St. Louis.

Forrester, W.D. (1980) - "Accuracy of Water Level Transfers", presented at the Second International Symposium on Problems Related to the Redefinition of North American Vertical Control Networks, Ottawa, May 26-30.

Hamon, B.V. (1966) - "Continental Shelf Waves and the Effects of Atmospheric Pressure and Wind Stress on Sea level', Journal of Geophysical Research, Vol. 71, No. 12, 2883.

Mather, R.S., R. Coleman, C. Rizos, and B. Hirsch (1977) - "A Preliminary Analysis of GEOS-3 Altimeter Data in the Tasman and Coral Seas, Australian Journal Geod., Photogr., Surv., 26, 27-46.

Miller, A.R. (1958) - "The Effects of Winds on Water Levels on the New England Coast", Limnology and Oceanography", Vol. III, No. 1.

Sunkel, H. (1977) - "Spline Functions and Geodetic Integral Formulas", presented at the International Symposium on Optimization of Design and Computation of Control Networks, Sopron, Hungrary, July 3-9.

West, G.B. (1980) - "Mean Earth Ellipsoid determined from SEASAT-1 Altimetric Observations", presented at the Spring Meeting of the American Geophysical Union, Toronto, May 22-26.

Wilson, B.W. (1960) - "Note on Surface Wind Stress over Water at Low and High Wind Speeds", Journal of Geophysical Research, Vol. 65, No. 10, 3377.